



JAEA-Review
2007-046

JAEA-Review

JAEA-Tokai TANDEM Annual Report 2006 April 1, 2006 – March 31, 2007

Department of Research Reactor and Tandem Accelerator

Nuclear Science Research Institute
Tokai Research and Development Center

January 2008

Japan Atomic Energy Agency

日本原子力研究開発機構

本レポートは日本原子力研究開発機構が不定期に発行する成果報告書です。
本レポートの入手並びに著作権利用に関するお問い合わせは、下記あてにお問い合わせ下さい。
なお、本レポートの全文は日本原子力研究開発機構ホームページ (<http://www.jaea.go.jp/index.shtml>)
より発信されています。このほか財団法人原子力弘済会資料センター*では実費による複写頒布を行っ
ております。

〒319-1195 茨城県那珂郡東海村白方白根 2 番地 4
日本原子力研究開発機構 研究技術情報部 研究技術情報課
電話 029-282-6387, Fax 029-282-5920

* 〒319-1195 茨城県那珂郡東海村白方白根 2 番地 4 日本原子力研究開発機構内

This report is issued irregularly by Japan Atomic Energy Agency
Inquiries about availability and/or copyright of this report should be addressed to
Intellectual Resources Section, Intellectual Resources Department,
Japan Atomic Energy Agency
2-4 Shirakata Shirane, Tokai-mura, Naka-gun, Ibaraki-ken 319-1195 Japan
Tel +81-29-282-6387, Fax +81-29-282-5920

© Japan Atomic Energy Agency, 2008

JAEA-Tokai TANDEM Annual Report 2006
April 1, 2006 – March 31, 2007

Department of Research Reactor and Tandem Accelerator

Nuclear Science Research Institute
Tokai Research and Development Center
Japan Atomic Energy Agency
Tokai-mura, Naka-gun, Ibaraki-ken

(Received October 30, 2007)

This annual report describes a summary of each research activity, which has been carried out using the JAEA-Tokai tandem accelerator with the energy booster from April 1, 2006 to March 31, 2007. The forty-eight summary reports were categorized into seven research/development fields, i.e., (1) accelerator operation and development, (2) nuclear structure, (3) nuclear reaction, (4) nuclear chemistry, (5) nuclear theory, (6) atomic physics and solid state physics, and (7) radiation effects in materials, in addition, lists of publications, personnel and cooperative researches with universities are contained. Regarding the number of summaries each of the fields is as follows: accelerator operation and development – 11, nuclear structure – 11, nuclear reaction – 6, nuclear chemistry – 5, nuclear theory – 4, atomic physics and solid state physics – 3, radiation effects in materials – 8.

Keywords : JAEA-Tokai Tandem Accelerator, Operation Results, Nuclear Structure, Nuclear Reaction, Nuclear Chemistry, Nuclear Theory, Atomic Physics, Solid State Physics, Radiation Effects in Materials, Progress Report.

Editors : Tetsuro ISHII, Yuichiro NAGAME, Satoshi CHIBA, Norito ISHIKAWA,
Yosuke TOH, Akihiko OSA and Masao SATAKA

原子力機構東海タンデム加速器 2006 年度年次報告

日本原子力研究開発機構
東海研究開発センター原子力科学研究所
研究炉加速器管理部

(2007 年 10 月 30 日受理)

本年次報告書は、原子力科学研究所の原子力機構東海タンデム加速器及びブースターを利用し、2006 年 4 月 1 日から 2007 年 3 月 31 日までの期間に実施された研究活動毎の要約をまとめたものである。

総数 48 件の要約は、(1) 加速器の運転状況と開発、(2) 原子核構造、(3) 原子核反応、(4) 核化学、(5) 原子核理論、(6) 原子物理及び固体物理、(7) 材料の照射効果 の 7 部門に分類され、またこれらに関係する各種リスト（公刊論文、発表会合、関与した職員、大学等との協力研究課題）も掲載されている。なお、部門ごとの件数は (1) : 11 件、(2) : 11 件、(3) : 6 件、(4) : 5 件、(5) : 4 件、(6) : 3 件、(7) : 8 件である。

原子力科学研究所：〒319-1195 茨城県那珂郡東海村白方白根 2-4

編集者：石井 哲朗、永目 諭一郎、千葉 敏、石川 法人、藤 暢輔、長 明彦、
左高 正雄

Foreword

This report covers research and development activities with the tandem accelerator, its superconducting booster and TRIAC radioactive ion accelerator at JAEA Tokai, for the period of FY 2006 (April 1, 2006 to March 31, 2007). During this period, the tandem accelerator was operated over a total of 201 days and delivered 26 different ions over 144 beam times to the experiments in the fields of nuclear physics, nuclear chemistry, atomic physics, solid state physics and radiation effects in materials. Forty research programs were carried out in collaboration with a total of about 220 researchers from universities and research institutes. The TRIAC was operated for 46 days. The following are some of the highlights in FY 2006.

In the development of the tandem accelerator and the booster, it was confirmed that superconducting cavities can be restored to the original field gradients by cleaning the niobium surfaces with high-pressure water-jet spray. We made a cryogenic test of a superconducting twin quarter-wave resonator designed for low-velocity beams and obtained a preliminary result of $E_{\text{acc}} = 2.8 \text{ MV/m}$ at 4W RF power. Techniques of stable production of the metal-ion beams from an ECR ion source were developed for applying them to the source at the high-voltage terminal.

In the development of TRIAC, we improved the charge breeding efficiency (ε_{CB}) for metallic ions and the vacuum at the low-energy beam line for better transport efficiency for highly charge-bred in order to achieve highly efficient acceleration of medium-mass radioactive ion beams. The ε_{CB} increased from 0.1% to as much as 2%. In the case of $^{129}\text{Xe}^{19+}$, the overall transmission from ISOL to the secondary target including ε_{CB} was as large as 2%.

In research of nuclear structure, the band properties of ^{187}Pt and ^{174}Re are investigated by in-beam γ -ray spectroscopy for investigating signature inversions and shape coexistence. A new isotope of the most neutron-rich Eu nucleus, ^{166}Eu , was found using the ISOL with a surface ionization ion source equipped with UC target. Excited states in ^{242}U , the heaviest uranium nucleus identified so far, were established up to 8^+ by in-beam γ -ray spectroscopy using the ($^{18}\text{O}, ^{20}\text{Ne}$) reaction. The systematics of the first 2^+ energies in neutron-rich actinide nuclei suggests the possibility of a spherical doubly magic nucleus $^{256}\text{U}_{164}$.

In research of nuclear reactions, fusion barrier distributions in the $^{76}\text{Ge}+^{208}\text{Pb}$ and $^{76}\text{Ge}+^{209}\text{Bi}$ reactions were extracted by measuring quasi-elastic backward scatterings. These reactions are candidates of cold-fusion reactions for producing super-heavy elements of $Z=114$ and 115, respectively. Fission cross-sections for the reaction $^{34}\text{S}+^{238}\text{U}$ were measured around the Coulomb barrier, and the results suggested that a new isotope ^{268}Hs can be found in the fusion

reaction at the sub-barrier energy. Astrophysical nuclear reaction rates of ${}^8\text{Li}(d,t){}^7\text{Li}$ and ${}^8\text{Li}(d,\alpha){}^6\text{He}$ were determined by using low-energy radioactive nuclear beam from TRIAC.

In research of nuclear chemistry, aqueous chemistry of element 104, rutherfordium (Rf) produced in the reaction ${}^{248}\text{Cm}({}^{18}\text{O}, 5n){}^{261}\text{Rf}$ was systematically investigated based on an atom-at-a-time scale. From trioctylphosphine oxide (TOPO) reversed-phase chromatography in hydrochloric acid solution, we observed characteristic chemical property of Rf compared to those of the homologues in the periodic table.

In research of nuclear theory, structure of exotic and heavy nuclei was investigated: Narrowing of the $N=28$ shell gap was predicted for $Z=14$ and 16 by shell model by taking account of the tensor force of a new shell model interaction in the sd - pf cross shell part. Potential energy surface calculation of heavy nuclei was extended to a wider parameter space to cover well the scission points. The investigation of bulk properties of kaonic nuclei in terms of relativistic mean field theory and chiral model for the KN interaction shows that the central density of some light nuclei is enhanced up to two times the saturation density.

In research of atomic and solid state physics, the diffusion coefficients of Li in β -LiGa with different Li content were investigated using ${}^8\text{Li}$ beams from TRIAC. It was found that the Li diffusion around stoichiometric composition (1:1) is faster than in the Li-excess and Li-deficient composition. This fact demonstrates that the motion of the vacancies on the Li atomic sites seems to be strongly promoted by the coexistence of Li-vacancies and Li anti-structure atoms.

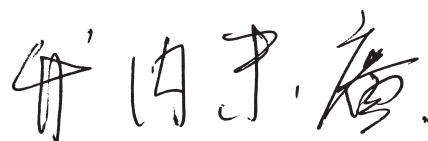
In research of radiation effects in materials, the microstructure evolution due to accumulation of ion-tracks and Xe-gas atoms was investigated. It was found that in Ce-based ceramics densely accumulated ion-tracks form small subdivided grains similar to the microstructure observed in high burn-up UO_2 fuels. It was also found that Xe-atom implantation promotes surface roughness which may be related to the formation of high burn-up structure.

Suehiro Takeuchi

Deputy Director

Department of Research Reactor

and Tandem Accelerator



Contents

1.	ACCELERATOR OPERATION AND DEVELOPMENT	1
1.1	Operation and Usage of Tandem Accelerator and Booster	3
1.2	Design of the Power Supply for the Bending Magnet on the High Voltage Terminal of the JAEA-Tokai Tandem	6
1.3	Stable Production of Metal Ion Beam from ECR Ion Source and Application to Terminal Ion Source	7
1.4	Screening Test of Relays Used under Pressurized Sulfur Hexafluoride (SF ₆)	9
1.5	Communication Fault in the Interlock System for the JAEA Tandem Accelerator Facility	11
1.6	Performance Test of Low β Superconducting Twin Quarter Wave Resonator	13
1.7	Effect of High Pressure Water Jet Rinsing to Superconducting Cavity	15
1.8	Acceleration Test of the Low-Speed Heavy Ion Beam by the JAEA-Tokai Tandem Booster	17
1.9	Ion Source Development of On-Line Isotope Separator for Radioactive Nuclear Beam	18
1.10	Ion Source Development for Off-Line Experiment	20
1.11	Development of a Thick Target for Ion Source of On-Line Mass Separation of Heavy Actinide Isotopes	22
2.	NUCLEAR STRUCTURE	23
2.1	Study of High-Spin States in $A \approx 30$ Nuclei	25
2.2	Lifetime Measurement of High-Spin States in ⁹² Zr	27
2.3	Development of Spin-Polarized Radioactive Nuclear Beam for Nuclear Spectroscopy through β -Delayed Decay of Spin-Polarized Nuclei Around Doubly Magic Nucleus ¹³² Sn	28
2.4	Coulomb Excitation Experiment of ¹³⁴ Xe	30
2.5	β Decay Half-Life of ¹⁶⁶ Eu and Levels in ¹⁶⁶ Gd	32
2.6	High-Spin States of Odd-Odd ¹⁷⁴ Re Nucleus	34
2.7	Spectroscopy of Neutron-Rich Tantalum Isotopes Produced in ¹⁸ O-Induced Transfer Reactions	36
2.8	Production of Long-Lived ^{186m} Re for Laser Ablation Laser-Induced Fluorescence Spectroscopy	37
2.9	Band Properties of the Transitional Nucleus ¹⁸⁷ Pt	38
2.10	Gamma-Rays in Neutron-Rich Nuclei ²³⁶ Th and ²⁴² U	40
2.11	Alpha Fine Structure Measurement for ²⁵⁵ No	42
3.	NUCLEAR REACTIONS	45
3.1	Direct Measurement of the Astrophysical Nuclear Reaction Rate of the ⁸ Li (d, t) ⁷ Li Reaction	47
3.2	Measurement of Spectroscopic Factor & Spin-Parity on ⁶² Ni (d, p) ⁶³ Ni* Reaction in Inverse Kinematics	49
3.3	Measurement of Quasi-Elastic Backscattering for ⁶⁴ Ni + ¹¹⁸ Sn	51
3.4	Quasi-Elastic Backward Scattering in ⁷⁶ Ge + ²⁰⁸ Pb, ²⁰⁹ Bi	53
3.5	Measurement of Fission Cross-Sections for ³⁴ S + ²³⁸ U	54
3.6	Correlation between α -Particle Emission and Fission in the ¹⁸ O + ²⁴⁴ Pu Reaction	56
4.	NUCLEAR CHEMISTRY	59
4.1	Trioctylphosphine Oxide (TOPO) Reversed-Phase Chromatography of Rutherfordium in HCl	61
4.2	Development of an Electrochemistry Apparatus for the Heaviest Elements	63

4.3	Elution Curves of Nb and Ta in Anion-Exchange Chromatography with HF/HNO ₃ Solutions	65
4.4	Production of RI Tracers for Chemistry of Transactinide Elements	67
4.5	Radioisotopes Incorporation in Fullerenes by Using Nuclear Recoil	68
5.	NUCLEAR THEORY	71
5.1	Significance of the Tensor Force in Exotic Nuclei in the SD-PF Shell	73
5.2	Extension of Calculation for Nuclear Potential Energy Surface to Large Deformation	75
5.3	Bulk Properties of Kaonic Nuclei	77
5.4	P-P Scattering Phase Shift in Momentum Space Including the Coulomb and a Short-Range Forces	79
6.	ATOMIC PHYSICS AND SOLID STATE PHYSICS	81
6.1	High-Resolution Zero-Degree Electron Spectroscopy of Neon Ions Passing through Carbon Foils	83
6.2	Measurement of the Diffusion Coefficients in β -LiGa by Using Short-Lived Radiotracer of ⁸ Li	85
6.3	Charge State Distribution of Sulfur Ions after Penetration of C-Foil Targets (IV)	87
7.	RADIATION EFFECTS IN MATERIALS	89
7.1	Microstructure and Ion Configuration of Spinel Compound Irradiated with Swift Heavy Ions	91
7.2	Effects of Accumulation of Ion Tracks and Pre-Implantation of Xe Ions on Microstructure Changes in CeO ₂	93
7.3	A Trial Usage of Microprobes for Improvement of a Scanning SQUID Microscope	95
7.4	Study on Irradiation-Induced Magnetic Transition in FeRh Alloys by Using X-Ray Magnetic Circular Dichroism	97
7.5	Electronic Sputtering of Nitrides and Oxides by High-Energy Heavy Ions	99
7.6	X-Ray Diffraction Study of CeO ₂ Irradiated with High-Energy Heavy Ions	101
7.7	Swift Heavy Ion Induced Structural Modifications in Single Crystalline α -Al ₂ O ₃	103
7.8	Hardness Modification in FeCu Alloys by Using Radiation Enhanced Segregation	105
8.	PUBLICATION IN JOURNAL AND PROCEEDINGS, AND CONTRIBUTION TO SCIENTIFIC MEETINGS	107
8.1	Accelerator Operation and Development	109
8.2	Nuclear Structure	111
8.3	Nuclear Reaction	116
8.4	Nuclear Chemistry	120
8.5	Nuclear Theory	125
8.6	Atomic Physics and Solid State Physics	131
8.7	Radiation Effects in Materials	132
9.	PERSONNEL AND COMMITTEE	137
9.1	Personnel	139
9.2	Research Planning and Assessment Committee	143

10. COOPERATIVE RESEARCHES, AND LIST OF COMMON USE PROGRAM IN JAEA	145
10.1 Cooperative Researches List.....	147
10.2 Common Use Program in JAEA.....	149

目 次

1. 加速器の運転状況及び開発	1
1.1 タンデム加速器とブースターの運転と利用	3
1.2 JAEA 東海タンデム加速器高電圧端子内偏向電磁石用電源の設計	6
1.3 ECR イオン源による金属イオンビームの安定生成とターミナルイオン源への応用	7
1.4 高圧 SF ₆ ガス環境下で使用するリレーのスクリーニング試験	9
1.5 JAEA タンデム加速器施設インターロックシステムにおける通信障害	11
1.6 低β超伝導加速空洞の性能試験	13
1.7 超伝導加速空洞に対する高圧純水洗浄の効果	15
1.8 JAEA タンデムブースターを用いた低速度イオンビームの加速試験	17
1.9 放射性核種ビームのためのオンライン同位体分離用イオン源の開発	18
1.10 オフライン実験のためのイオン源の開発	20
1.11 重アクチノイド核種質量分離用イオン源の開発	22
2. 原子核構造	23
2.1 質量数 30 領域の原子核の高スピン状態の研究	25
2.2 ⁹² Zr 高スピン状態の寿命測定	27
2.3 核スピン偏極した二重魔法数 ¹³² Sn 近傍核のβ遅発粒子測定による核分光	28
2.4 ¹³⁴ Xe のクーロン励起実験	30
2.5 中性子過剰核 ¹⁶⁶ Eu の半減期と ¹⁶⁶ Gd の励起準位	32
2.6 奇々核 ¹⁷⁴ Re の高スピン状態	34
2.7 酸素 18 ビームを用いた核子移行反応による中性子過剰 Ta 同位体の核分光	36
2.8 レーザーアブレーション共鳴分光のための長半減期核種 ^{168m} Re の生成	37
2.9 遷移領域核 ¹⁸⁷ Pt のバンドの性質	38
2.10 中性子過剰核 ²³⁶ Th、 ²⁴² U のγ線遷移	40
2.11 ²⁵⁵ No のα線微細構造測定	42
3. 原子核反応	45
3.1 ⁸ Li (d, t) ⁷ Li 天体核反応率の直接測定	47
3.2 ⁶³ Ni 励起状態の分光学的因子及びスピン・パリティの測定	49
3.3 ⁶⁴ Ni + ¹¹⁸ Sn の後方準弾性散乱の測定	51
3.4 ⁷⁶ Ge + ²⁰⁸ Pb、 ²⁰⁹ Bi 反応における後方準弾性散乱	53
3.5 ³⁴ S + ²³⁸ U 反応の核分裂断面積の測定	54
3.6 ¹⁸ O + ²⁴⁴ Pu 反応におけるα放出と核分裂の相関	56
4. 核化学	59
4.1 HCl 溶液におけるラザホージウムの TOP0 逆相クロマトグラフィー	61
4.2 重元素に向けた電気化学装置の開発	63
4.3 HF/HNO ₃ 溶液中での陰イオン交換クロマトグラフィーにおける Nb と Ta の溶離曲線	65
4.4 超アクチノイド元素化学のための RI トレーサー製造	67
4.5 核反跳を利用したフラーレンへの放射性同位体の導入	68

5.	原子核理論	71
5.1	sd-pf 殻のエキゾチック核におけるテンソル力の重要性	73
5.2	原子核のポテンシャルエネルギー計算の大変形状態の拡張	75
5.3	K 中間子原子核のバルクな性質	77
5.4	運動量空間におけるクーロン力と短距離力を含む p-p 散乱に対する位相のずれ	79
6.	原子物理及び固体物理	81
6.1	炭素薄膜通過 Ne イオンのリュドベリ状態からの放出電子スペクトル	83
6.2	短寿命核トレーサー ⁸ Li を用いた β -LiGa 中リチウム拡散係数測定	85
6.3	炭素薄膜通過後の硫黄イオンの電荷分布 (IV)	87
7.	材料の照射効果	89
7.1	高速重イオン照射したスピネル結晶中のイオントラック構造とイオン配列	91
7.2	CeO ₂ の微細構造変化に対するイオントラック蓄積と Xe イオン予注入効果	93
7.3	走査型 SQUID 顕微鏡改良のためのマイクロプローブ使用の試み	95
7.4	X線磁気円二色性測定による鉄ロジウム合金の照射誘起磁性変態の研究	97
7.5	高エネルギー重イオンによる窒化物及び酸化物の電子励起スパッタリング	99
7.6	高エネルギー重イオン照射した CeO ₂ における X 線回折の研究	101
7.7	単結晶 α -Al ₂ O ₃ における高エネルギー重イオン照射による構造変化	103
7.8	照射促進偏析を用いた FeCu 合金における硬さの改質	105
8.	雑誌及び国際会議等の刊行物、学会発表	107
8.1	加速器の運転状況及び開発	109
8.2	原子核構造	111
8.3	原子核反応	116
8.4	核化学	120
8.5	原子核理論	125
8.6	原子物理及び固体物理	131
8.7	材料の照射効果	132
9.	関連課室職員及び委員会	137
9.1	課室職員	139
9.2	委員会	143
10.	共同・協力研究及び施設供用リスト	145
10.1	共同・協力研究リスト	147
10.2	施設供用リスト	149

This is a blank page

CHAPTER 1

Accelerator Operation and Development

- 1.1 Operation and Usage of Tandem Accelerator and Booster
- 1.2 Design of the Power Supply for the Bending Magnet on the High Voltage Terminal of the JAEA-Tokai Tandem
- 1.3 Stable Production of Metal Ion Beam from ECR Ion Source and Application to Terminal Ion Source
- 1.4 Screening Test of Relays Used under Pressurized Sulfur Hexafluoride (SF₆)
- 1.5 Communication Fault in the Interlock System for the JAEA Tandem Accelerator Facility
- 1.6 Performance Test of Low β Superconducting Twin Quarter Wave Resonator
- 1.7 Effect of High Pressure Water Jet Rinsing to Superconducting Cavity
- 1.8 Acceleration Test of the Low-Speed Heavy Ion Beam by the JAEA-Tokai Tandem Booster
- 1.9 Ion Source Development of On-Line Isotope Separator for Radioactive Nuclear Beam
- 1.10 Ion Source Development for Off-Line Experiment
- 1.11 Development of a Thick Target for Ion Source of On-Line Mass Separation of Heavy Actinide Isotopes

This is a blank page

1.1 OPERATION AND USAGE OF TANDEM ACCELERATOR AND BOOSTER

M. SATAKA, S. TAKEUCHI, Y. TSUKIHASHI, K. HORIE, I.OHUCHI, S. HANASHIMA,
S. ABE, N. ISHIZAKI, H. TAYAMA, A. OSA, M. MATSUDA, Y. NAKANOYA,
H. KABUMOTO, M. NAKAMURA, K. KUTSUKAKE and Y. OTOKAWA

The tandem accelerator and booster have been operated for experiments over two periods, May 19 to September 21 and December 5 to March 29. The total operation time of the tandem accelerator was 201 days and 65 different beams were delivered for experiments during the operation time. The experimental proposals and usage of the beam times from May 19, 2006 to March 29, 2007 are summarized in Table 1. and Table 2, respectively.

Table 1. Experimental Proposals.

Research Proposals Accepted by the Program Advisory Committee:	
In-house Staff Proposals	4
Collaboration Proposals	35
Number of Experiment proposed	40
Number of Scientists participating in Research	
from out side	219
in-house	232
Number of Institutions presented	41

Table 2. Usage of Beam-times in Different Research Fields.

Research Fields	Beam time	Beam delibary
Nuclear Physics	83 days 41.3%	27 times
Nuclear Chemistry	29 18.4	13
Atomic and Solid State Physics	46 22.1	27
Radiation effects in Materials	23 11.4	17
Accelerator Development	20 10.0	18
Total	201 days	102 times

Distribution of the terminal voltage and ion species are listed in Table 3 and Table 4, respectively. The stable high voltage limit of the tandem accelerator was gradually increasing without aggressive conditioning, after the whole accelerator tubes were replaced in the beginning of FY 2003 by the new compressed geometry tubes which were cleaned by a

high-pressure water jet. A six days experiment was carried out with very stable beam at 18MeV.

Table 3. Distribution of Terminal Voltages.

17-18	MV	6	days	2.9	%
16-17		10		4.9	
15-16		72		35.1	
14-15		50		24.4	
13-14		18		8.8	
12-13		14		6.8	
11-12		4		2.0	
10-11		5		2.4	
9-10		11		5.4	
8-9		9		4.4	
7-8		4		2.0	
6-7		2		1.0	
5-6		-			

With respect to the ion beams, the accelerator has provided a total 26 different kinds of ion species for research. Most of the beams were extracted from SNICS-2 sputter sources, which produce negative charged ions, injected into the tandem accelerator. The hydrogen beam and multiply charged ion beams of nitrogen, oxygen and rare gases were accelerated from the on-terminal ECR ion source, which were used about 25% of all the beam time. In this fiscal year, the on-terminal 14GHz ECR ion injector was prepared. This will be replaced of 10GHz ECR within next fiscal year.

The $^{16,18}\text{O}$ beams stood out most in popularity commanding over 15% of the beam time. They were mostly used for nuclear chemistry on actinides. The ^{136}Xe beams were used for research of radiation effects. The ^1H , $^6,7\text{Li}$ beams contributed to generating radioactive ion beams for Tokai Radioactive Ion Accelerator Complex (TRIAC).

The super-conducting booster was operated for a total of 27 days to boost the energies of 7 different beams from the tandem accelerator. The booster also played a role of the beam transport line to the booster experiment hall for total 18 days. There was no big trouble in FY 2006 as before. Forty super-conducting resonators were in good condition to run, although the average acceleration field gradients decreased to 4MV/m. The niobium surfaces were cleaned for resonators with a high-pressure water jet-spray to recover the original field gradient. The

details are described elsewhere in this report. All the boosted beams were used for nuclear physics and it means that 33% of the beam time for nuclear physics needed an energy boost.

Table 4. Distribution of Beam Species accelerated for Experiment.

^1H	28 days	^{31}P	1 days
$^{6,7}\text{Li}$	28	$^{32,34}\text{S}$	13
^{11}B	2	^{40}Ar	5
$^{12,13}\text{C}$	7	$^{58,64}\text{Ni}$	13
^{14}N	8	^{76}Ge	4
$^{16,18}\text{O}$	32	^{86}Kr	3
^{19}F	9	^{100}Mo	1
^{22}Ne	5	$^{134,136}\text{Xe}$	24
^{27}Al	3	^{197}Au	6
$^{28,30}\text{Si}$	4		

Table 5. Boosted Ion Beams for Experiment.

^{18}O	180 MeV	4 days
^{40}Ar	157-181	2
^{64}Ni	215-290	9
^{76}Ge	333-390	4
^{86}Kr	280	3
^{100}Mo	360	2
^{134}Xe	410	3

The TRIAC facility, which has been installed in the tandem accelerator facility in collaboration with KEK, have experimental proposals with use of radioactive beams. The accelerator provided ion beams for 46 days to the TRIAC for experimental and development use. Some experiments with ^8Li beam and ^{126}In were successfully carried out. The ion source development for TRIAC and the details of experiments using radioactive ion beams are described elsewhere in this report.

1.2 DESIGN OF THE POWER SUPPLY FOR THE BENDING MAGNET ON THE HIGH VOLTAGE TERMINAL OF THE JAEA-TOKAI TANDEM

S. HANASHIMA

In this fiscal year, we carried forward design work of the new power supply for the 180° bending magnet on the high voltage terminal of the tandem. The magnet is named as BM TL-1. On the terminal, electric power is precious, so we are designing the supply as switch mode power supply (SMPS) with power factor correction to improve the efficiency. It also needs special care for cooling, because the supply works in the atmosphere of up to 0.6 MPa of SF₆. Improvement of the efficiency will reduce burden for cooling. The new supply consists of a control module and 4 power modules working parallel. The final output power is 200A @32V. The primary power is 400Hz 3-phase 200V.

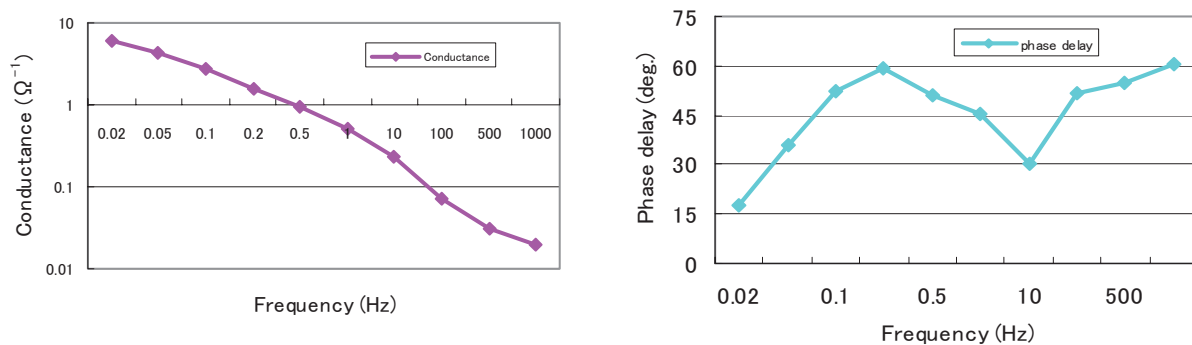


Fig. 1. Conductance (left) and phase delay (right) vs frequency, for the bending magnet.

Measurement of the conductance of BM TL-1 was made for the design. DC resistance of the coil was known as about 0.16 Ω. But the AC impedance or the conductance were not known. It is more difficult to reduce output ripple or output error on the SMPS than on a supply with series regulation technique. The conductance of the magnet coil means the ratio between the current ripple and the voltage ripple. So it is used for setting the allowance of the voltage ripple for the power supply. It is also useful for designing feedback loop. The measurement was made from 0.02Hz to 100kHz. Figure1 shows the results of 0.02Hz to 1kHz. The magnet yoke of BM TL-1 is made of iron block, so the eddy current loss increases in a higher frequency region. For example, conductance is about 0.03 Ω⁻¹ at 400Hz. If current ripple of 2mA_{p-p} is allowed at the frequency, voltage ripple of 2mA/0.03 Ω⁻¹ ≐ 67mV p-p is allowed. At 0.1Hz, the conductance is about 100 times greater than at 400Hz. Thus, the ripple voltage must be limited less than about 0.7mV_{p-p} for the same current ripple criteria at the frequency.

1.3 STABLE PRODUCTION OF METAL ION BEAM FROM ECR ION SOURCE AND APPLICATION TO TERMINAL ION SOURCE

T. NAKANOYA and M. MATSUDA

An electron cyclotron resonance (ECR) ion source with permanent magnets has been installed in the high voltage terminal as a terminal ion source (TIS) [1]. The TIS produces intensive positive ion beams from gaseous atoms and molecules. We are developing metal ion beams from the ECR ion source which can be use in high voltage terminal.

We have already produced 17 kinds of metal ion beams with oven method at a test bench. Considering the operating period of accelerator, a metal ion beam by oven method is required to have stability and long life time. We tested long time stability of ion beam by Zn sample. This result is shown in Fig.1. A Zn ion beam could produce relatively stable for over 50 h without any handling. The consumption of Zn sample was only 20 % at this test. More stable operation is expected if radio-frequency (RF) is tuned and temperature of oven is adjusted. It would be possible to use the sample about 10 days if RF input and oven temperature are automatically stabilized.

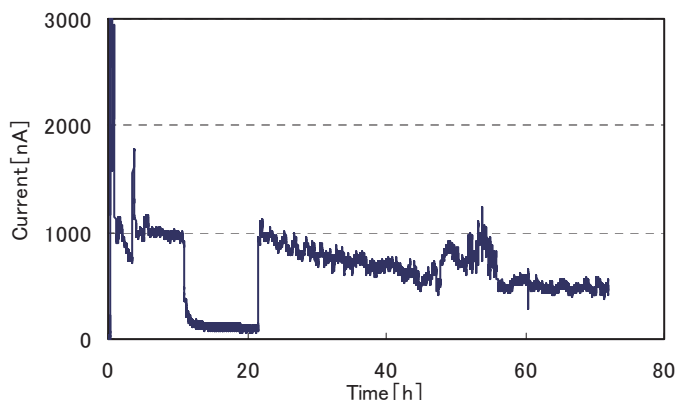


Fig.1. Beam current change of Zn^{6+} as a function of extraction time. Oven power 0.8W; RF power 20W. The sudden decrease during the time of 10 to 22 hour is caused by out of matching of RF resonance .

We have designed a new oven assembly for the TIS as shown in Fig.2. The size of each part is shown in Tab.1. The basic structure of the oven head was the same shape as reported in ref [2]. But the parts outside of vacuum are modified for in-tank use. The tank of tandem accelerator is filled with SF_6 gas of 0.45 MPa. On the other hand, the pressure of plasma chamber is less than 10^{-5} Pa. So the oven is required to stand such a large pressure difference. Moreover the space for oven is very limited, because the high voltage terminal shell where the new TIS to be mounted is very narrow and congested with many equipment. It must be secure of 250 mm back stroke space for replacing oven assembly. For withstanding the pressure difference, we exclude o-rings as much as possible, compared to the test bench model. An oven rod and a shield tube are connected by metallic seal. A shield tube and insulation tube are connected by same way. These parts compose a threefold tube structure. The rear part of RF cube consists of metal and alumina insulator only. The isolation valve between plasma chamber and oven was removed for shorting the full length. The shield tube has two functions. One is plasma shielding, and the other is heat shielding. At ECR zone in the plasma chamber, bare oven head is damaged by plasma sputtering. The shield tube can reduce the damage of the oven head. The oven head can be heated up to 1500°C for producing metal ion beams. Thermal radiation might have harmful influence on permanent magnet system. In this case, the shield tube

works as a heat shield to prevent direct thermal radiation. For this reason, a part of shield tube was exposed to SF₆ gas atmosphere and equipped with radiator fins for cooling. We aim to use this oven near future.

Table 1. Dimensions of the oven assembly.

Plasma chamber	Inner diameter	25 mm
Oven rod	Diameter	8 mm
	Length	450 mm
Shield tube	Diameter	12 mm
	Length	390 mm
Insulation tube	Diameter	18 mm
	Length	50 mm

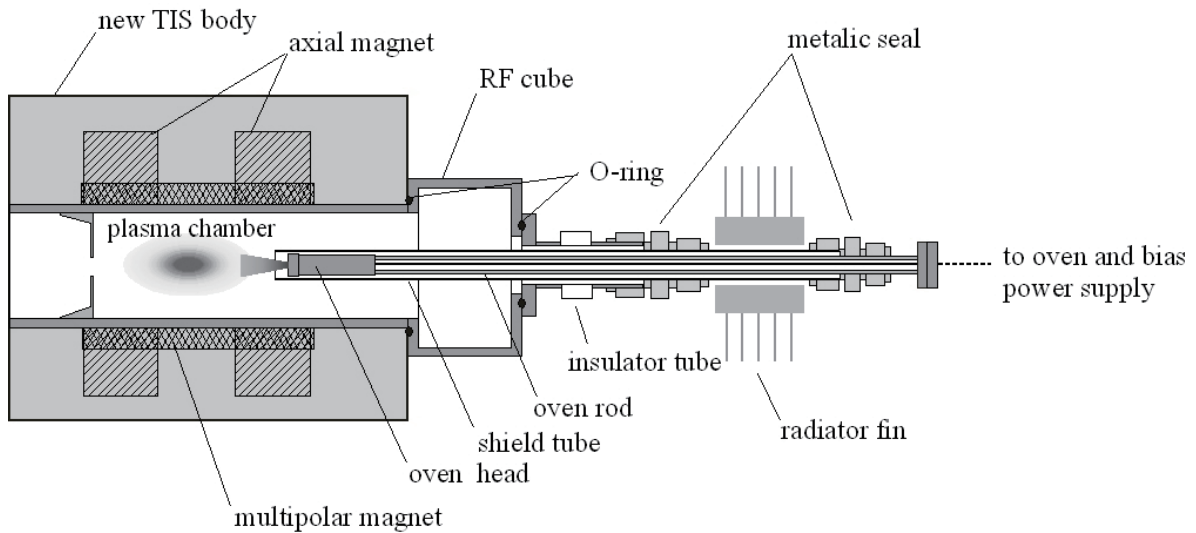


Fig. 2. Schematic view of the new TIS and the oven assembly.

References

- [1] M. Matsuda, C. Kobayashi and S. Takeuchi, Proc. of 14th Int. Workshop on ECR sources. CERN, Geneva, Switzerland, 3-6 May. 1999.
- [2] T. Nakanoya and M. Matsuda, JAEA-Review 2005-004 (2005)12.

1.4 SCREENING TEST OF RELAYS USED UNDER PRESSURIZED SULFUR HEXAFLUORIDE (SF₆)

K. KUTSUKAKE, M. MATSUDA, S. HANASHIMA and K. OBARA¹

Many measurement and control devices are installed inside of a high voltage terminal of the JAEA-Tokai tandem accelerator and operated under pressurized sulfur hexafluoride (SF₆) of 0.5MPa [1]. A screening test has been carried out by turning on and off a power supply of a dummy load, to select a relay usable under the pressurized SF₆ from relays which work under the normal atmospheric condition (standard specification, not a hermetic type).

Three kinds of relays were tested: electromechanical relay (EMR), magnet contactor (MAG) and hybrid relay (HYB). Each relay was set up in a test chamber of the SF₆ of 0.5MPa, and connected to a resistance load rated three-phase current of 200V/3A. Then contacts of the relay were repeatedly opened and closed at a fixed periodic time. Temperature of the relay, voltage, electric current and a change of appearance of the relay before and after the test were measured and observed. Major specifications of the relays tested on the screening test are shown in Table 1, and the HYB before set up in the test chamber is shown in Fig. 1.

Table 1. Specifications of the relays tested on the screening test.

		EMR	MAG	HYB
Durability ¹⁾	Mechanically	5×10^7 ²⁾	1×10^6 ³⁾	1×10^7 ²⁾
	Electrically	2×10^5 ³⁾	1×10^7 ³⁾	1×10^7 ³⁾
Allowable temperature (°C)		-25~40	-10~+55	-25~+60
Number of contacts		3	3	1
Dimensions (mm) & weight (g)		27×30×35H, 50	50×50×70H, 200	27×20×35H, 25

¹⁾ Total number of open & close of contact. ²⁾ Periodic time: 0.2 sec. ³⁾ Periodic time: 2 sec.

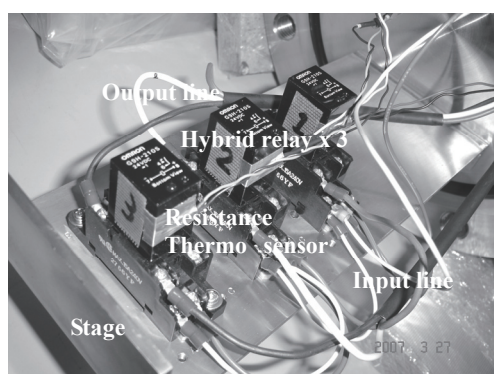


Fig. 1. Three Hybrid relays before set up in the test chamber.

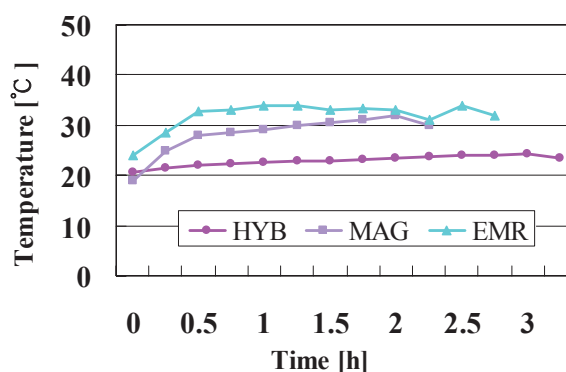


Fig. 2. Temperature changes of the relays during the test in the pressurized SF₆ of 0.5MPa.

¹ Nippon Advanced Technology Co. Ltd

The temperature changes during repetition opening and closing of the relays are shown in Fig. 2. As for periodic time, the EMR was tested at 1cycle/1sec, while the MAG and the HYB were tested at 1cycle/1.62sec. The contacts of the EMR and the MAG showed irregular contact after several minutes of the test. By this time, input voltage and electric current to an operational coil of the relay was feed normally. The highest temperature of the EMR and the MAG showed about 35 °C and 32 °C, respectively, but these temperatures did not reach an allowable temperature limit. Concerning the visual inspection of the EMR and the MAG after the test, melting and dark-gray products were observed around the contacts. It is estimated that the dark-gray products are sulfide or fluoride, and these compounds are formed by chemical reaction between metals and sulfur or hydrogen fluoride due to dissociation of SF₆ in electric arcs [2]. In addition, a contact resistance of the MAG increased up to several 100kΩ due to the sticking compounds that seemed to be silver sulfide.

On the other hand, for the HYB, there were not any troubles including melting and generation of dust. The HYB is basically composed of an electromechanical relay and a solid state relay. The sequence of the mechanism, at the beginning of turning on and off the power supply, the electric current flows through a semiconductor relay (triode AC switch, TRIAC), then the current flows through an electromechanical relay at steady state. Therefore the arcs can be avoided in the HYB, in addition, a temperature rising becomes low. As a result, the performance of the HYB is better than the EMR and the MAG, and it is available in the pressurized SF₆ of 0.5MPa in spite of the standard specification.

In the future, we are planning the test of solid state relays (SSR) as a next step. The generation of heat is a problem in the SSR, but the electric arcs are not generated; therefore an application of the SSR is expected as good as the HYB.

References

- [1] Tandem Accelerator & Tandem Booster, Pamphlet by Tandem Accelerator Section, Nuclear Science Research Institute, JAEA (1997).
- [2] SF₆ Technical Reference, Honeywell Industrial Fluorines (2000).

1.5 COMMUNICATION FAULT IN THE INTERLOCK SYSTEM FOR THE JAEA TANDEM ACCELERATOR FACILITY

M. NAKAMURA and S. HANASHIMA

We developed a new interlock system for the JAEA tandem accelerator facility. The central controller module communicates with other modules (entrance monitor x7, switch control x4, LED driver x3, announcement x1) connected each other in a serial bus (RS-485@250kbps) [1]. These modules are controlled by Peripheral Interface Controllers (PICs, Microchip Technology Inc.) programmed in an assembly language.

We found that a communication fault occurred in the system and it caused the system halt at intervals of several hours. As a result of our investigation, we understood the halt was caused by the complex problems of hardware and software. We observed communication signals between the central controller and other modules with a logic-analyzer and an oscilloscope in parallel with debugging the program of the system. The following shows their details.

Signals measured with the logic analyzer were entangled when the system halted. (The process of transmitting or receiving signals is handled alternately when the system operates normally.) We observed with the oscilloscope that a base of received signals was dropping gradually along the number of modules to about 2 V. The appearance of the dropping signals is shown in Fig.1 A.

A differential signaling is used in the communication system. But we thought that the unintended drop of over 2 V might cause the communication fault. We observed signals at a transmit port of entrance monitors to investigate the cause of the drop. Then we found that the drop disappeared when a grounding terminal of the oscilloscope was connected to the module's one. And we found that the observed grounding impedance was high, and the drop decreased when another grounding wire was added to a communication path. So we thought that the drop was caused by the rising of a grounding potential. The modules except for entrance monitors were not affected because they were installed near to a grounding system of the central controller.

In adding another grounding wire to a signal line of the system to decrease the grounding potential, we found a short circuit between a +5 V power source and the signal line in the entrance monitor #4. A short circuit current observed with a DC clamp on current probe was about 0.1 A from the power source to the signal line. The drop disappeared when the power of

this module was shut off. Unfortunately, the short circuit recovered when we were investigating it in more detail by opening the chassis of this module. But we found a small damage on the cable had possibilities of the cause. We confirmed that the system works normally after we had taken measures to those problems. Signals refined are shown in Fig.1 B.

The program had bugs which halted the interlock system from a lack of the waiting time at the communication fault. We modified it to 1.0 ms for the system to recover even if the central controller received an invalid data momentarily. And we modified the program of entrance monitors to display an error message if the system halted.

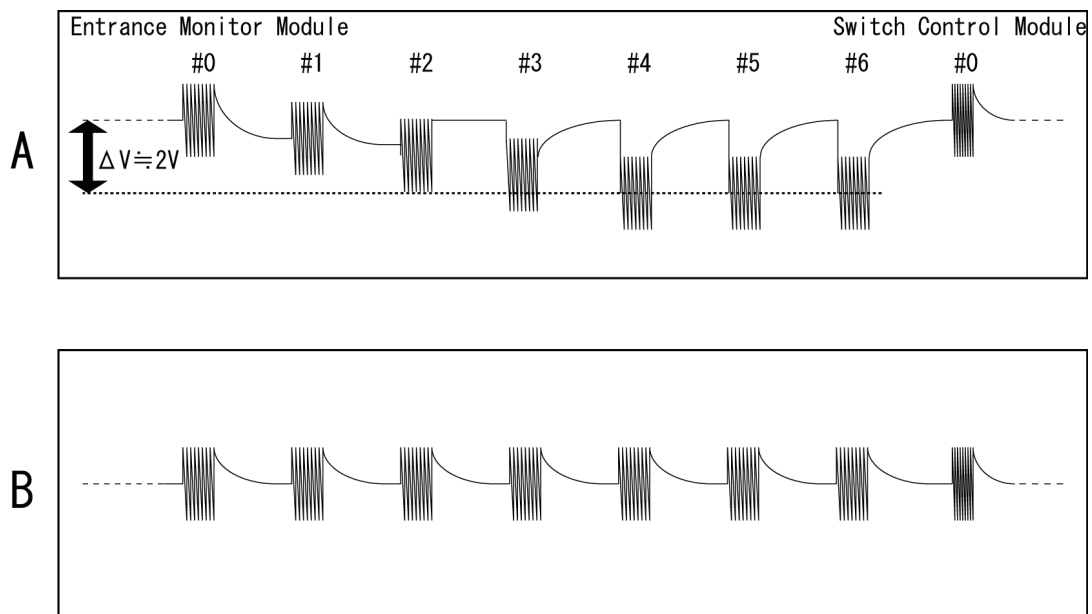


Fig.1 (Sketched) typical received signals of the central controller.

‘A’ shows the dropping signals and ‘B’ shows the normal one after refinement.

Reference

- [1] S. HANASHIMA et al, JAEA-Tokai Tandem Annu. Rep. 2005, JAEA-Review 2006-029 (2006) 16.

1.6 PERFORMANCE TEST OF LOW BETA SUPERCONDUCTING TWIN QUARTER WAVE RESONATOR

H. KABUMOTO, S. TAKEUCHI and Y. OTOKAWA

We have started development of low beta superconducting twin quarter wave resonator (twin-QWR) in FY2004, and have fabricated a prototype twin-QWR in FY2005. We have carried out performance test of this twin-QWR in FY2006.

Figure 1 shows a cutaway drawing of the twin-QWR. The top end plate and outer conductor are connected by superconducting gasket made of niobium. We could not carry out electro-polishing (EP) for rim of outer conductor. Instead of EP, we carried out chemical-polishing (CP) for this area. After final assembling and high pressure water jet rinsing, we carried out off-line performance test of twin-QWR.

Figure 2 shows the result of off-line performance tests. In the first test, the temperature rising was observed around niobium gasket, and the quality factor (Q_0) was 8×10^7 at 4.2K at low electric field, the acceleration electric field (E_{acc}) was 2.0MV/m at RF power input of 4.0W. We thought that the connection between top end plate and outer conductor was insufficient, and we tightened up the connection screws to press the niobium gasket (estimated to $4 \sim 5 \times 10^5$ N). The performance was improved to $Q_0 = 2 \times 10^8$, $E_{acc} = 2.8$ MV/m at 4.0W.

It is thought that the frequency stability of twin-QWR is worse than QWR. Because twin-QWR has two inner conductors that are narrow and low mechanical strength. This frequency instability happens because of the deformation of the top board by the helium pressure. Twin-QWR has support screws at root of inner conductors to prevent this deformation. Figure 3 shows the frequency shift due to the helium pressure. The frequency shift was about 1.23 kHz/(kgf/cm²), and it was about 4 times as large as QWR's 0.27 kHz/(kgf/cm²).

We are planning to carry out performance test again after changing niobium gasket in FY 2007.

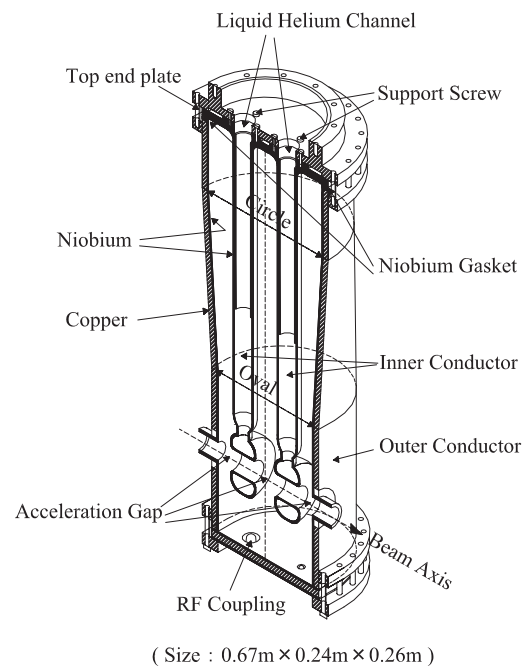


Fig.1. Cutaway drawing of twin-QWR.

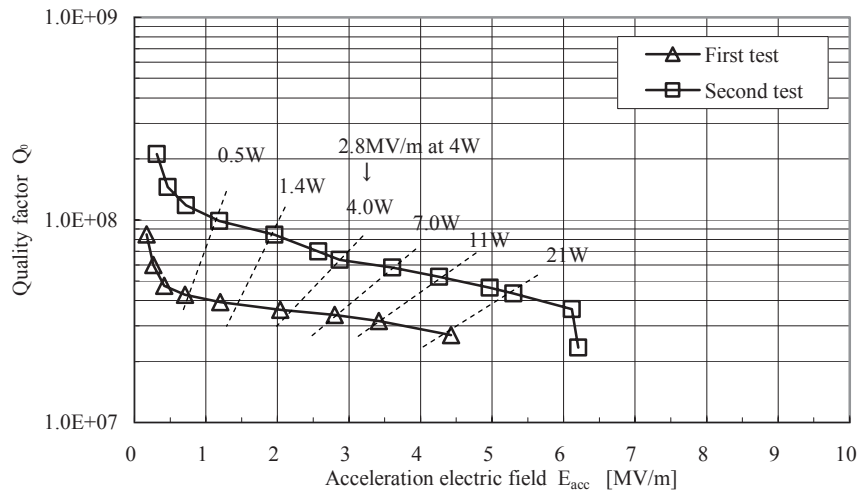


Fig.2. Resonator Q_0 -values at 4.2K in off-line tests.

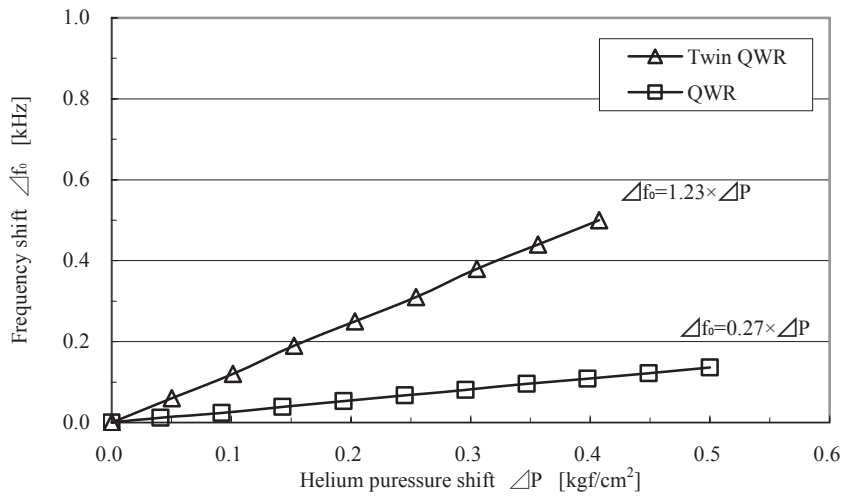


Fig.3. Frequency shift due to the helium pressure.

References

- [1] H. Kabumoto et al., JAEA –Tokai Tandem Annu.Rep.2005, JAEA-Review 2006-029 (2006) 12.
- [2] H. Kabumoto et al., JAERI Tandem Annu.Rep.2003, JAERI-Review 2004-027 (2004) 13.

1.7 EFFECT OF HIGH PRESSURE WATER JET RINSING TO SUPERCONDUCTING CAVITY

H. KABUMOTO, S. TAKEUCHI, N. ISHIZAKI, A. IJIMA¹, T. YOSHIDA¹,
T. USAMI¹, T. ISHIGURO¹ and K. YAMAGUCHI¹

Superconducting booster was built in 1994, and the operations of 20~40days were offered every year. When it was built, the acceleration electric field (E_{acc}) of superconducting cavity was 5.0MV/m on the average. The performance decrease little by little, and it become 4.0MV/m now. Some of the cavities generate X-ray from low acceleration electric field. It is thought that field emission is occurred by small contamination accumulated on the surface of niobium. We decide to examine the high pressure water jet rinsing (HPWR).

High pressure water jet rinsing is a well known method to remove contamination of superconducting cavity recently. Figure 1 shows the picture of HPWR. Ultra pure water of $18M\Omega \cdot cm$ is generated by ion exchange filter for 6 liters per minute. Water is pressurized to 6~8MPa by mechanical compressor, and sprayed on surface of the niobium. We have constructed the HPWR system in FY2005.

We carried out washing test to 4 cavities (on-line L37~L40). Figure 2 shows the effect of HPWR to on-line L40 cavity. Before HPWR, X-ray was generated from 3.0MV/m, and E_{acc} was 3.6MV/m at RF power input of 4.0W. After HPWR, X-ray was not generated even at high acceleration electric field, and E_{acc} was improved to 6.5MV/m. Table 1 shows the result of HPWR to on-line L37~L40 cavities. Acceleration electric fields were improved in all cavities, and the average of E_{acc} were improved from 4.3MV/m to 5.9MV/m at 4.0W. It was confirmed that the performance of superconducting cavity were improved by HPWR. We are planning to carry out HPWR for other on-line cavities in FY2007.

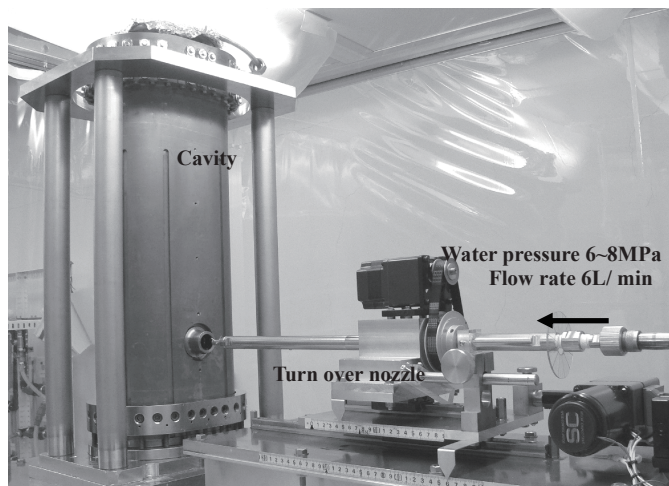


Fig.1. Picture of HPWR.

¹ ATOX CO., LTD.

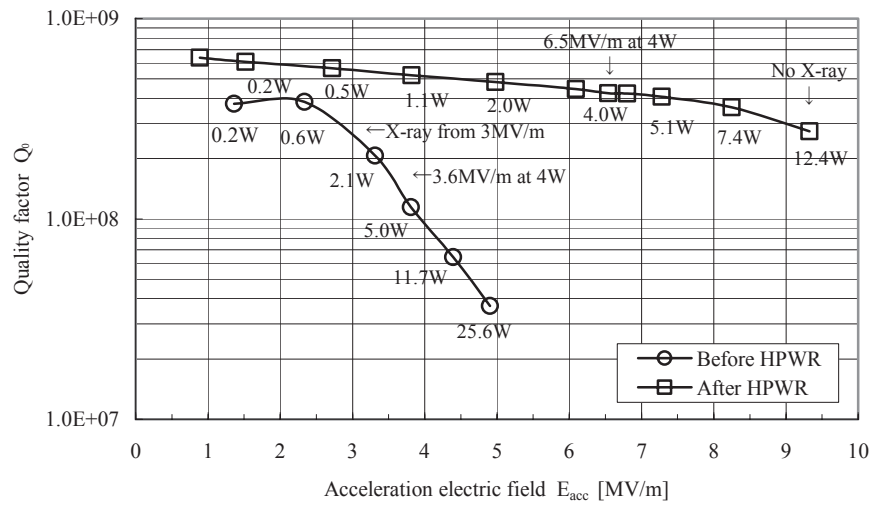


Fig.2. Effect of high pressure water jet rinsing to on-line L40 cavity.

Tab.1. Change of E_{acc} gain at input RF power of 4.0W before and after the HPWR.

Cavity No.	Before HPWR	After HPWR	Gain ΔE_{acc} [MV/m]
	E_{acc} [MV/m]	E_{acc} [MV/m]	
L37	4.7	5.3	+0.6
L38	3.5	5.9	+2.4
L39	5.4	6.0	+0.6
L40	3.6	6.5	+2.9
Average	4.3	5.9	+1.6

1.8 ACCELERATION TEST OF THE LOW-SPEED HEAVY ION BEAM BY THE JAEA-TOKAI TANDEM BOOSTER

M. MATSUDA

The Tokai Radioactive Ion Accelerator Complex (TRIAC) was installed at the JAEA Tandem Accelerator facility as a joint project of the JAEA-Tokai and the KEK-IPNS. The low energy Radioactive Nuclear Beam (RNB) having its energy up to 1.1MeV/u are utilized for various scientific projects [1]. In future, we are going to connect TRIAC to the existing JAEA Super Conducting (SC) booster in order to accelerate the energy up to 5~8MeV/u. The SC booster is an independently phased linac composed of 46 super conducting quarter wave resonators of an optimum velocity of $\beta=10\%$. However, the acceleration efficiency of the beam of 1.1MeV/u from TRIAC is only 10%. For the SC booster to accelerate efficiently, the pre-booster which accelerates ion beams up to 2MeV/u ($\beta=6.5\%$) is necessary. On the other hand, it was shown by the test calculation[2] that the exit energy of the TRIAC could be accelerated up to 1.4MeV/u by the modified acceleration mode. The possibility of the early realization of the future plan without the pre-booster was shown. The acceleration test of such low-speed beams were actually done with the SC booster.

The incident beam to the SC booster was $^{40}\text{Ar}^{10+}$ which charge exchanged from $^{40}\text{Ar}^{4+}$ with energy 1.3MeV/u and 1.4MeV/u by using post stripper foil from the in-terminal ion source of the tandem accelerator. The setting of the synchronous phase of each resonator was done in usual operating method which applied the bunch beam phase detector [3]. The average electric field of the resonator was 2.7 MV/m and a synchronous phase was set to -30 degrees. Each result of acceleration tests were shown in table 1 and table 2. The transmission efficiency is normalized at the beam current of faraday cup at the booster entrance (B1-1).

Table 1. $^{40}\text{Ar}^{10+}$ (A/q=4), $E_{\text{in}}/A=1.3\text{MeV/u}$ ($\beta=5.28\%$) $\Rightarrow E_{\text{out}}/A=3.9\text{MeV/u}$

FC position	04-1 tandem exit	B1-1 Booster entrance	B1-2 middle	B3-1 end	B3-2 After debuncher	B4-1 After booster analyzing magnet
Current [nAe]	14	11	11	2.4	2.1	1.9
Transimission			100%	22%	19%	17%

Table 2. $^{40}\text{Ar}^{10+}$ (A/q=4), $E_{\text{in}}/A=1.4\text{MeV/u}$ ($\beta=5.48\%$) $\Rightarrow E_{\text{out}}/A=4.5\text{MeV/u}$

FC position	04-1	B1-1	B1-2	B3-1	B3-2	B4-1
Current [nAe]	34	27	24	2.8	2.7	2.6
Transimission			89%	10%	10%	10%

As a result of the acceleration test, either of the booster exit energy agree with the calculated value approximately and it succeeded in the acceleration in usual way. However, the beam transmission efficiency was worse than about 50 % of usual high-speed ion beams ($\beta>7\%$). A lot of beams were lost in main acceleration part of booster. By the optimization of the beam transportation system, we think transmission efficiency to be improved. Also, the difference of emittance of the beam from the tandem and from TRIAC must be considered.

References

- [1] H. Miyatake et al. , Nucl. Instrum. Methods B204 (2003) 746.
- [2] S. Arai , private communication.
- [3] S. Takeuchi et al. , Nucl. Instrum. Methods A382 (1996) 153.

1.9 ION SOURCE DEVELOPMENT OF ON-LINE ISOTOPE SEPARATOR FOR RADIOACTIVE NUCLEAR BEAM

A. OSA, M. MATSUDA, Y. OTOHKAWA, S. ICHIKAWA,
T.K. SATO and S.C. JEONG¹

According to the JAEA-KEK joint radioactive nuclear beam (RNB) project, we have developed integrated-target-ion source systems to produced heavy neutron-rich RNBs with particle-induced fission of ^{238}U [1]. In order to evaluate the release performance of the integrated-target-ion source system, release time of mass-separated fission products were measured.

A graphite fiber based uranium carbide target was bombarded with a 32-MeV proton beam (25 MeV on target) with intensity of about 60 nA. For the release time measurements of fission products, the mass separated products were collected on an aluminized Mylar tape in a tape transport system and were periodically transported to a measuring position where an HPGe detector was placed for γ -ray measurements.

A faraday cup located in a connection beam line upstream from the ion source is held in the “out” position, that means proton beam irradiate the target and the reaction products are generated and saturated in the ion source. After that, the faraday cup is held in the “in” position. Proton beam no longer irradiate the target and the direct generation of radioactive isotopes inside the target is stopped. The atoms present in the target continue to be released and radioactive ions continue to be collected on the tape. In a cycle, collection, tape transport and measurement is repeated 16 times at typical intervals of 3 seconds. 4k channels γ -ray spectra of each interval are stored in 64k channels memory divided by 16 blocks. Storing block is switched at the same time as the collected radioactive source is transported to the measuring position. The whole measurement cycle can be repeated in order to increase the statistics.

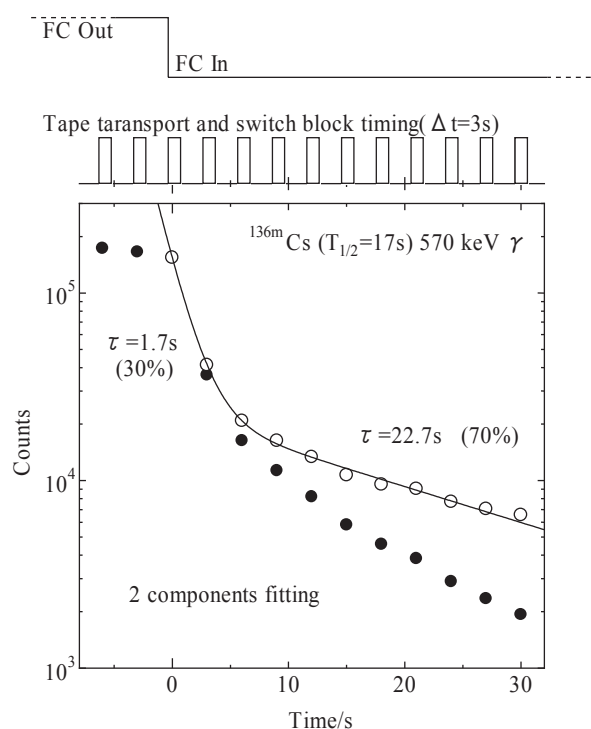


Fig.1. Release time distribution of $^{136\text{m}}\text{Cs}$ and time-sequence diagram.

¹ High Energy Accelerator Research Organization

Table 1. Release times and fractional rates deduced from the one and/or two exponential fit to the release data.

Isotope	Ion source	half-life/s	Release time/s	Fractional rate	Literature
⁹⁴ Rb	SIS	2.072	τ_1 : 1.1 τ_2 : 10.7	84% 16%	3.2 s ^[2] , 8.2 s ^[3] , 0.8 s ^[4]
^{136m} Cs	SIS	17	τ_1 : 1.7 τ_2 : 22.7	30% 70%	2.5 s ^[2] , 21.6 s ^[3]
¹⁴⁵ Ba	SIS	4.3	τ_1 : 9	100%	10.3 s ^[2] , 107 s ^[3]
¹⁶⁰ Eu	SIS	38	τ_1 : 12	100%	
⁹¹ Kr	FEBIAD	5.98	τ_1 : 3.1 τ_2 : 46.9	21% 79%	2.2 s ^[2] , 3.5 s ^[3]
^{123g} In	FEBIAD	39.68	τ_1 : 7	100%	2.5 s ^[2] , 8.7 s ^[5]
	SIS		τ_1 : 1.7@2250°C	100%	6.2 s, 2.3 s, 1.6 s ^[3]
¹³⁹ Xe	FEBIAD	8.57	τ_1 : 12 τ_2 : very long		32 s ^[2] , 11.7 s ^[3]

The fission products are delayed-released from the target-ion-source system. For example, release time distribution of Cs from the ion source and time-sequence diagram are shown in Fig.1. Filled and open circle presents γ -ray raw count (N) and nuclear decay corrected one (N') for the data after $t=0$, respectively. Time dependences of the corrected count are fitted by following equation: $N'(t) = \sum_{i=1,2} A_i \exp(-\lambda_i t)$. The release time, $\tau_i = 1/\lambda_i$, for several elements, ionized with a surface ionization ion source(SIS) and/or a Forced Electron Beam Induced Arc-Discharge (FEBIAD) type ion source, are shown in Table 1.

In this study, suppression of the separation yield for short-lived isotopes, which half-lives are less than the release time for the element, was observed. It caused decay loss in the target-ion-source system. It should speed up release time, which depends on the temperature of the target-ion-source system and base material of target. We are constructing a high temperature FEBIAD type ion source for separation of short-lived In isotopes. As a base material, graphite disk which is molded graphite powder in low pressure make a good performance. Change of base material of the target is under studying.

References

- [1] A. Osa, Nucl. Instrum. Methods B 261 (2007) 1048-1052.
- [2] B. Fogelberg, M. Hellström, L. Jacobsson, D. Jerrestam, L. Spanier and G. Rudstam, Nucl. Instrum. Methods B70 (1992) 137.
- [3] A.H.M. Evensen et al., Nucl Instrum Methods B126 (1997) 160.
- [4] P.L. Reeder, R.A. Warner, G.P. Ford, H. Willmes, Phys. Rev. C 32 (1985) 1327.
- [5] A. Andrighetto et al., Nucl Instrum Methods B204 (2003) 267.

1.10 ION SOURCE DEVELOPMENT FOR OFF-LINE EXPERIMENT

A. OSA, Y. OTOHKAWA, S. ICHIKAWA, T.K. SATO and SC.JEONG¹⁾

We have modified a surface ionization ion source (SIS) to provide stable ion beam for development test of the CB-ECRIS[1]. In order to evaluate the performance of the modified SIS (SIS-III), operating method dependence of beam intensity with same input power was measured.

The original plan of this modification was to improve ionization performances of surface ionization type target-integrated-ion source system (SIS-II). In a general way, the mechanism to generate ions in SIS is surface ionization (surface ionization (SI) mode). To enhance the ionizing power, we added an electron impact mechanism (electron impact (EI) mode) in the SIS-III. Schematic view of the SIS-III is shown in Fig. 1.

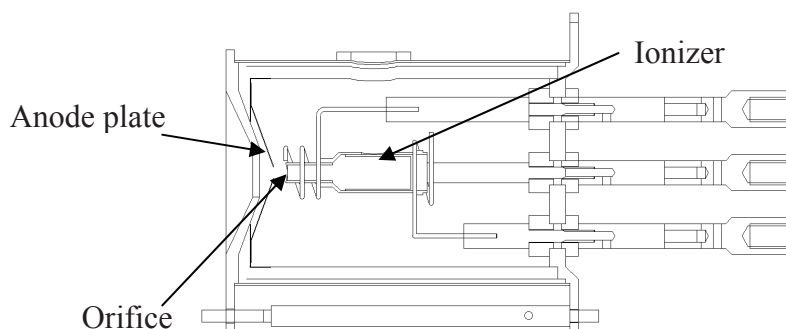


Fig. 1. Schematic view of the SIS-III.

We put an anode plate in front of the orifice of the ionizer. Several hundred volts are applied between the plate and the ionizer so that thermal electrons impact atoms vaporized from the ionizer orifice. In the off-line test, BaO powder is fed to the ionizer as a seed of Ba vapor. We compared the beam intensity in the EI mode with the one in the SI mode.

Table 1. Observed ion species measured in off-line test of SIS-III.

	Ionization energy/eV	EI mode	SI mode
Ba ⁺	5.212	950 nA	200 nA
Ba ²⁺	10.00	300 nA	6.8 nA
N ₂ ⁺	15.58	160 nA	unseen
Operation parameter			
Electron bombardment		395V/0.26A	450V/0.21A
Filament-1		4.6V/35A	4V/36.8A
Filament-2		7V/36.6A	7.3V/38.1A
Total input power		520W	520W

1) High Energy Accelerator Research Organization

We observed high yield Ba^+ ion beam in the EI mode operation though we input same total power. In addition, multiply-charged ion of Ba and nitrogen molecule ion, which are generally impossible to ionize with the SIS-II, were observed. In the EI mode operation, Ba^+ ion beam is simultaneously observed that electron impact current ($\sim 0.01A$) begins to pass, which is smaller than necessary input power for ionization of Ba in the SI mode. At the input power $\sim 500W$, the temperature of the ionizer achieves $1500^\circ C$. At this temperature, the vapor pressure of BaO is a few Pa. The difference of yields between the EI mode and the SI mode depends on the ionizing power of each mode.

When we provide enough intense ion beam (~ 100 nA) with the SI mode operation for development test of the CB-ECRIS, we have to control input power all of the time to keep intensity. In addition, the seed of Ba vapor have been exhausted in several hours. On the other hand, when we use the SIS-III with the EI mode operation, we can continuously provide beam in several day. Unfortunately, the performance of the SIS-III with the EI mode does not appear in the on-line experiment; it is worse than the SIS-II with the SI mode. In the on-line experiment, we have to heat the ionizer up to $2500^\circ C$ which is needed to evaporate reaction products from target. In addition, in the off-line test, high dense vapor is ejected from the ionizer orifice compared with the rarefied reaction products vapor in the on-line experiment. We considered that disappearance of the EI mode in the on-line experiment is caused by these differences of operating condition.

Reference

- [1] A. Osa, Nucl. Instrum. Methods B 261 (2007) 1048-1052.

1.11 DEVELOPMENT OF A THICK TARGET FOR ION SOURCE OF ON-LINE MASS SEPARATION OF HEAVY ACTINIDE ISOTOPES

T.K. SATO, A. OSA, K. TSUKADA, M. ASAI and S. ICHIKAWA

Isotope separation on-line (ISOL) with unambiguous mass identification and rapid separation is a powerful method for study of short-lived actinide isotopes. We developed a gas-jet coupled thermal ion source in the JAEA-ISOL [1]. With this system neutron-deficient Am, Cm and Bk isotopes were successfully mass-separated and their decay properties were studied. To extend this research program to the region of heavy actinide isotopes, we have developed a thick target ion-source technique.

Experiments were performed using a thermal ion-source [2] in the JAEA-ISOL connected with the tandem accelerator at JAEA, Tokai. Temperature dependence of ion beam intensities of ^{239}Am produced in the $^{238}\text{U}(^6\text{Li}, 5n)$ reaction was measured after mass-separation. A 25 mg/cm^2 thick ^{238}U target, impregnated with a graphite fiber ($\phi=100\ \mu\text{m}$, Tokai carbon, Co., Ltd.), was irradiated by a 45 MeV ^6Li beam with an intensity of about 100 particle-nA.

Figure 1 shows mass-separated ^{239}Am beam intensities as a function of the ion-source temperature. The calculated ionization efficiency is also shown in the figure. The separation efficiency of ^{239}Am was 0.8% and the beam intensity was 1.3×10^3 atoms/s at the ion-source temperature of 2600 K. The observed beam intensity is about 10 times higher than that expected with the gas-jet coupled thermal ion source system.

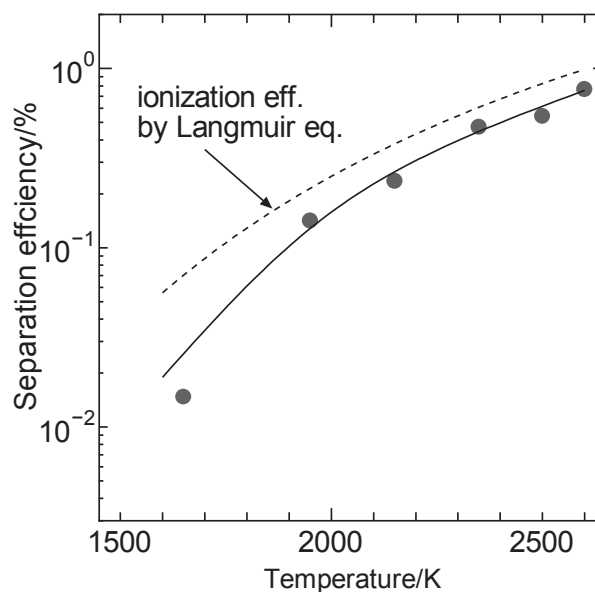


Fig. 1. Separation efficiency for ^{239}Am as a function of ionizer temperature. Dashed line shows a calculation using the Langmuir equation.

References

- [1] S. Ichikawa et al. Nucl. Inst. and Meth. B187 (2002) 548-554.
- [2] S. Ichikawa et al. Nucl. Inst. and Meth. A274 (1989) 259-264.

CHAPTER 2

Nuclear Structure

- 2.1 Study of High-Spin States in $A \approx 30$ Nuclei
- 2.2 Lifetime Measurement of High-Spin States in ^{92}Zr
- 2.3 Development of Spin-Polarized Radioactive Nuclear Beam for Nuclear Spectroscopy through β -Delayed Decay of Spin-Polarized Nuclei Around Doubly Magic Nucleus ^{132}Sn
- 2.4 Coulomb Excitation Experiment of ^{134}Xe
- 2.5 β Decay Half-Life of ^{166}Eu and Levels in ^{166}Gd
- 2.6 High-Spin States of Odd-Odd ^{174}Re Nucleus
- 2.7 Spectroscopy of Neutron-Rich Tantalum Isotopes Produced in ^{18}O -Induced Transfer Reactions
- 2.8 Production of Long-Lived $^{186\text{m}}\text{Re}$ for Laser Ablation Laser-Induced Fluorescence Spectroscopy
- 2.9 Band Properties of the Transitional Nucleus ^{187}Pt
- 2.10 Gamma-Rays in Neutron-Rich Nuclei ^{236}Th and ^{242}U
- 2.11 Alpha Fine Structure Measurement for ^{255}No

This is a blank page

2.1 STUDY OF HIGH-SPIN STATES IN $A \approx 30$ NUCLEI

M.L. LIU¹, E. IDEGUCHI¹, T. MORIKAWA², Y. TOH, M. KOIZUMI, A. KIMURA,
H. KUSAKARI³, M. OSHIMA, B. CEDERWALL⁴, K. FURUTAKA, Y. HATSUKAWA,
S. MITARAI², M. SUGAWARA⁵ and Y. ZHENG¹

High-spin states in $A \approx 30$ nuclei have been extensively studied in the past few years [1,2]. In this region several interesting phenomena can be investigated such as violation of mirror symmetry, cluster structure, shape coexistence, and the interplay between single-particle and collective motion [1,2]. In ^{32}S and ^{36}S , presences of superdeformed structure were predicted [3,4] but they were not experimentally confirmed. In order to investigate collective structures at high-spin, ^{36}S and its neighboring nuclei were studied.

An in-beam γ -ray spectroscopic experiment was performed to study high-spin states of ^{36}S and its neighboring nuclei through the $^{18}\text{O} + ^{24}\text{Mg}$ fusion-evaporation reaction. The ^{18}O beam of 70MeV was provided by the tandem accelerator of Japan Atomic Energy Agency. The targets used were an isotopically enriched ^{24}Mg foil of 1 mg/cm² thickness with 8 mg/cm² ^{nat}Pb backing and a 490 $\mu\text{g}/\text{cm}^2$ thick self-supporting one. The GEMINI-II array [5] consisting of 14 HPGe detectors with BGO anti-Compton shields was used to detect γ rays. The HPGe detectors were placed at 47° (4 Ge's), 72° (2 Ge's), 90° (2 Ge's), 105° (4 Ge's), 144° (1 Ge) and 147° (1 Ge) with respect to the beam direction. In order to select evaporation channels, a charged particle detector array consisting of 20 ΔE Si detectors [6] surrounding the target was used. Events were collected when at least two HPGe detectors and one Si detector were fired in coincidence.

Based on the γ - γ coincidence relations and γ -ray energy sum, a level scheme for ^{36}S was constructed as shown in Figure 1. The ordering of transitions in the level scheme was determined by the γ -ray relative intensity balance. Previously proposed level scheme [7] was confirmed in the present study up to the 6.69MeV level. After making charged particle gates, γ rays emitted from ^{33}P , ^{34}S , ^{35}Cl , ^{38}Ar and ^{39}K were also observed. Three new 1026-, 1297- and 2141-keV γ rays were identified in ^{33}P , which de-excite high-lying states with spin $\sim 15/2 \hbar$, as shown in Figure 2A. In the experiment ^{35}Cl was populated most strongly and most of the known yrast and non-yrast transitions [8] were observed. In the present analysis, the highest observed level is the 11^- state at 11.617 MeV in ^{38}Ar . By gating on the 1441-keV transition, which de-excites the 11^- level, γ rays of low-lying states in ^{38}Ar [9] were clearly confirmed (Figure 2B). Data analysis is still in progress.

¹CNS, University of Tokyo

²Kyushu University

³Chiba University

⁴Royal Institute of Technology

⁵Chiba Institute of Technology

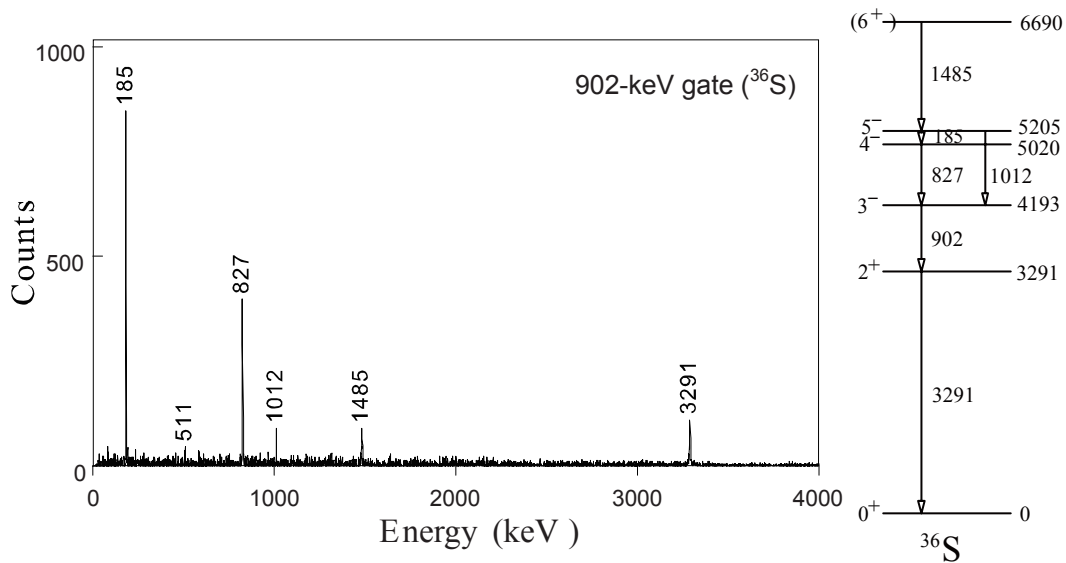


Fig. 1. γ -ray spectrum by gating on 902 keV transition (left) and a level scheme of ^{36}S (right).

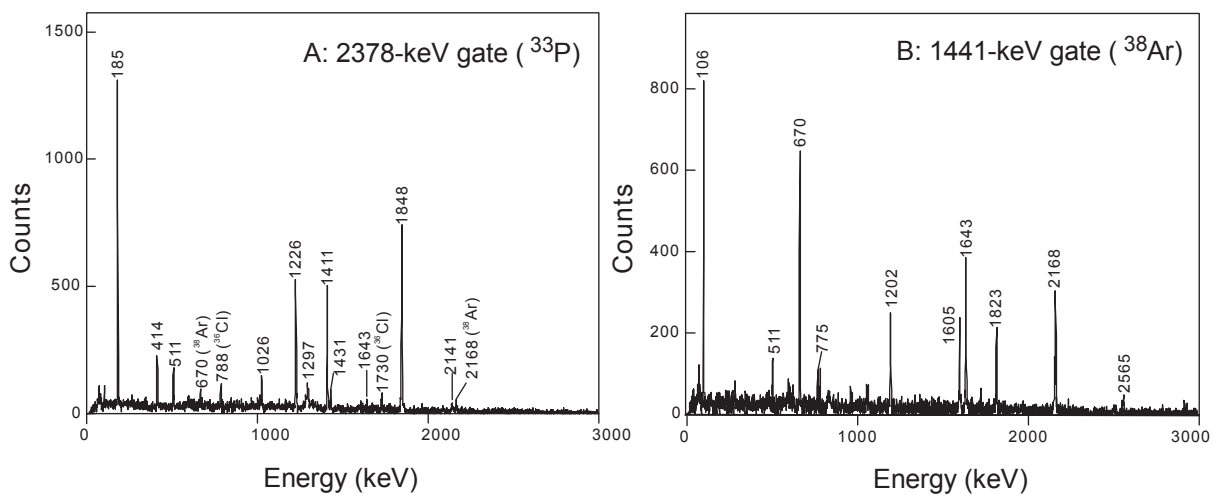


Fig. 2. γ -ray spectra by gating on (A) 2378 and (B) 1441 keV transitions in ^{33}P and in ^{38}Ar , respectively.

References

- [1] P. Mason et al., Phys. Rev. C 71 (2005) 014316.
- [2] F. Della Vedova et al., Phys. Rev. C 75 (2007) 034317, and references therein.
- [3] H. Molique, J. Dobaczewski and J. Dudek, Phys. Rev. C 61 (2000) 044304.
- [4] T. Inakura, S. Mizutori, M. Yamagami and K. Matsuyanagi, Nucl. Phys. A 728 (2003) 52.
- [5] K. Furuno et al., Nucl. Instrum. Methods Phys. Res. A421 (1999) 211.
- [6] T. Kuroyanagi et al., Nucl. Instrum. Methods Phys. Res. A316 (1992) 289.
- [7] X. Liang et al., Phys. Rev. C 66 (2002) 014302.
- [8] R. Kshetri et al., Nucl. Phys. A 781 (2007) 277.
- [9] D. Rudolph et al., Phys. Rev. C 65 (2002) 034305.

2.2 LIFETIME MEASUREMENT OF HIGH-SPIN STATES IN ^{92}Zr

M. SUGAWARA¹, Y. TOH, M. OSHIMA, M. KOIZUMI,
A. KIMURA, Y. HATSUKAWA, T. KIN and H. KUSAKARI²

It has been a main subject in nuclear structure physics for a long time to study the shape and phase evolution as a function of several control parameters characterizing nuclear states such as the proton number Z , the neutron number N , and the nuclear spin I . A new way called E-GOS (E-Gamma Over Spin) was proposed a few years before now to illuminate a possible transition between vibrational and rotational collective modes as a function of nuclear spin[1]. In this approach, the ratio, $R = E_\gamma(I \rightarrow I-2)/I$ is considered, which is expressed as $\hbar\omega/I$ and $(\hbar^2/2\mathfrak{I})(4-2/I)$ in the limits of vibrator and rotor, respectively, and behaves quite differently as a function of spin between the two. This E-GOS plot is shown for ^{92}Zr as an example in Fig. 1. The sharp, hyperbolic decrease with spin, a signature of vibrator, is clearly visible up to 12^+ state, while above that a gradual increase with spin, a signature of rotor, succeeds. Therefore a structural transition from a vibrator to a rotor is suggested for ^{92}Zr around 12^+ .

It is needed to measure the lifetimes of high-spin states for proving the existence of suggested transition from a vibrator to a rotor. Accordingly the lifetime measurement was made on high-spin states in ^{92}Zr using the Doppler shift attenuation method through the reaction of $^9\text{Be}(^{86}\text{Kr}, \text{p})$. All the 1011 of 0.5 mm thickness backed with Au of 29.6 mg/cm² thickness was bombarded with an ^{86}Kr beam of 280 MeV. Emitted γ -rays were detected with an array of 12 HPGe detectors with BGO Compton suppressors (GEMINI-II). Total events of 2.2×10^8 were collected for 3 days of beam time. In this reaction, the recoil velocity of ^{92}Zr nucleus was estimated to be around 6 % relative to the light velocity and the energy difference between stopped and fully shifted components amounted to about 50 keV for the detector at $\theta=144^\circ$ with respect to the beam direction. Since we have also detectors at $\theta=47^\circ$ in GEMINI-II frame, it is possible to check the consistency of the deduced lifetimes by analyzing the γ -ray lineshapes of both the detectors simultaneously. Detailed analysis is in progress.

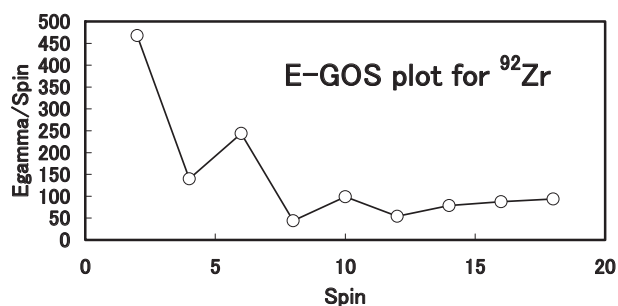


Fig. 1. E-GOS plot for ^{92}Zr .

Reference

[1] P. H. Regan et al., Phys. Rev. Lett. 90 (2003) 152502.

¹Chiba Institute of Technology

²Chiba University

2.3 DEVELOPMENT OF SPIN-POLARIZED RADIOACTIVE NUCLEAR BEAM FOR NUCLEAR SPECTROSCOPY THROUGH β -DELAYED DECAY OF SPIN-POLARIZED NUCLEI AROUND DOUBLY MAGIC NUCLEUS ^{132}Sn

Y. HIRAYAMA¹, M. MIHARA², S.C. JEONG¹, H. MIYATAKE¹, K. MATSUTA², Y.X. WATANABE¹, T. HASHIMOTO, N. IMAI¹, H. ISHIYAMA¹, S. ICHIKAWA, T. ISHII, T. IZUMIKAWA³, D. KAMEDA⁴, I. KATAYAMA¹, H. KAWAKAMI¹, H. KAWAMURA⁵, J. KOMURASAKI², S. MITSUOKA, S. MOMOTA⁶, J. MURATA⁵, K. NARITA⁵, D. NISHIMURA², A. OSA, T.K. SATO, T. SHIMODA² and N. YOSHIKAWA¹

Spin-polarized radioactive nuclear beam (RNB) is a useful tool to study nuclear structures through nuclear moment measurements and β -delayed decay spectroscopy [1], and to study materials through electromagnetic property measurements. For nuclear spectroscopy around the doubly magic nucleus ^{132}Sn at TRIAC facility, we decided to introduce the tilted-foil (TF) technique [2] for the production of spin-polarized RNBs.

The production process of nuclear polarization by the TF technique is as follows: First atomic polarization is produced in an asymmetric electron transfer process between outgoing atoms and those in the surface of the tilted foils. Then nuclear polarization is induced by hyperfine interaction between the nucleus and the polarized electron.

The features of this method are as follows: The method is applicable to any elements in principle and is suited to the low energy RNBs of a few hundred keV per nucleon. The produced polarization increases with the number of foils [3] and the tilt angle between the beam axis and the normal axis of the foils [4]. The direction of polarization is easily reversed by reversing the normal axis of the foils.

A study of the TF method has been performed at TRIAC facility by using the ^8Li ($\tau_{1/2} = 838$ ms, $I^\pi = 2^+$, $g = 0.8268$) beam at the energies of 178 and 240 keV/A. The typical beam intensity was 10^5 pps. ^8Li nuclei were implanted in an annealed platinum stopper foil of 10 μm thick at room temperature, where the magnetic field of $B_0 \sim 0.05$ T was applied to preserve the nuclear polarization. The β -NMR technique was applied to the measurement of the nuclear polarization. Figure 1 shows the obtained polarization as a function of the number of foils by varying the foil materials, beam energies and tilt angles in order to search an optimum condition. In the experiment in Nov. 2005, the ten carbon foils of thickness 10 $\mu\text{g}/\text{cm}^2$ were used with the tilt angle of 70° . The polarization was achieved to be $3.7 \pm 1.1\%$ with the 10 foils. The induced polarization wasn't saturated. Although higher polarization is expected by increasing the number of foils, the carbon foil is so thick that ^8Li ions cannot pass through more than ten foils. Therefore, we developed a thinner polystyrene foil of about 3 $\mu\text{g}/\text{cm}^2$

¹ High Energy Accelerator Research Organization (KEK)

² Osaka University

³ Niigata University

⁴ Institute of Physical and Chemical Research (RIKEN)

⁵ Rikkyo University

⁶ Kochi University of Technology

thickness. At the experiment in Jan. 2007, the polarization of $5.9 \pm 0.5\%$ was achieved at the beam energy of 178 keV/A by using the 15 polystyrene foils at the tilt angle of 70° . From this result, polarization of 8% is expected with 20 foils, which is limited by energy loss of ^8Li ions passing through the foils.

We are now preparing for nuclear spectroscopic experiments of radioactive indium isotopes polarized with the TF technique.

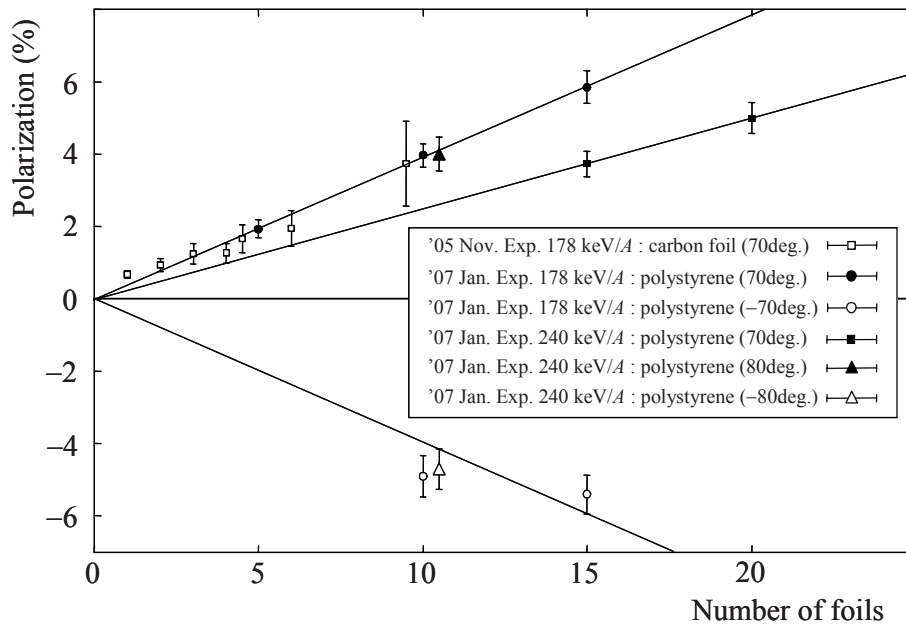


Fig. 1. ^8Li polarization produced by varying number of sheets of foil, the foil materials, beam energies and tilt angles.

References

- [1] Y. Hirayama, T. Shimoda, H. Izumi, A. Hatakeyama, K.P. Jackson, C.D.P. Levy, H. Miyatake, M. Yagi, H. Yano, Phys. Lett. B 611 (2005) 239.
- [2] Y. Nojiri and B.I. Deutch, Phys. Rev. Lett. 51 (1983) 180.
- [3] G. Goldring and Y. Niv, Hyperfine Interact. 21 (1985) 209.
- [4] N.H. Tolk, L.C. Feldman, J.S. Kraus, J.C. Tully, M. Hass, Y. Niv and G.M. Temmer, Phys. Rev. Lett. 47 (1981) 487.

2.4 COULOMB EXCITATION EXPERIMENT OF ^{134}Xe

M. KOIZUMI, Y. TOH, M. OSHIMA, A. OSA, A. KIMURA, Y. HATSUKAWA, K. FURUTAKA, H. HARADA, G. KITATANI, S. NAKAMURA, M. OHTA, K. HARA, H. KUSAKARI¹, M. SUGAWARA², T. MORIKAWA³ and Y. KOJIMA⁴

Being located in a transitional region, Xe isotopes gradually change their properties from a γ -unstable rotational character ($A \approx 124$) to a vibrational ($A = 134$). In terms of dynamic symmetry of IBM, the change is considered as a shape phase transition from O(6) to U(5) symmetry. Theoretical calculations suggested that the E(5) critical point of the phase shape transition of Xe would appear at around $A = 130$ [1,2]. In order to make detailed discussion, information on electromagnetic properties such as B(E2)s and quadrupole moments are required.

Coulomb excitation is a useful method for measurements of electromagnetic properties near ground states of nuclei [3,4]. Our systematic study revealed nuclear properties and evolutions of structures of stable nuclei in the mass region around $A \approx 70$ [5-12]. Applying the same techniques, we have started systematic study of low-lying structure of Xe isotopes.

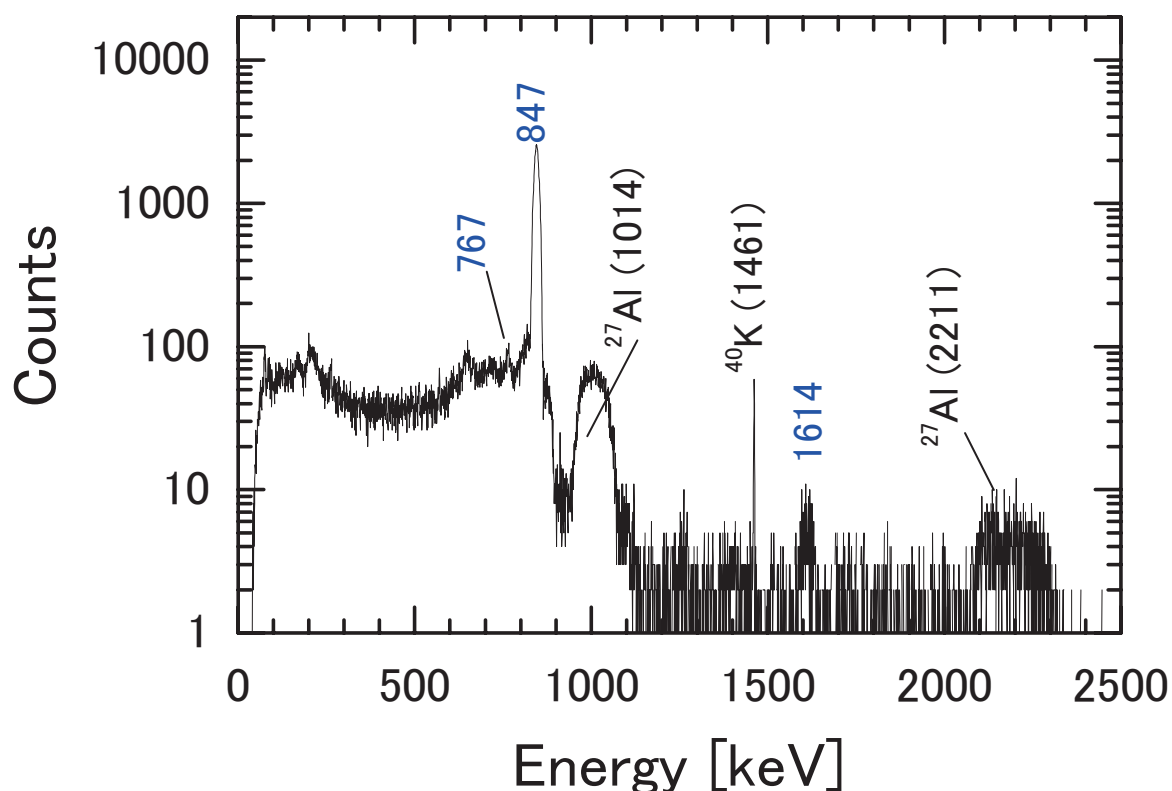


Fig. 1. A particle- γ coincidence spectrum measured with a Ge detector placed at 90° to the beam direction. The unit of the γ -energy given in the spectrum is keV.

¹Chiba University

²Chiba Institute of Technology

³Kyushu University

⁴Hiroshima University

A Coulomb excitation experiment of ^{134}Xe was carried out using a 410-MeV ^{134}Xe beam with the beam current of about 1.4 pA. A 16- μm aluminum target was used for the experiment. Because of the inverse kinematics, the scattering angle of ^{134}Xe less than 10 degrees. De-excitation γ -rays were measured with a γ -ray detector array, GEMINI-II [13], and the recoiled particles with a position sensitive particle detector array, LUNA [14]. Particle- γ -coincidence events were recorded event by event on magnetic tapes. Totally, about 5×10^6 events were obtained. Figure 1 is a particle- γ coincidence spectrum measured with a Ge detector placed at 90° to the beam direction. No Doppler correction has been done for the spectrum. Because the scattered Xe particles are not dispersed, the widths of the Xe de-excitation γ -peaks are narrow (about 16 keV FWHM). Three peaks are identified as ^{134}Xe de-excitation γ -rays: the 766.7-keV $2_2^+ \rightarrow 2_1^+$ transition, the 847.0-keV $2_1^+ \rightarrow 0^+$ transition, and the 1613.8-keV $2_2^+ \rightarrow 0^+$ transition. De-excitation γ -rays from Al target, which are broader than those from ^{134}Xe , are also seen in the spectrum: 843.38-keV $1/2_1^+ \rightarrow 5/2_1^+$ transition, 1014.5-keV $3/2_2^+ \rightarrow 5/2_1^+$ transition, and 2211-keV $7/2_2^+ \rightarrow 5/2_1^+$ transition. Since the neutron number of ^{134}Xe is close to the magic number, the nucleus is considered to have a spherical shape. Data analysis of this experiment is in progress.

References

- [1] D.L. Zhabg and Y.X. Liu, Chin. Phys. Lett. 20 (2003) 1028.
- [2] R. Fossin, Dennis Bonatsos, and G.A. Lalazissis, Phys. Rev. C73 (2006) 044310.
- [3] K. Alder and A. Winther, Coulomb Excitation (Academic, NewYork, 1966).
- [4] K. Alder and A. Winther, Electromagnetic Excitation (North Holland, Amsterdam, 1975).
- [5] Y. Toh et al., J. Phys. G 27 (2001) 1475.
- [6] Y. Toh et al., Eur. Phys. J. A 9 (2000) 353.
- [7] A. Osa, T. Czosnyka, et al., Phys. Lett. B 546 (2002) 48.
- [8] M. Zielinska, T. Czosnyka, et al., Nucl. Phys. A 712 (2002) 3.
- [9] M. Koizumi, A. Seki, Y. Toh, et al., Eur. Phys. J. A 18 (2003) 87.
- [10] M.Sugawara et al., Eur. Phys. J. A 16 (2003) 409.
- [11] M. Koizumi et al., Nucl. Phys. A 736 (2003) 46.
- [12] T. Hayakawa et al., Phys. Rev. C 67 (2003) 064310.
- [13] K. Furuno et al., Nucl. Instrum. Methods Phys. Res. A 421 (1999) 211.
- [14] Y. Toh et al., Rev. Sci. Inst. 73 (2002) 47-50.

2.5 β DECAY HALF-LIFE OF ^{166}Eu AND LEVELS IN ^{166}Gd

T.K. SATO¹, A. OSA¹, M. ASAI¹, K. TSUKADA¹, H. HAYASHI², M. SHIBATA³,
Y. KOJIMA⁴ and S. ICHIKAWA¹

A β -decay half-life of a new neutron-rich isotope ^{166}Eu produced in the proton-induced fission of ^{238}U has been determined, using an on-line isotope separator at JAEA. Excited states of daughter nuclide ^{166}Gd have been established for the first time. Level energies of the first 2^+ states of even-even Gd isotopes were found to show an irregular behavior at ^{162}Gd and increasing deformation toward the neutron midshell around $N\sim 104$.

A ^{nat}U target was used in the form of uranium carbide with target thickness of 630 mg/cm^2 . The target was bombarded by a 33 MeV proton beam with the intensity of about 300 nA. Fission products were diffused-out from the target, and then ionized in a surface-ionization type ion source. The mass-separated ions of interest were implanted into an aluminum-coated Mylar tape in a tape transport system, and periodically transported to a measuring position. The measuring position was equipped with a sandwich-type plastic scintillator for β -ray measurements, a short coaxial n -type HPGe detector (ORTEC LOAX), and a 36% n -type HPGe detector (ORTEC

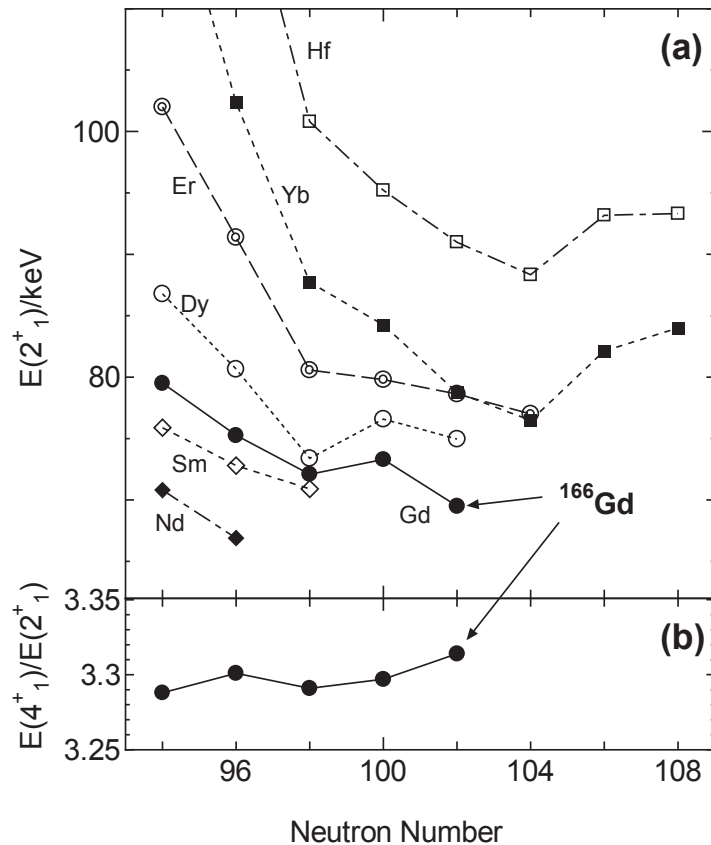


Fig. (a) Level energies of the first 2^+ states in even-even Nd, Sm, Gd, Dy, Er, Yb and Hf isotopes. (b) Energy ratios between the 4_1^+ and 2_1^+ states $E(4_1^+)/E(2_1^+)$ for even-even Gd isotopes.

¹JAEA

²Nagoya University

³Nagoya University RIRC

⁴Hiroshima University

GAMMA-X). β - γ and x/γ - γ coincidences between these detectors were recorded event by event together with time information used in a half-life analysis.

In this study, the observed K x rays following the β -decay of the products in the mass-separated fraction provided direct identification of isotopes. From decay curves of the Gd K x ray and assigned γ -rays, β -decay half-life of new neutron-rich Eu isotope was determined to be 1.7(4) s for ^{166}Eu . In addition, the observed 69.7(1) and 160.79(4) keV γ rays following the β -decay of ^{166}Eu were assigned to the $2^+_{1} \rightarrow 0^+_{1}$, and $4^+_{1} \rightarrow 2^+_{1}$ transitions in the ground state-band of ^{166}Gd , respectively. Therefore, we determined the $E(2^+)$ and $E(4^+)$ energies of $^{166}\text{Gd}_{102}$ which is the most neutron-rich Gd isotope to be 69.7(1) keV and 230.49(10) keV, respectively. The $E(2^+_{1})$ energies of Gd isotopes take the first minimum at $N=98$ (^{162}Gd), rises at $N=100$ (^{164}Gd), and decrease again at $N=102$ (^{166}Gd). In the previous decay-studies for Tb isotopes, the same tendency was already found in even-even Dy isotopes [1]. The $E(4^+_{1})$ energies of Gd and Dy isotopes also show the same tendency. Although, the deformed sub-shell closure expected at $N=98$ in this region, the second minimum of the first 2^+_{1} state of Gd, Dy isotopes exists around $N \approx 104$ neutron midshell, which is reasonably explained as the maximum deformation at the midshell.

Reference

- [1] M. Asai *et al.*, Phys. Rev. C 59 (1999) 306.

2.6 HIGH-SPIN STATES OF ODD-ODD ^{174}Re NUCLEUS

Y.H. ZHANG¹, S. GUO¹, X.H. ZHOU¹, M. Long¹, M. OSHIMA, Y. TOH, M. KOIZUMI, A. OSA, A. KIMURA, Y. HATSUKAWA, M. SUGAWARA² and H. KUSAKARI³

In the past few years, efforts have been made in our group to study the band structures of prolate-deformed odd-odd nuclei at the upper end of rear-earth region [1]. As for the odd-odd ^{174}Re , the high-spin data are scarce; the level scheme accepted in Ref. [2] deviates evidently from the systematics [1], and it could not be confirmed in the recent work using the $^{159}\text{Tb}(^{20}\text{Ne},5n\gamma)^{174}\text{Re}$ reaction [3]. Therefore, we have performed an in-beam γ -spectroscopy experiment to study the high-spin states of ^{174}Re using the $^{152}\text{Sm}(^{27}\text{Al},5n\gamma)^{174}\text{Re}$ reaction.

The ^{27}Al beam was provided by the JAEA tandem accelerator and impinged on an enriched ^{152}Sm metallic foil of 2.0 mg/cm^2 thickness with a 10 mg/cm^2 Pb backing. The γ -ray detection array consisted of 13 large volume HPGe's with BGO anti-Compton shields. γ -ray excitation functions were measured at 125-, 132-, and 140-MeV beam energies and the γ - γ coincidence measurement was performed at 140-MeV beam energy. A total of 2×10^8 γ - γ coincidence events were accumulated in this experiment and analyzed in a same way as described in Ref. [1].

The level scheme of ^{174}Re have been constructed and shown in Fig. 1. The bands reported in Ref. [3] have been confirmed and extended significantly. Bands 3 and 5 were newly identified in this work. Of most importance, the present work has established spectroscopic connection between bands 1 and 2 due to a number of inter-band transitions. According to systematics [1], spin-and-parity assignment and quasiparticle configurations have been proposed and indicated in Fig. 1.

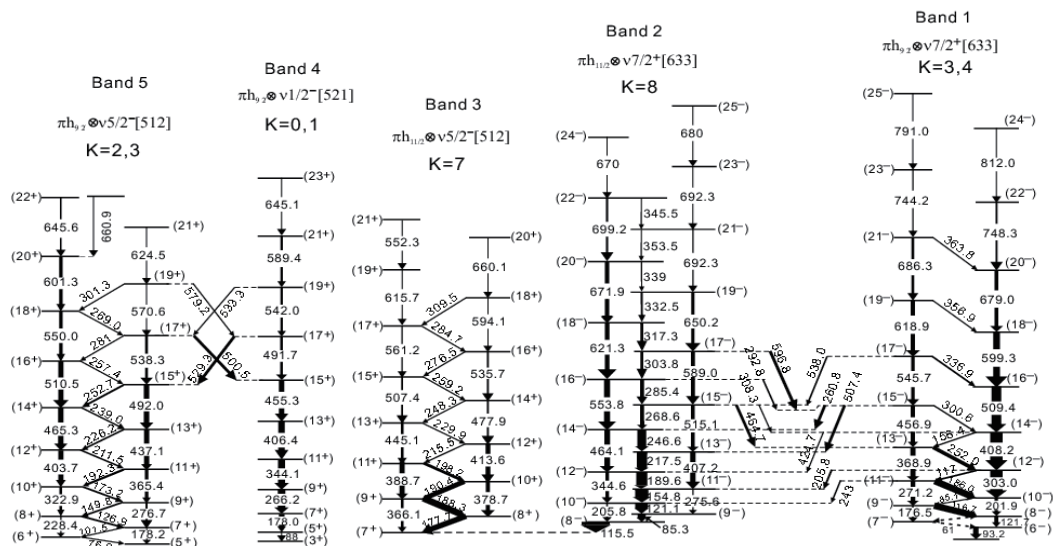


Fig. 1 Partial level scheme of ^{174}Re deduced from the present work.

¹ Institute of Modern Physics, CAS, Lanzhou, China

² Chiba Institute of Technology, Narashino, Chiba 275-0023, Japan

³ Chiba University, Inage-ku, Chiba 263-8512, Japan

We have plotted the quantity $S(I)$ (defined as in [1]) as a function of spin for bands 1 and 2 in Fig. 2. The (15^-) levels are corrected by 2 keV considering the level interaction effect. In such a plot, the points (associated with levels I 's) that have negative values are energetically favored over those with positive ones. The expected favored signatures are 1 and 0 for bands 1 and band 2, corresponding to the odd and even spin sequences, respectively. It can be seen in this figure that, it is the unfavored-signature branches that are favored energetically at low and medium spins rather than the expected favored ones. Such a behavior has been referred to as the low-spin signature inversion. With increasing angular momentum, the inverted signature splitting becomes decreasing, and the two signature branches cross with each other at the high spins beyond which normal signature splitting is observed. The low-spin signature inversion in ^{174}Re fits well into systematics as as presented in Ref. [1].

Further analysis is still in progress and the final result will be published in a coming article.

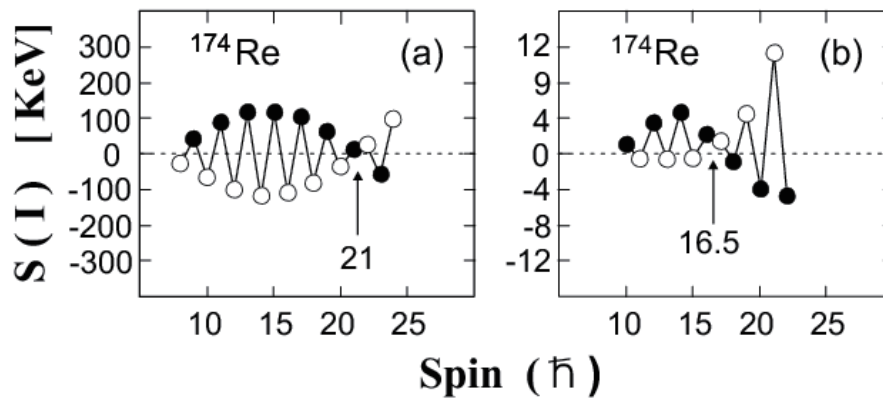


Fig. 2 Plot of signature splitting $S(I)$ vs I for (a) the $\pi h_{9/2} \otimes \nu i_{13/2}$ band and (b) the $\pi h_{11/2} \otimes \nu i_{13/2}$ band in ^{174}Re . The arrow indicates the signature inversion spin.

References

- [1] Y. H. Zhang et al, Phys. Rev. C68 (2003) 054313.
- [2] R. B. Firestone et al., Table of Isotopes (8th edition) Vol. II (1995) 2071.
- [3] Y. H. Zhang et al., Eur. Phys. J. A7 (2000)19.

2.7 SPECTROSCOPY OF NEUTRON-RICH TANTALUM ISOTOPES PRODUCED IN ^{18}O -INDUCED TRANSFER REACTIONS

T. SHIZUMA, T. ISHII, H. MAKII, T. HAYAKAWA, M. MATSUDA and M. FUJIWARA¹

The emergence of high- K isomers, where K is the angular momentum projection on the nuclear symmetry axis, based on multi-quasiparticle excitation is a characteristic of nuclei in the $A \approx 180$ region. The majority of the known high- K isomers lie on the neutron-deficient side of the valley of β stability, because the access to the neutron-rich nuclei in this region has been limited by the restriction of using fusion-evaporation reactions with stable beam and target combination. However recent progress in γ -ray spectroscopic techniques using ^{18}O -induced transfer reactions has been proven to be effective for investigating the near-yrast structures of neutron-rich nuclei [1,2].

Excited states in neutron-rich Ta nuclei have been populated in ^{18}O -induced neutron transfer reactions on ^{181}Ta . The 180MeV ^{18}O beam was provided by the tandem accelerator at Japan Atomic Energy Agency, Tokai. The target thickness of 3.9 mg/cm^2 was thick enough to stop residual nuclei inside the target material. In-beam γ rays were measured by eight HP-Ge detectors. Outgoing projectile-like ions were detected by four sets of surface barrier Si $\Delta E - E$ detectors placed at a position close to the grazing angle of the reaction. Events were recorded on magnetic tapes when the silicon detector and one or more Ge detectors were fired in coincidence.

Figure 1 shows a γ -ray energy spectrum in coincidence with scattered particles. Intense γ -ray peaks from ^{181}Ta of which excited states are populated via inelastic scattering or Coulomb excitation can be seen. In the preliminary analysis of the data, γ -ray peaks from neutron-rich Ta isotopes produced in neutron transfer reactions have been observed. Further analysis is in progress.

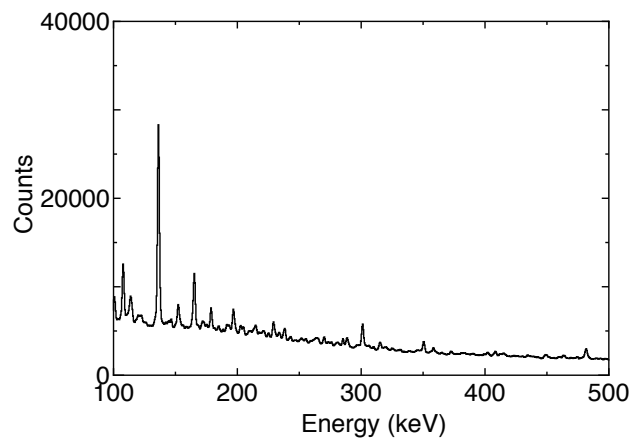


Fig.1 A γ -ray single spectrum obtained in the ^{18}O -induced transfer reaction on ^{181}Ta .

References

- [1] T. Ishii *et al.*, Phys. Rev. C 72 (2005) 021301(R).
- [2] T. Shizuma *et al.*, Eur. Phys. J. A 391 (2006) 30.

¹Osaka University

2.8 PRODUCTION OF LONG-LIVED $^{186\text{m}}\text{Re}$ FOR LASER ABLATION LASER-INDUCED FLUORESCENCE SPECTROSCOPY

H. IIMURA, M. KOIZUMI, M. MIYABE, M. OHBA, Y. ISHIDA¹, and
T. HORIGUCHI²

The rhenium isotopes ($Z=75$) with mass number around $A=180$ are of particular interest because these nuclei have been theoretically predicted to have axially asymmetric deformation. Mean square charge radii obtained by high-resolution laser spectroscopy are sensitive information on the deformation of nuclei. However, the laser spectroscopy of Re isotopes have not been made except stable isotopes $^{185,187}\text{Re}$. Radioactive isotopes have yet to be measured mainly because Re is one of refractory elements and hard to be atomized. In this work we use laser ablation to atomize Re sample, and then ablated atoms are irradiated by tunable dye laser for the fluorescence detection. We set long-lived $^{186\text{m}}\text{Re}$ ($T_{1/2}=2\times 10^5$ y) as the first candidate to be measured by using this method. So far the known production method of $^{186\text{m}}\text{Re}$ is thermal neutron capture, but this can not be used for laser spectroscopy because the irradiated sample contains stable Re isotopes which mask the fluorescence from the trace amount of $^{186\text{m}}\text{Re}$. Thus we use $^{186}\text{W}(p,n)$ reaction to produce $^{186\text{m}}\text{Re}$, although the production yield of this reaction has not been known. As the first step of the experiment we have estimated this yield.

A 98.2%-enriched ^{186}W powder was used as a target. It was pressed into a disk-shaped pellet with a thickness of 650 mg/cm^2 . The target was irradiated with 13.0 MeV protons at a beam current of approximately $0.8\text{ }\mu\text{A}$. The irradiation continued for about 18 h. After three years of cooling period, γ -ray measurements were carried out with a Ge detector. It is known that the only strong γ -transition following the decay of $^{186\text{m}}\text{Re}$ is the 137.2-keV transition in ^{186}Os ($Z=76$). From the measurements, we found that this transition overlapped with the 136.5-keV transition of ^{57}Co , which was produced from Fe impurity in the target. By subtracting the contribution from ^{57}Co , we determined the count rate of the 137.2-keV γ -ray, which was then used to estimate the number of $^{186\text{m}}\text{Re}$ atoms. As a result, the yield of $^{186\text{m}}\text{Re}$ was calculated to be 4×10^{11} atoms. This yield can be compared with that of $^{184\text{m}}\text{Re}$ (165 d), which was produced simultaneously from ^{184}W contained in the target with 1.7%. From the intensity of 105-keV isomeric transition in $^{184\text{m}}\text{Re}$, the yield of $^{184\text{m}}\text{Re}$ after the irradiation was obtained to be 1×10^9 atoms, which corresponds to 7×10^{10} atoms when the number of target ^{184}W atoms is the same as ^{186}W . Although the spin of $^{186\text{m}}\text{Re}$ has yet to be established, roughly comparable values of the production yields for the (p,n) reactions could support that $^{186\text{m}}\text{Re}$ has the same spin as $^{184\text{m}}\text{Re}$ ($I=8$).

In order to do laser spectroscopy with this yield we are now improving the sensitivity of our set up for laser ablation laser-induced fluorescence spectroscopy. One thing in progress is chemical separation of Re from irradiated W target, which is expected to be effective for reducing the background from the scattered laser light. This is also preferable for γ -ray measurements, and more precise production yield of $^{186\text{m}}\text{Re}$ could be obtained.

¹Institute for Physical and Chemical Research, RIKEN

²Hiroshima International University

2.9 BAND PROPERTIES OF THE TRANSITIONAL NUCLEUS ^{187}Pt

X.H. ZHOU¹, M. OSHIMA, Y. TOH, M. KOIZUMI, A. OSA, Y. HATSUKAWA,
Y.H. ZHANG¹ and M. SUGAWARA²

The neutron-deficient Pt-Hg nuclei are well known to exhibit shape coexistence phenomenon [1], which has provided the motivation for extensive studies both experimentally and theoretically. In the even-A Pt isotopes from A=170 to A=190 [1], nuclear structure studies have presented strong evidence for the shape coexistence at low energy. The spectroscopic information of ^{187}Pt is of particular interest as it lies between the two nuclei ^{186}Pt and ^{188}Pt where the change in collective structure should be most drastic.

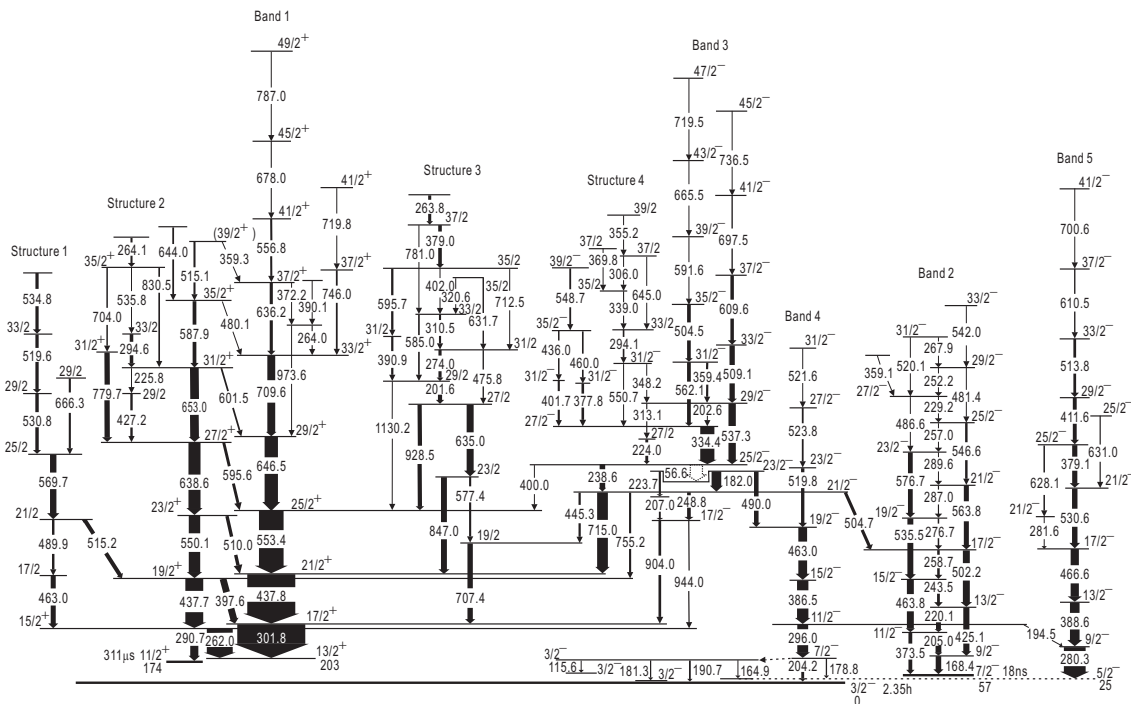


Fig. 1. The level scheme of ^{187}Pt .

The excited states in ^{187}Pt were populated via the $^{173}\text{Yb}(^{18}\text{O}, 4n)$ reaction. The ^{18}O beams at energies of 78 and 85 MeV were provided by the tandem accelerator at the Japan Atomic Energy Agency. Standard in-beam spectroscopic measurements were carried out. Assignments of the observed new γ rays to ^{187}Pt were based on the coincidences with the known γ rays [2]. Based on the analysis of γ - γ coincidence relationships, a complicated level scheme for ^{187}Pt has been proposed and presented in Fig. 1.

The $i_{13/2}$ configuration has been assigned to band 1. One of the interesting findings in the present work is the observation of the unfavored signature branch up to high spin, while in the heavier odd-A Pt nuclei only was a short sequence observed [2]. The first band crossing for the $i_{13/2}$ band should be resulted from the alignment of a pair of $i_{13/2}$ neutrons (BC and AD crossings) due to the appreciable negative γ deformation. The $i_{13/2}$ band displays very large signature splitting in the whole spin region observed experimentally. We have proposed that it

¹Institute of Modern Physics, P. R. China

²Chiba Institute of Technology

is the negative values of γ and β_4 that cause this phenomenon. The TRS calculations indicate that the $i_{13/2}$ configurations have large and negative equilibrium hexadecapole deformation of about -0.04. A large negative value of β_4 can bunch the single particle levels and brings the low- Ω orbits closer to the Fermi surface. The triaxiality can induce a similar effect.

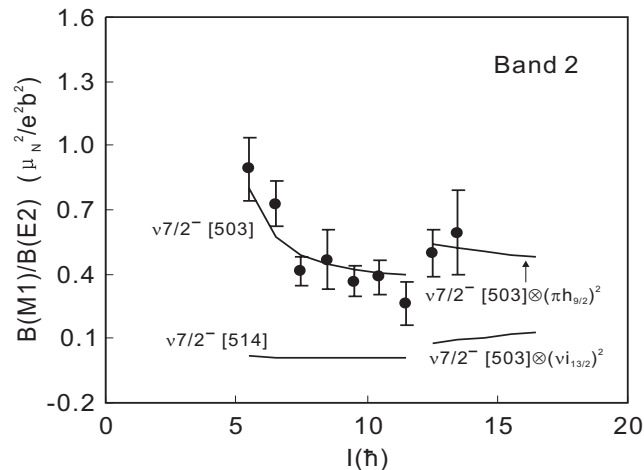


Fig.2. Experimental $B(M1)/B(E2)$ ratios as a function of initial spin I for the $7/2^- [503]$ band, and theoretical predictions.

The band-head spin and parity of band 2 were assigned to be $7/2^- [2]$. This strongly coupled band experiences a sharp backbending at $\hbar\omega=0.25$ MeV with gain of $7.0\hbar$ in alignment. The $B(M1)/B(E2)$ ratios for a coupled band have been proven to be quite useful in characterizing the specific intrinsic orbit and the quasi-particles associated with band crossing. The experimental data is shown in Fig.2 together with theoretical estimates obtained from semiclassical formulae. The detailed information for the calculation was presented in ref. [3]. As clearly shown in Fig. 2, the experimental values are well reproduced by the configuration of $7/2^- [503]$, while the calculated values associated with the $7/2^- [514]$ configuration are far below the experimental observations. Therefore, we propose that band 2 is based on the rather pure $7/2^- [503]$ configuration. We examined the effects of γ variations on the theoretical ratios, and found that the $7/2^- [503]$ configuration is strongly preferred in the γ interval from -20° to $+20^\circ$. The experimental $B(M1)/B(E2)$ ratios for the $7/2^- [503]$ band show a pronounced increase of a factor of 2 in the band crossing region. In the mass region of the present interest, the $i_{13/2}$ neutrons and $h_{9/2}$ protons should be responsible for the band crossing. As shown in Fig.2, the two alignments result in opposite trends in the $B(M1)/B(E2)$ values after the crossing. Therefore, the experimentally observed increase in the $B(M1)/B(E2)$ ratios strongly suggest that the band crossing is due to the $h_{9/2}$ proton alignment.

Band 4 is built on the ground state with the $3/2^- [512]$ Nilsson configuration. The alignment process of band 4 is closely similar with that of the $7/2^- [503]$ band, and the band crossing is likely caused by the $h_{9/2}$ proton alignment.

Band 5 has a decoupled structure. We propose that band 5 is associated with the $1/2^- [521]$ configuration. It is very possible that the band crossing of band 5 was caused by the alignment of $h_{9/2}$ protons.

References

- [1] D. T. Joss, et al., Phys. Rev. C74 (2006) 014302.
- [2] B. Roussiere et al., Nucl. Phys. A548 (1992) 227.
- [3] X. H. Zhou, et al., Phys. Rev. C75 (2007) 034314.

2.10 GAMMA-RAYS IN NEUTRON-RICH NUCLEI ^{236}Th AND ^{242}U

T. ISHII, H. MAKII, M. ASAI, H. KOURA, S. SHIGEMATSU¹, K. TSUKADA, A. TOYOSHIMA, M. MATSUDA, A. MAKISHIMA², T. SHIZUMA, J. KANEKO³, H. TOUME⁴, I. HOSSAIN⁵, S. ICHIKAWA, T. KOHNO¹ and M. OGAWA³

The ground-state bands of neutron-rich nuclei ^{236}Th and ^{242}U were established by in-beam γ -ray spectroscopy using the (^{18}O , ^{20}Ne) two-proton pickup reactions with a ^{238}U and a ^{244}Pu target. Deexcitation γ rays in ^{236}Th and ^{242}U were identified by selecting the kinetic energies of ^{20}Ne using Si ΔE - E detectors. An E - ΔE plot obtained from the ^{236}Th experiment is shown in Fig. 1. Figures 2 (a) and (b) show γ -ray spectra obtained by setting the gates on ^{20}Ne with the kinetic energies in the region (a) and (b) in Fig. 1, respectively. In Fig. 2 (a), almost equally spaced transitions of 112, 169, 224 and 273 keV were observed. In Fig. 2 (b), γ rays in the ground-state band of ^{234}Th , which were identified previously [1,2], were observed. Since the reaction Q -values for the region (b) are lower than those for the region (a) by 12 MeV, excitation energy in ^{236}Th for the region (b) is high enough to evaporate two neutrons. The observation of γ rays in ^{234}Th for the region (b) suggests that the γ rays coincident with the region (a) are the deexcitation γ rays in ^{236}Th . Following the same analysis, we have identified γ rays in ^{242}U produced by the $^{244}\text{Pu}(^{18}\text{O}, ^{20}\text{Ne})$ reaction. Note that the cross section of the two-proton pickup reactions were on the order of μb . Assuming that those γ rays form the ground-state rotational bands, we have established level schemes of ^{236}Th and ^{242}U up to spin 10 and 8, respectively, shown in Fig. 3. Although the $2^+ \rightarrow 0^+$ γ transitions were not observed because of the large internal conversion coefficients, $\alpha_T > 300$, we can estimate these energies precisely from the moments of inertia deduced from the higher levels.

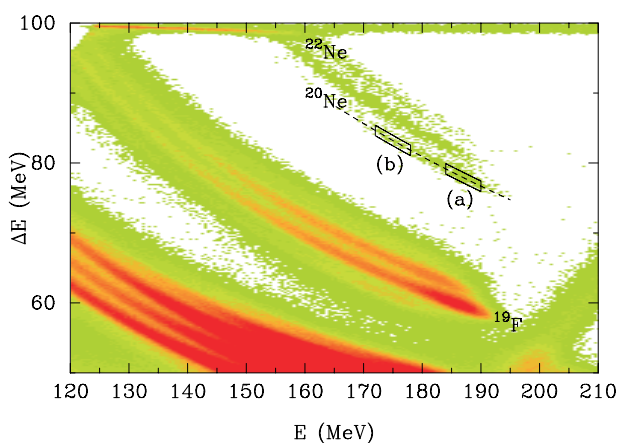


Fig. 1. E - ΔE plot of scattered nuclei measured by a Si ΔE - E detector in the reaction of a 200-MeV ^{18}O beam with a ^{238}U target. The dashed line represents a calculated energy loss for ^{20}Ne nuclei.

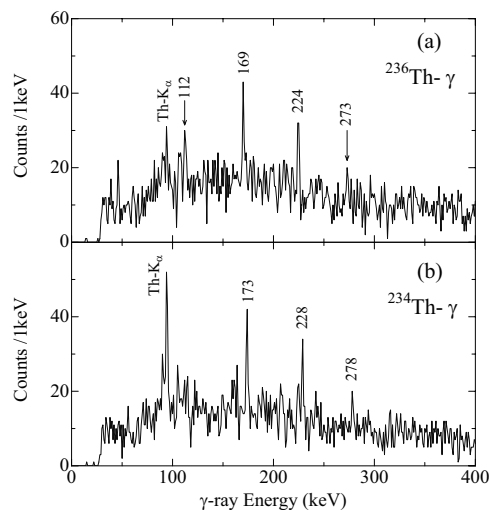


Fig. 2. γ -ray spectra obtained by setting the gates on ^{20}Ne with the kinetic energies in the regions (a) and (b) in Fig. 1, respectively.

¹Tokyo Institute of Technology, ²National Defense Medical College,

³Komazawa University, ⁴Ibaraki University, ⁵Osaka University

We have established five new data of the first 2^+ energies, $E(2_1^+)$, by a series of our in-beam γ -ray study of neutron-rich nuclei ^{236}Th , $^{240,242}\text{U}$, ^{246}Pu and ^{250}Cm [3,4]. By extending the systematics of $E(2_1^+)$, we have found that the $E(2_1^+)$ values in U and Pu have local minima at $N \sim 146$. This fact suggests the possibility of the spherical shell closure of $N = 164$ in the U region as an opposite side of the spherical shell closure of $N = 126$. Calculation of single particle levels using the Koura-Yamada (KY) potential [5] supports this suggestion. This calculation gives 1.8 MeV energy gaps both at $N = 164$ and at $Z = 92$ for ^{256}U . These energy gaps are comparable size to those calculated by the KY potential for an expected doubly-magic superheavy nucleus of $^{298}114$ (2.5 MeV at $N = 184$ and 1.6 MeV at $Z = 114$), and are about half of those for a typical doubly magic nucleus of ^{208}Pb .

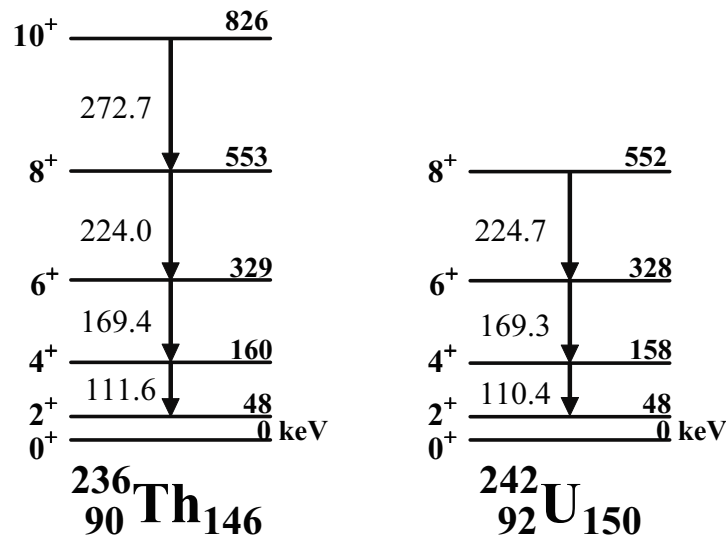


Fig. 3 . Level schemes of ^{236}Th and ^{242}U . The γ -ray and level energies are in units of keV. The 2^+ energies in ^{236}Th and ^{242}U were estimated to be 48.4(3) and 47.8(3) keV, respectively, from the higher energy levels.

References

- [1] K. E. Rehm, D. Frekers, T. Humanic *et al.*, ANL-83-25 (1983) 91.
- [2] J. Gerl, Ch. Ender, D. Habs *et al.*, Phys. Rev. C 39 (1989) 1145.
- [3] T. Ishii, S. Shigematsu, M. Asai *et al.*, Phys. Rev. C 72 (2005) 021301(R).
- [4] T. Ishii, S. Shigematsu, H. Makii *et al.*, J. Phys. Soc. Jpn. 75 (2006) 043201.
- [5] H. Koura and M. Yamada, Nucl. Phys. A671 (2000) 96.

2.11 ALPHA FINE STRUCTURE MEASUREMENT FOR ^{255}No

M. ASAI, K. TSUKADA, Y. ISHII, A. TOYOSHIMA, T. ISHII, I. NISHINAKA and
Y. NAGAME

Fine structure of α spectra provides rich information on nuclear level structure. Excited states in daughter nuclei are established through measured α transition energies, and spin-parities and single-particle configurations are estimated from deduced hindrance factors of α transitions. For short-lived heavy actinide and transactinide nuclei, however, no precise data of α fine structure have been obtained, because the coincidence summing effect between α particles and subsequently emitted internal conversion electrons, Auger electrons, and low-energy X rays significantly distorts the measured α particle spectra. Placing Si detectors at a longer source-to-detector distance than usual ones, one can achieve a better energy resolution of α peaks as well as reduce the influence of the coincidence summing effect. Under such condition, we have measured α fine structure of a short-lived heavy actinide nucleus ^{255}No very precisely.

The nucleus ^{255}No was produced by the $^{248}\text{Cm}(^{12}\text{C}, 5n)$ reaction. The beam energy was 77 MeV on target. Reaction products were transported by a He jet into a rotating wheel α -detection system, and deposited on a thin foil eighty of which were set on the wheel [1]. The wheel rotated at 90-s intervals, and moved the deposited sources to six consecutive detector stations each of which was equipped with a Si PIN photodiode detector ($18 \times 18 \text{ mm}^2$ active area). The first four detectors were placed at a source-to-detector distance of 12.2 mm, and $17 \text{ mm}\phi$ apertures were set in front of them. The efficiency of each of the detectors was 10%. The last two detectors were placed at a source-to-detector distance of 2.2 mm whose efficiencies were 40%. The last two detectors were only used to obtain “distorted” α spectra to see the influence of the coincidence summing effect.

Figure 1 shows a sum of α -particle spectra measured with the 2nd, 3rd, and 4th detectors. Three intense α lines were observed at 7748, 7909, and 8100 keV which correspond to the transitions to the $1/2^+[620]$, $1/2^+[631]$, and $5/2^+[622]$ states in ^{251}Fm , respectively. These α transitions were also observed in previous α -singles and α - γ experiments [2-4]. On the other hand, some weak α lines were clearly observed for the first time at the low-energy side of the intense peaks, owing to the good energy resolution and small low-energy tailing of the measured α peaks. The α transitions to the $9/2^- [734]$ ground state and the first excited $11/2^-$ state in the $9/2^- [734]$ band were also observed separately. Alpha-transition energies and branching intensities were determined without the influence of the coincidence summing effect.

On the basis of the present and the previous α - γ coincidence results [4], we have established a more detailed level scheme of ^{251}Fm (Fig. 2) than the previous one [4]. Rotational bands built on the $1/2^+[620]$, $1/2^+[631]$, and $5/2^+[622]$ states were established for the first time. Hindrance factors for all the α transitions observed are very similar to those in the α decays of the lighter $N = 153$ isotones ^{253}Fm and ^{251}Cf . The moment of inertia of each rotational band is also similar to those in neighboring nuclei. These results confirm the present spin-parity and Nilsson orbital assignments in Fig. 2.

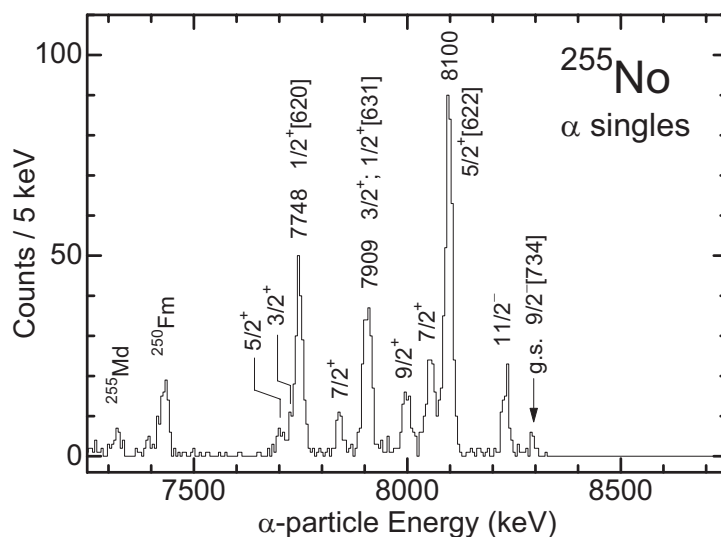


Fig. 1. Alpha-singles spectrum of ^{255}No .

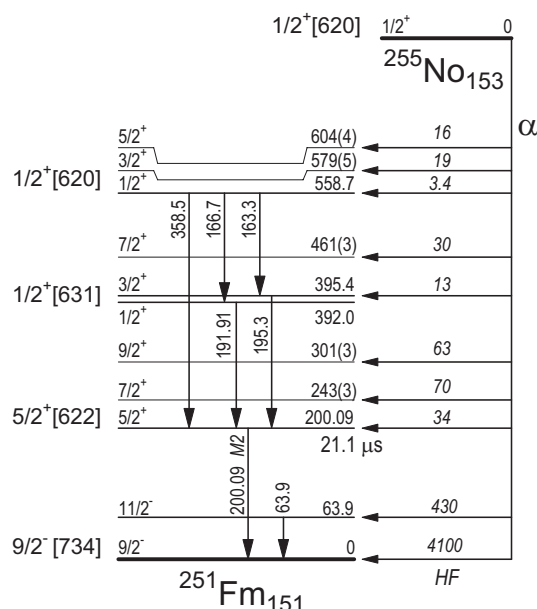


Fig. 2. Level scheme of ^{251}Fm established on the basis of the present and the previous α - γ coincidence results [4].

References

- [1] Y. Nagame, M. Asai, H. Haba, S. Goto, K. Tsukada, I. Nishinaka, K. Nishio, S. Ichikawa, A. Toyoshima, K. Akiyama, H. Nakahara, M. Sakama, M. Schädel, J. V. Kratz, H. W. Gäggeler and A. Türler, *J. Nucl. Radiochem. Sci.* 3 (2002) 85.
- [2] C. E. Bemis, Jr., D. C. Hensley, P. F. Dittner, C. D. Goodman and R. J. Silva, *ORNL-4706* (1971) 62.
- [3] F. P. Heßberger, S. Hofmann, D. Ackermann, S. Antalic, B. Kindler, I. Kojouharov, P. Kuusiniemi, M. Leino, B. Lommel, R. Mann, K. Nishio, A. G. Popeko, B. Sulignano, S. Saro, B. Streicher, M. Venhart and A. V. Yeremin, *Eur. Phys. J. A* 29 (2006) 165.
- [4] M. Asai, K. Tsukada, H. Haba, A. Toyoshima, T. Ishii, Y. Nagame, I. Nishinaka, T. Ichikawa, Y. Kojima and K. Sueki, *JAEA-Review* 2006-029 (2006) 41.

This is a blank page

CHAPTER 3

Nuclear Reactions

- 3.1 Direct Measurement of the Astrophysical Nuclear Reaction Rate of the ${}^8\text{Li}(\text{d}, \text{t}){}^7\text{Li}$ Reaction
- 3.2 Measurement of Spectroscopic Factor & Spin-Parity on ${}^{62}\text{Ni}(\text{d}, \text{p}){}^{63}\text{Ni}^*$ Reaction in Inverse Kinematics
- 3.3 Measurement of Quasi-Elastic Backscattering for ${}^{64}\text{Ni} + {}^{118}\text{Sn}$
- 3.4 Quasi-Elastic Backward Scattering in ${}^{76}\text{Ge} + {}^{208}\text{Pb}$, ${}^{209}\text{Bi}$
- 3.5 Measurement of Fission Cross-Sections for ${}^{34}\text{S} + {}^{238}\text{U}$
- 3.6 Correlation between α -Particle Emission and Fission in the ${}^{18}\text{O} + {}^{244}\text{Pu}$ Reaction

This is a blank page

3.1 DIRECT MEASUREMENT OF THE ASTROPHYSICAL NUCLEAR REACTION RATE OF THE ${}^8\text{Li}(d, t){}^7\text{Li}$ REACTION

H. ISHIYAMA¹, T. HASHIMOTO, Y.X. WATANABE¹, Y. HIRAYAMA¹, N. IMAI¹, M.H. TANAKA¹,
Y. FUCHI¹, N. YOSHIKAWA¹, H. MIYATAKE¹, S.C. JEONG¹, M. OKADA¹, S. ARAI¹,
H. KAWAKAMI¹, I. KATAYAMA¹, T. NOMURA¹, S. MITSUOKA, K. NISHIO, M. MATSUDA, A. OSA,
T.K. SATO, S. ICHIKAWA, H. IKEZOE, S.K. DAS², Y. MIZOI², T. FUKUDA² and T. SHIMODA³

The nuclear reactions via ${}^8\text{Li}$ are thought to play important roles for nucleosynthesis at the early stage of rapid neutron capture (r-) process [1] and the early universe [2] in neutron-rich environment. A systematic study for astrophysical nuclear reaction rates via ${}^8\text{Li}$ is in progress at the tandem facility of JAEA. Excitation functions of ${}^8\text{Li}(d, p)$, (d, t) , (d, α) reactions have been measured. The ${}^8\text{Li}(d, t)$ and (d, α) reactions destroy ${}^8\text{Li}$ nuclei and prevent production of heavier elements than lithium. Direct measurements of these reactions were performed by M.J. Balbes et al. at University of Notre Dam [3]. But measured excitation functions did not cover the energy region of astrophysical interest. In this report, the excitation function and astrophysical nuclear reaction rate of the ${}^8\text{Li}(d, t)$ reaction in the interest energy region are presented.

The ${}^8\text{Li}$ beam provided at 7 different energies, $E_{\text{cm}} = 1.1, 1.0, 0.8, 0.7, 0.5, 0.4, 0.3$ MeV, by the Tokai Radioactive Ion Accelerator Complex (TRIAC) was irradiated on a $1.4 \mu\text{m}$ thick CD_2 foil. The typical intensity and the energy resolution of the ${}^8\text{Li}$ beam were 1×10^5 pps and 3%(FWHM), respectively. The detector system consisted of a ΔE -E telescope ($45\text{mm} \times 45\text{mm}$, a $43 \mu\text{m}$ thick double sided stripped Si detector and $375 \mu\text{m}$ thick Si detector), two Si detectors ($18\text{mm} \times 18\text{mm}$), two single stripped Si detectors ($50\text{mm} \times 50\text{mm}$) to detect reaction products, and a plastic scintillator to monitor the intensity of the ${}^8\text{Li}$ beam. The angular distributions of the reaction were obtained at 7 different energies. The total cross sections were determined taking into account the obtained angular distributions.

Figure 1 shows the measured excitation function of the ${}^8\text{Li}(d, t){}^7\text{Li}$ reaction. The present experiment provides the first data of the cross sections below $E_{\text{cm}} = 1.2$ MeV and covers almost all of the Gamow peaks from $T_9 = 1$ to 3. Unexpected large cross sections were observed around $E_{\text{cm}} = 0.8$ MeV. The large cross section may suggest the existence of one or more unknown excited states around 22.4 MeV in ${}^{10}\text{Be}$. Figure 2 shows the obtained

¹ Institute of Particle and Nuclear Studies, KEK

² Osaka Electro-Communication University

³ Osaka University

astrophysical reaction rate. It is about ten times larger than the expected one [3].

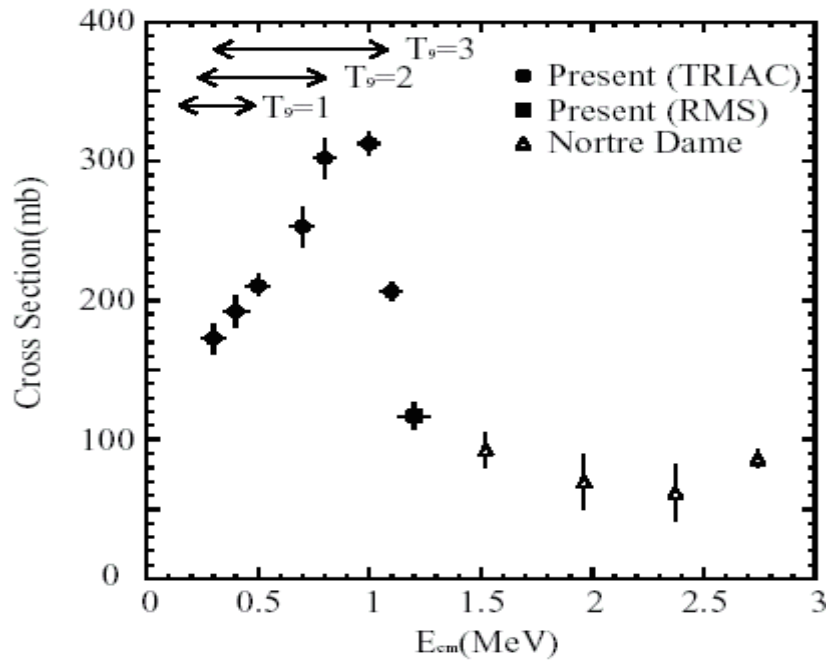


Fig.1. Excitation function of the ${}^8\text{Li}(d, t){}^7\text{Li}$ reaction. The closed circles and square show the present results. The square was obtained using the ${}^8\text{Li}$ beam provided by a recoil mass separator before operation of the TRIAC. The open triangles show the results by M.J. Balbes [3].

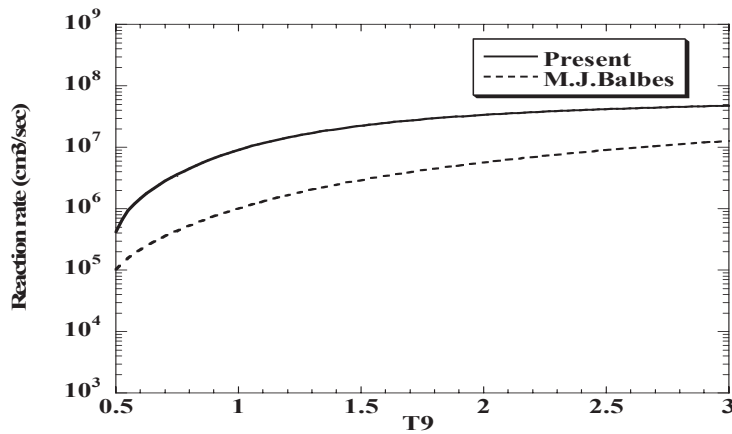


Fig.2. Reaction rate of the ${}^8\text{Li}(d, t){}^7\text{Li}$. The solid line shows the present result. The dashed line shows the expected rate by M.J. Balbes [3].

References

- [1] M. Terasawa, K. Sumiyoshi, T. Kajino, I. Tanihata, et al., Nucl. Phys. A688 (2001) 581c.
- [2] T. Kajino and R.N. Boyd, Astrophys. J. 359 (1990) 267.
- [3] M.J. Balbes, M.M. Farrell, R.N. Boyd, X. Gu, et al., Nucl. Phys. A584 (1995) 315.

3.2 MEASUREMENT OF SPECTROSCOPIC FACTOR & SPIN-PARITY ON $^{62}\text{Ni}(d,p)^{63}\text{Ni}^*$ REACTION IN INVERSE KINEMATICS

K.H. TSHOO¹, N. IMAI², S.C. JEONG², H. BHANG¹, S. CHOI¹, T. HASHIMOTO,
Y. HIRAYAMA², T. ISHII, H. ISHIYAMA², S. MITSUOKA,
H. MIYATAKE², K. NISHIO and Y.X. WATANABE²

The overproduction of Ni isotope has been a long standing problem in the calculation of s-process nucleosynthesis in massive star [1]. The origin of overproduction is considered to be due to the uncertainties in the nuclear physics input parameters such as MACS(Maxwellian averaged cross section) of the Ni isotope [2]. The largest overproduction in the survey by Rauscher *et al.* was ^{62}Ni [2]. In theoretical calculation on $^{62}\text{Ni}(n,\gamma)^{63}\text{Ni}^*$ reaction, nonresonant direct p-wave neutron capture process is dominant contribution. This contribution is entirely due to the capture in the $1/2^+$ state at $E_x=2.955$ MeV, where E_x indicates excited energy [3]. Recently, the neutron capture cross section of ^{62}Ni was measured at stellar energies [4]. However the predicted direct p-wave capture process was not observed [4].

Theoretical calculation was based on the nuclear structure data. The spectroscopic factor of the $1/2^+$ state of ^{63}Ni at $E_x=2.955$ MeV is determined by Anfinsen *et al.*(1970). Since the experimental angular distribution at $E_x=2.955$ MeV is very different from DWBA analysis, its spectroscopic factor and spin-parity are considered to be questionable.

In the present experiment, we have measured the angular distributions of the cross sections on $^{62}\text{Ni}(d,p)^{63}\text{Ni}$ reaction in the inverse kinematics by using CD_2 target at the JAEA tandem accelerator facility. The background protons were predicted to be produced by the fusion reaction with carbon in the CD_2 target. In order to estimate the background quantitatively, we performed another measurement with a C target. Through the comparison of the proton energy spectra with the CD_2 and carbon targets, the background can be removed. The $^{62}\text{Ni}^{13+}$ beam was accelerated up to 3.5 MeV/nucleon by the tandem accelerator. The thicknesses of CD_2 target was $130 \mu\text{g}/\text{cm}^2$. Figure 1 shows a schematic drawing of the experimental setup. Two SSD telescopes of $50 \times 50 \text{ mm}^2$ were mounted to detect recoiled particles. The angular regions covered by the telescopes were from 48.9 to 71.1 degrees and from 97.7 to 162.4 degrees in the laboratory frame, respectively. The forward telescope consisted of 0.325 mm-

¹ Seoul National University

² High Energy Accelerator Research Organization (KEK)

thick SSD and 16x16-channels doubly sided striped SSD of 1mm-thickness, while the backward telescope was composed of 16-channels singly sided stripped SSD of 65 μm -thickness and 0.325 mm thick SSD. In addition to the telescopes, we placed an annular type SSD of 0.3 mm thickness, which was divided to 10 strips along radial axis. This detector covered angular region from 13.6 to 36.8 degrees.

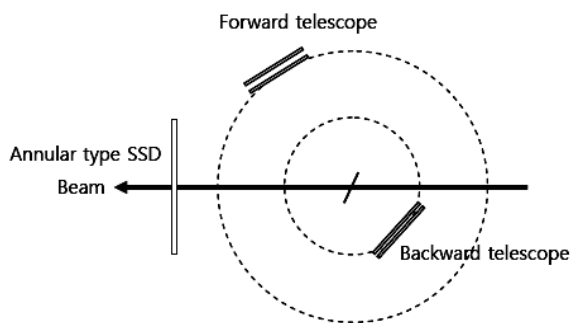


Fig1. A schematic view of the experimental setup

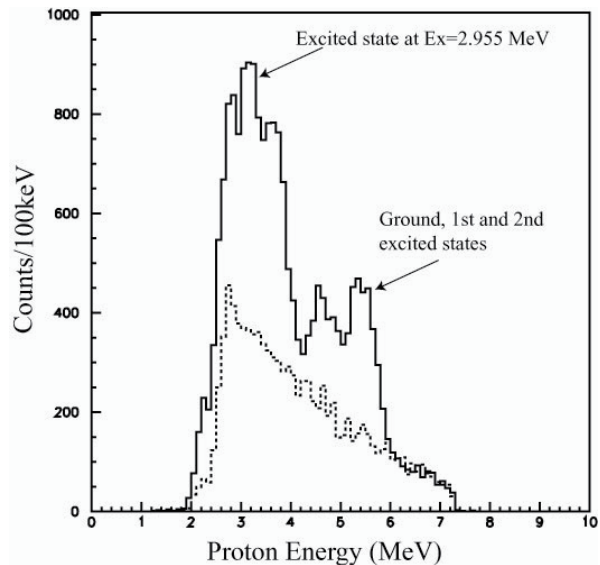


Fig2. Proton energy spectra measured by a strip of the backward telescope. See the text for details.

The solid line in Fig. 2 shows the proton energy spectrum measured by a strip of the backward telescope with the CD_2 target, while the dashed line indicates the spectrum with the carbon target normalized by the number of protons in the energy range from 6MeV to 8MeV. The shapes of solid line and dashed line are almost same above 6MeV. It is clearly seen that the tail of the CD_2 spectrum at higher energy region is background coming from the carbon. The spectroscopic factor and spin-parity of the excited state of ^{63}Ni at $E_x=2.955$ MeV will be determined through the DWBA analysis of the measured angular distribution of $^{62}\text{Ni}(d,p)^{63}\text{Ni}^*$.

References

- [1] F.X. Timmes, S.E. Woosley, and T.A. Weaver, *ApJS* 98 (1995) 617.
- [2] T. Rauscher, A. Heger, R.D. Hoffman, and S.E. Woosley, *ApJ* 576 (2002) 323.
- [3] T. Rauscher, and K.H. Guber, *Phys. Rev. C* 66 (2002) 028802.
- [4] A. Tomyo *et al.*, *ApJ* 623 (2005) L153.

3.3 MEASUREMENT OF QUASI-ELASTIC BACKSCATTERING FOR $^{64}\text{Ni}+^{118}\text{Sn}$

Y.X. WATANABE¹, S. MITSUOKA, K. NISHIO, S.C. JEONG¹, T. HASHIMOTO,
Y. HIRAYAMA¹, N. IMAI¹, H. ISHIYAMA¹, H. MIYATAKE¹ and H. IKEZOE

In the entrance channel of the fusion process, the projectile nucleus gets over a barrier generated by the Coulomb potential and the nuclear potential, and then is captured by the target nucleus. They undergo the non-equilibrium process, forming a compound nucleus or getting apart from each other as deep-inelastic scattering or quasi-fission. The entrance barrier may be modified by the tunnel effect, collective excitations, and nucleon transfer channels. The effect of collective excitations is well described by coupled channel formalism [1], but the effect of nucleon transfer channels still remains an open question. The fusion cross sections of $^{40}\text{Ca}+^{96}\text{Zr}$ were measured at the Laboratori Nazionali di Legnaro, and they showed an extraordinary enhancement than those of $^{40}\text{Ca}+^{90}\text{Zr}$ at energies below the Coulomb barriers [2]. It was suggested due to the neutron transfer channels with positive Q-values. However, in the fusion-evaporation cross sections for the systems of $^{132}\text{Sn}+^{64}\text{Ni}$ and $^{124}\text{Sn}+^{64}\text{Ni}$ measured at Oak Ridge National Laboratory [3], the former did not show any enhancements of the cross sections although it has 5 neutron stripping channels with positive Q-values.

In order to investigate a possible effect of neutron transfer channels on fusion reactions, we intended to deduce the barrier distributions by detecting quasi-elastic backscattering for two combinations of isotopes which form the same compound nucleus in the fusion reaction; one has several neutron transfer channels with positive Q-values and the other has no channels. Comparing the barrier distributions and fusion excitation functions between the two systems would give information about the effect of the neutron transfer channels on the process before the collision and on the non-equilibrium process after the collision in the fusion reaction. We adopted the two systems of $^{64}\text{Ni}+^{118}\text{Sn}$ and $^{58}\text{Ni}+^{124}\text{Sn}$, which form the same compound nucleus ^{182}Pt . The former has no neutron transfer channels with positive Q-values, while the latter has 9 channels. The fusion excitation functions of them have been measured [4], so we can compare them with the deduced barrier distributions.

In FY2006, we performed the measurement for the system of $^{64}\text{Ni}+^{118}\text{Sn}$. Using the tandem accelerator and the superconducting booster linac, ^{64}Ni beams were accelerated,

¹ High Energy Accelerator Research Organization (KEK)

and impinged on the ^{118}Sn target, which were made on the carbon film by sputtering method with the thickness of about $100 \mu\text{g}/\text{cm}^2$. The quasi-elastic backscattered particles were detected by solid state detectors located at angles of 162° and 172° to the beam direction. Varying the voltages of the superconducting booster linac, beam energies were altered between 215 and 260 MeV by 1.5 MeV step. Correcting the centrifugal potential for each energy and each angle, the excitation function of the quasi-elastic backscattering for 56 incident energies was obtained and the barrier distribution was deduced from the first order derivative of the excitation function. Figure 1 shows the differential quasi-elastic cross sections relative to Rutherford and the barrier distribution.

The barrier distribution of $^{64}\text{Ni}+^{118}\text{Sn}$ has an extent corresponding to the estimation from the Stelson model [5], which is a phenomenological one dealing with the effect of the neutron transfer channels. The result suggests no large contribution of the neutron transfer channels to the entrance channel of the fusion reaction for that system. In FY2007, we will perform the measurement for the system of $^{58}\text{Ni}+^{124}\text{Sn}$ where 9 neutron transfer channels have positive Q-values, and compare the barrier distributions and fusion cross sections between two systems.

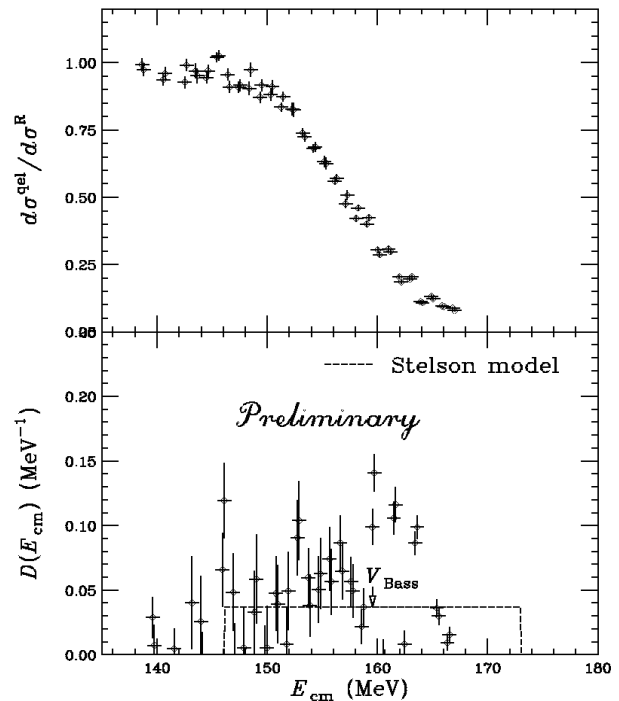


Fig. 1. The ratio of the differential quasi-elastic scattering cross sections relative to Rutherford ($d\sigma^{\text{qel}}/d\sigma^{\text{R}}$) (upper panel) and deduced barrier distribution ($D(E_{\text{cm}})$) (lower panel) for $^{64}\text{Ni}+^{118}\text{Sn}$. The abscissa indicates the energy in the center-of-mass system. Dashed line shows the barrier distribution from the Stelson model [5].

References

- [1] C.H. Dasso et al., Nucl. Phys. A405 (1983) 381.
- [2] H. Timmers et al., Phys. Lett. B399 (1997) 35.
- [3] J.F. Liang et al., Phys. Rev. Lett. 96 (2006) 029903.
- [4] K.T. Lesko et al., Phys. Rev. C34 (1986) 2155.
- [5] P.H. Stelson, Phys. Lett. 205 (1988) 190.

3.4 QUASI-ELASTIC BACKWARD SCATTERING IN $^{76}\text{Ge}+^{208}\text{Pb}$, ^{209}Bi

S. MITSUOKA, H. IKEZOE, K. NISHIO, S.C. JEONG¹ and Y.X. WATANABE¹

Coulomb barrier distribution in heavy-ion reaction gives us important information about the interaction potential for nucleus-nucleus collision. Especially, the barrier height is a key quantity for the synthesis of super-heavy elements by cold fusion reactions, because the incident energy is selected in the vicinity of the Coulomb barrier. Up to now, the Bass potential has been frequently used to estimate the Coulomb barrier height. However, there is no experimental evidence that the Bass barrier height is applicable to such massive projectile and target systems. The Coulomb barrier distribution could be experimentally derived from quasi-elastic (QE) scattering measured at backward angles of nearly 180 degree, where head-on collision is dominant. We adopted this method in the reactions of $^{76}\text{Ge}+^{208}\text{Pb}$ and $^{76}\text{Ge}+^{209}\text{Bi}$, relating to Pb/Bi-based cold fusion for the production of super-heavy elements $Z=114$ and 115 , respectively.

Enriched targets of ^{208}Pb and ^{209}Bi in the form of a strip (3 mm width in horizontal plane) were bombarded by ^{76}Ge beam from the tandem-booster accelerator in the energy steps of 1.5 MeV. The backward QE scattering was detected by solid state detectors at the laboratory angles of 172° , -168° and 162° , and the Rutherford scattering was monitored at $\pm 45^\circ$ with respect to the beam axis. Here the negative sign means the counterclockwise rotation in the reaction plane. The barrier distributions were obtained by taking the first derivative of the QE excitation function $\sigma_{\text{QE}}(E)$ relative to the Rutherford scattering $\sigma_{\text{R}}(E)$, that is $-d\{\sigma_{\text{QE}}(E)/\sigma_{\text{R}}(E)\}/dE$. Detailed analysis is in progress for QE cross sections where deep-inelastic scattering should be excluded by considering the reaction Q-values of inelastic and transfer channels.

We have systematically extracted the barrier distributions in ^{48}Ti , ^{54}Cr , ^{56}Fe , ^{64}Ni and $^{70}\text{Zn}+^{208}\text{Pb}$ relating to cold fusion for $Z=104$, 106 , 108 , 110 and 112 , respectively. It was found that the mean values of the barrier distributions showed a deviation from the Bass barrier height by amount of 4-7 MeV toward the low energy side. It has been considered so far that the extensively small cross sections of super-heavy elements synthesized at GSI and RIKEN were due to the entrance channel effect, because the excitation functions of one-neutron (1n) evaporation channel had the peak below the Bass barrier. However, the present data show the 1n peak position is not in the sub-barrier region. In $^{48}\text{Ti}+^{208}\text{Pb}$, for intense, 1n channel is just on the barrier, so the excitation function is sharply cut in the lower energy side. As the projectile becomes heavier, the 1n peak position locates in higher side of the present barrier distributions and the excitation function becomes a bell shape. Even 0n channel would be opened in ^{70}Zn and ^{76}Ge projectile cases. This suggests a new possibility for future experiments of super-heavy synthesis by radiative-capture in cold fusion.

¹ High Energy Accelerator Research Organization (KEK)

3.5 MEASUREMENT OF FISSION CROSS-SECTIONS FOR $^{34}\text{S} + ^{238}\text{U}$

K. NISHIO, H. IKEZOE, S. MITSUOKA, Y. WATANABE¹, I. NISHINAKA,
T. OHTSUKI², Y. NAGAME and K. TSUKADA

Understanding of the fusion reactions using actinide target nuclei is important for the synthesis of superheavy nuclei (SHN). Because of the prolate deformation of actinide nuclei, Coulomb barrier height depends on the incident angle of the projectile to the symmetric axis of the target. By bombarding rather light projectiles at subbarrier energies, where contact at polar side of target nucleus occurs, new isotopes ^{264}Sg and ^{270}Hs were produced in the reactions of $^{30}\text{Si} + ^{238}\text{U}$ [1] and $^{26}\text{Mg} + ^{248}\text{Cm}$ [2], respectively. Formation of the compound nucleus may be sensitive to the orientation of the deformed target nuclei when projectile is much heavier, and the possible advantage of the equatorial collisions to form the compound nucleus is discussed in the reactions of ^{48}Ca beam and actinide targets [3]. To understand the fusion mechanism and to predict cross-sections producing SHN, measurement of capture cross-sections is important. For reactions leading to the fissile compound nucleus, the capture cross-section is approximated to the fission cross-section.

We have measured the fission cross-sections for $^{34}\text{S} + ^{238}\text{U}$. The measurement is motivated by the possible production of a new isotope ^{268}Hs as 4n channel in the subbarrier fusion reaction. This reaction is also important to study the systematic behavior of the orientation effects in fusion, which should depend on the projectile mass.

The experiment was performed at JAEA tandem accelerator. Two fission fragments are detected in coincidence by using two parallel plate avalanche counters (PPACs) located on both sides of the uranium target. The detector has sensitive area of 200 mm \times 120 mm. The ^{238}U target with thickness of 100 $\mu\text{g}/\text{cm}^2$ was prepared by electrically depositing natural uranium on a nickel foil of 90 $\mu\text{g}/\text{cm}^2$ thick.

We have measured the time difference between the signals from two PPACs, charge

¹ High Energy Accelerator Research Organization

² Institute for Nuclear Physics, Tohoku University

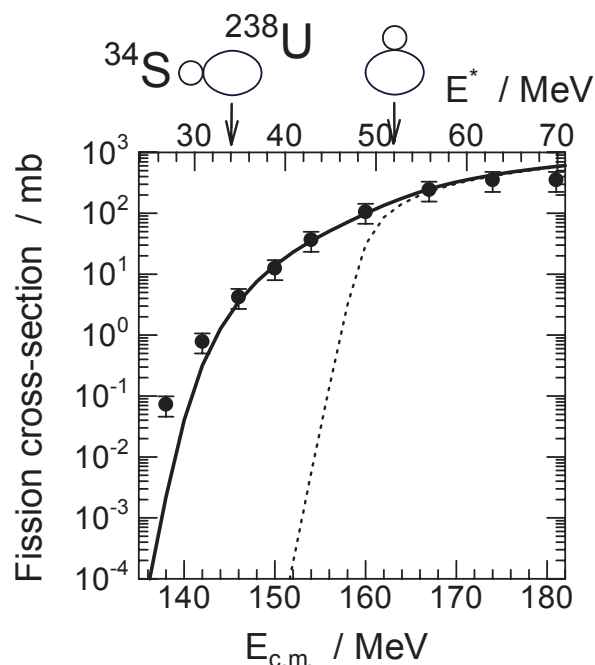


Fig. 1 Fission cross-sections for $^{34}\text{S} + ^{238}\text{U}$ as a function of c.m. energy. Excitation energy E^* of the compound nucleus ^{272}Hs is also shown in the upper abscissa. The Coulomb barrier height corresponding to the two extreme touching configurations are shown by arrows on the upper

in the PPACs induced by the fragments, and the emission angle of the fragments (θ_1 and θ_2) relative to the beam axis. Fission fragments are separated from other reaction products such as scattered projectiles, recoiled targets, and other light particles. The cross-section was determined by detecting the elastically scattered projectiles by a silicon detector located at an angle 29° to the beam axis.

The experimental results are shown in Fig. 1 as a function of center-of-mass energy. The solid curve is the results of the coupled-channel (CC) calculation [4] which takes into account the prolate deformation of ^{238}U , $(\beta_2, \beta_4) = (0.275, 0.05)$ [1,5]. In this calculation, couplings to the 2^+ state in ^{34}S (2.13 MeV) and 3^- state in ^{238}U (0.73 MeV) are also included [6]. The one-dimensional barrier penetration model, where the deformation of ^{238}U and couplings to the vibrational states of the nuclei are ignored, is also shown by the dotted curve.

The CC calculation reproduces the experimental data well except the extremely deep sub-barrier energy of $E_{c.m.} < 145$ MeV, and shows large enhancement of the cross-section relative to the one-dimensional model due to the lowering of the Coulomb barrier at polar collisions. Large enhancement of the cross-section at sub-barrier energies suggests the possible production of the new isotope ^{268}Hs around $E_{c.m.} = 150$ MeV ($E^* = 40$ MeV).

References

- [1] K. Nishio, S. Hofmann, F.P. Hessberger, D. Ackermann, S. Antalic, V.F. Comas, Z. Gan, S. Heinz, J.A. Heredia, H. Ikezoe, J. Khuyagbaatar, B. Kindler, I. Kojouharov, P. Kuusiniemi, B. Lommel, R. Mann, M. Mazzocco, S. Mitsuoka, Y. Nagame, T. Ohtsuki, A.G. Popeko, S. Saro, H.J. Schoett, B. Sulignano, A. Svirikhin, K. Tsukada, K. Tsuruta, A.V. Yeremin, *Eur. Phys. J. A* 29, 281 (2006).
- [2] J. Dvorak, W. Bröchle, M. Chelnokov, R. Dressler, Ch.E. Düllmann, K. Eberhardt, V. Gorshkov, E. Jäger, R. Krücken, A. Kuznetsov, Y. Nagame, F. Nebel, Z. Novackova, Z. Qin, M. Schädel, B. Schausten, E. Schimpf, A. Semchenkov, P. Thörle, A. Tüler, M. Wegrzacki, A. Yakushev, A. Yeremin, *Phys. Rev. Lett.* 97, 242501 (2007).
- [3] Yu.Ts. Oganessian, *J. Phys. G* 34, R165 (2007).
- [4] K. Hagino (unpublished). The code is based on the CCFULL code. K.Hagino *et al.*, *Computer Phys. Comm.* 123, 143 (1999).
- [5] K. Nishio, H. Ikezoe, Y. Nagame, M. Asai, K. Tsukada, S. Mitsuoka, K. Tsuruta, K. Satou, C.J. Lin, T. Ohsawa, *Phys. Rev. Lett.* 93, 162701 (2004).
- [6] R.B. Firestone and V.S. Shirley, Edt. *Table of Isotopes*, Eighth Edition, Vol. 1 and 2 John Wiley and Sons, Inc., New York, 1996.

3.6 CORRELATION BETWEEN α -PARTICLE EMISSION AND FISSION IN THE $^{18}\text{O} + ^{244}\text{Pu}$ REACTION

I. NISHINAKA, M. TANIKAWA¹, Y. NAGAME, M. ASAI, K. TSUKADA,
A. TOYOSHIMA, Y. KASAMATSU, K. NISHIO and A. YOKOYAMA²

The incomplete fusion reaction makes it possible to study the fission of nuclides that are not produced in other reactions. However, the process of the incomplete fusion reaction is not yet completely understood. In our previous work for the 103 and 113 MeV $^{18}\text{O} + ^{244}\text{Pu}$ reactions [1], it was found that the nuclear fission of ^{258}Fm at several excitation energies could be studied via the incomplete fusion reaction of $^{244}\text{Pu}(^{18}\text{O}, \alpha)^{258}\text{Fm}$ by measuring fission fragments in coincidence with α -particles. The α -particle spectra measured in coincidence with fission fragments at a forward angle of 20 deg. to the beam direction suggest that the preequilibrium α -particle emission in the incomplete fusion reaction plays an important role. In this work, we have experimentally determined the probabilities of the α -particle emission in both the incomplete fusion reaction $^{244}\text{Pu}(^{18}\text{O}, \alpha)^{258}\text{Fm}$ and the complete fusion reaction $^{18}\text{O} + ^{244}\text{Pu}$ by measuring α -particle spectra in coincident with fission fragments at both forward and backward angles to the beam direction.

In the 103 MeV $^{18}\text{O} + ^{244}\text{Pu}$ reaction, light charged particles including α -particles were measured in coincidence with fission fragments by two ΔE - E telescopes. Figure 1 shows a schematic view of the experimental setup. The ΔE - E telescopes set at angles of 20 and 160 deg. to the beam direction have respective solid angles of 0.49 msr and 0.12 msr. Each ΔE - E telescope consists of 30 μm and 2 mm thick silicon surface barrier detectors. Fission fragments were measured by position sensitive parallel plate avalanche counters PPAC. A Faraday cup is located at the end of the beam line.

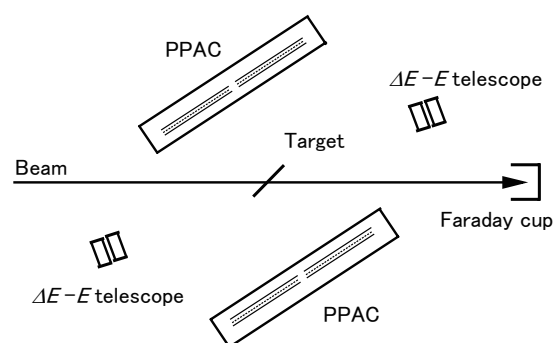


Fig. 1. The experimental setup.

In Fig. 2 α -particle spectra are shown as a function of energy in the center-of-mass system by solid circles for “single” events and open circles for “coincident” events. No α -particles in coincident with fission fragments was observed by the ΔE - E telescope located at the angle of 160 deg. to the beam direction. A limit of the probability of α -particle emission from the compound nucleus in the complete fusion reaction of 103 MeV $^{18}\text{O} + ^{244}\text{Pu}$ has been determined to be less than 0.6 mb. These results obviously show that the α -particle spectrum measured in coincident with fission fragments by the ΔE - E telescope at the angle of 20 deg. originates only from the α -particle emission in the incomplete fusion reaction of $^{244}\text{Pu}(^{18}\text{O}, \alpha)^{258}\text{Fm}$. Because the α -particles evaporated from the compound nucleus emit isotropically in the center-of-mass system while those from the incomplete fusion-fission reaction emit at forward angles to the beam direction [2].

¹University of Tokyo

²Kanazawa University

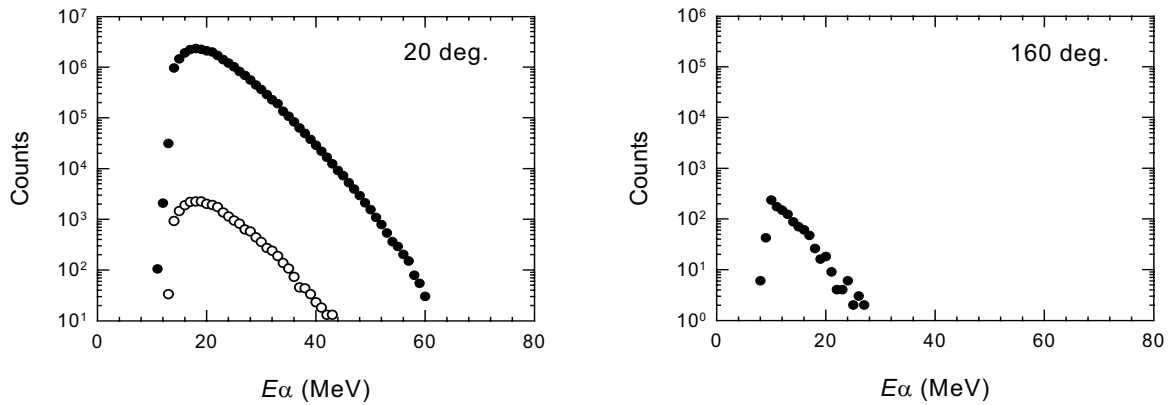


Fig. 2. α -particle energy spectra measured at 20 and 160 deg. to the beam direction in the 103 MeV $^{18}\text{O} + ^{244}\text{Pu}$ reaction. Solid and open circles show “single” and “coincident” events, respectively.

References

- [1] I. Nishinaka, M. Tanikawa, Y. Nagame, M. Asai, K. Tsukada, A. Toyoshima, T. Ichikawa and A. Yokoyama, JAEA-Review 2006-029 (2006) 49.
- [2] W. Augustyniak, C. Borcea, M. Lewitowicz, N. Hoai Chau, Yu. E. Penionzhkevich, V. G. Sandukovski, M. Sowinski and S. Chojnacki, Z. Phys. A 332 (1989) 209.

This is a blank page

CHAPTER 4

Nuclear Chemistry

- 4.1 Trioctylphosphine Oxide (TOPO) Reversed-Phase Chromatography of Rutherfordium in HCl
- 4.2 Development of an Electrochemistry Apparatus for the Heaviest Elements
- 4.3 Elution Curves of Nb and Ta in Anion-Exchange Chromatography with HF/HNO₃ Solutions
- 4.4 Production of RI Tracers for Chemistry of Transactinide Elements
- 4.5 Radioisotopes Incorporation in Fullerenes by Using Nuclear Recoil

This is a blank page

4.1 TRIOCTYLPHOSPHINE OXIDE (TOPO) REVERSED-PHASE CHROMATOGRAPHY OF RUTHERFORDIUM IN HCl

A. TOYOSHIMA, Y. KASAMATSU, K. TSUKADA, M. ASAI, Y. ISHII, H. TOUME, T.K. SATO, I. NISHINAKA, Y. NAGAME, H. HABA¹, K. AKIYAMA², Y. OURA², S. GOTO³, H. KUDO³, K. OOE⁴, A. SHINOHARA⁴ and K. SUEKI⁵

Previously we studied anion-exchange behavior of rutherfordium (Rf) in 4.0 - 11.5 M HCl solutions together with its homologues Zr and Hf using the automated ion-exchange separation apparatus coupled with the detection system for alpha spectroscopy (AIDA) [1]. The adsorption probabilities of Rf on the anion-exchange resin increased beyond 7.0 M HCl and the sequence of those among the group-4 homologues was $Rf \geq Zr > Hf$. The EXAFS study of Zr and Hf in HCl and those on the anion-exchange resin equilibrated with HCl verified that the adsorption onto the resin is based on the chloride complexation in HCl [2], suggesting that the chloride complexation of Rf is stronger than that of the homologues. Recently, we investigated the tributylphosphate (TBP) extraction behavior of Rf, Zr, and Hf in 7.0 - 8.0 M HCl using a reversed-phase chromatography technique [3]. The extraction trend among the elements was $Zr > Hf \geq Rf$ which is different from the sequence found in the anion-exchange study. It was suggested that the stability of the TBP complex of Rf tetrachloride is lower than those of Zr and Hf. In the present study, we performed the trioctylphosphine oxide (TOPO) reversed-phase chromatography of Rf, Zr, and Hf in 2.0 - 7.0 M HCl in order to further investigate extraction of Rf from HCl into phosphorous-bonded-oxygen extractants. TOPO has the phosphorous oxygen, which solvates to neutral chloride-complexes, with higher electronegativity than that of TBP.

The isotopes ²⁶¹Rf (78 s) and ¹⁶⁹Hf (3.42 min) were produced in the ²⁴⁸Cm(¹⁸O,5n) and ^{152enrich}Gd(¹⁸O,xn) reactions at the JAEA tandem accelerator. We produced the ¹⁶⁹Hf isotope for monitoring the chemical yield and extraction probabilities during repetitive chromatographic experiments. Reaction products were transported by a He/KCl gas-jet technique to the chemistry laboratory and deposited onto the collection site of AIDA. After the collection, products were dissolved with hot 11.5 M HCl and were subsequently fed onto the TOPO reversed-phase column of 1.6 mm i.d. × 7.0 mm long. The effluent from the column was discarded. Then, 2.0, 3.5, 5.0, or 7.0 M HCl was fed into the column and the effluent was collected on a Ta disc as fraction 1 with preparation by evaporation to dryness for α -spectrometry. A fraction of the products adsorbed on the column was then stripped with the 2.0 M HCl. The effluent was collected on another Ta disc as fraction 2 and was evaporated to dryness. The pair of discs was then subjected to α -spectrometry with 600 mm² PIPS detectors. Elution behavior of ⁸⁵Zr (7.86 min) and ¹⁶⁹Hf produced simultaneously by the ^{nat}Ge(¹⁸O,xn) and ^{nat}Gd(¹⁸O,xn) reactions, respectively, in 2.0 - 10 M HCl were also measured in separate experiments under the same conditions as those of ²⁶¹Rf and ¹⁶⁹Hf.

Figure 1 shows the variations of the percent extraction (%Ext) of Rf, Zr, and Hf as a function

¹ The Institute of Physical and Chemical Research (RIKEN)

² Tokyo Metropolitan University

³ Niigata University

⁴ Osaka University

⁵ University of Tsukuba

of HCl concentration. The %Ext values are evaluated using the equation of $\%Ext = 100 \times A_2 / (A_1 + A_2)$ where A_1 and A_2 represent radioactivities in fractions 1 and 2, respectively. The %Ext values of Rf, Zr, and Hf are plotted by closed circles, open triangles, and open squares, respectively, and the Cm/Gd and Ge/Gd in parenthesis show the targets used in the experiments. The %Ext values of the three elements similarly increase in the range of 2.0 - 7.0 M HCl which is lower than that for the TBP extractions of 7.0 - 8.0 M. It suggests that the phosphorous oxygen of TOPO with high electronegativity solvates to neutral chloride-complexes of Rf, Zr, and Hf even in dilute HCl and the resulting solvated complexes are extracted into the organic TOPO phase. On the other hand, the extraction trend into TOPO among the homologues is the same as that into TBP: $Zr > Hf \geq Rf$, suggesting that the stability of TOPO complex of Rf tetrachloride is also weaker than that of homologues.

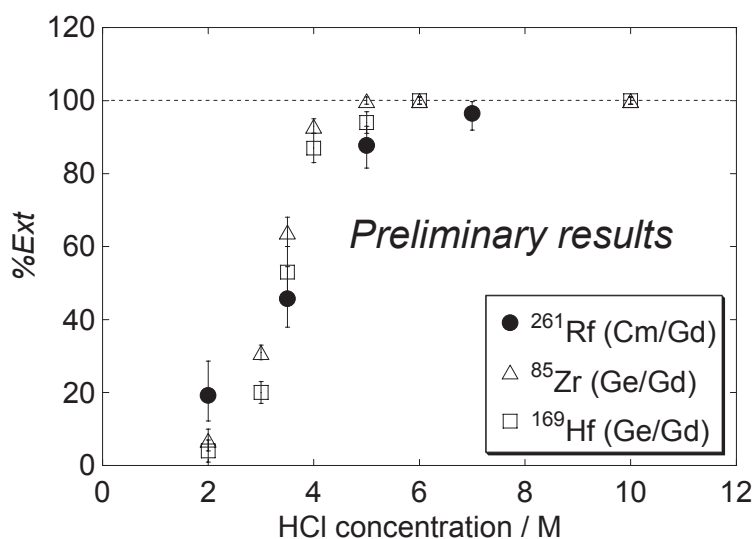


Fig. 1. Variations of percent extraction (%Ext) of Rf, Zr, and Hf into TOPO from HCl.

References

- [1] H. Haba, K. Tsukada, M. Asai, S. Goto, A. Toyoshima, I. Nishinaka, K. Akiyama, M. Hirata, S. Ichikawa, Y. Nagame, Y. Shoji, M. Shigekawa, T. Koike, M. Iwasaki, A. Shinohara, T. Kaneko, T. Maruyama, S. Ono, H. Kudo, Y. Oura, K. Sueki, H. Nakahara, M. Sakama, A. Yokoyama, J. V. Kratz, M. Schädel and W. Bröchle, *J. Nucl. Radiochem. Sci.* 3, (2002) 143.
- [2] H. Haba, K. Akiyama, K. Tsukada, M. Asai, A. Toyoshima, T. Yaita, M. Hirata, K. Sueki and Y. Nagame to be submitted.
- [3] H. Haba, K. Tsukada, M. Asai, A. Toyoshima, Y. Ishii, H. Toume, T. Sato, I. Nishinaka, T. Ichikawa, S. Ichikawa, Y. Nagame, W. Sato, K. Matsuo, Y. Kitamoto, Y. Tashiro, A. Shinohara, J. Saito, M. Ito, T. Ikezawa, M. Sakamaki, S. Goto, H. Kudo, H. Kikunaga, M. Arai, S. Kamataki, A. Yokoyama, K. Akiyama, K. Sueki, Y. Oura, M. Schädel, W. Bröchle and J. V. Kratz, *Radiochim. Acta*, 95 (2007) 1.

4.2. DEVELOPMENT OF AN ELECTROCHEMISTRY APPARATUS FOR THE HEAVIEST ELEMENTS

A. TOYOSHIMA, Y. KASAMATSU, Y. KITATSUJI, K. TSUKADA, H. HABA¹,
A. SHINOHARA² and Y. NAGAME

It is of great importance to study oxidation states of the heaviest atoms and to determine the oxidation-reduction (redox) potential in aqueous solution. The heaviest elements placed at *d*- and *f*-transition blocks of the periodic table are expected to take various oxidation states. Theoretical calculations predict that oxidation states and redox potentials of the heaviest atoms are influenced by relativistic effects [1]. Thus, electrochemical properties of the heaviest elements will give valuable information on the relativistic effects. However, an electric current originated from a redox reaction of the heaviest element is not measurable because of an atom-at-a-time situation. Thus, we fabricated an electrochemistry apparatus combined with a chromatographic separation technique available even to single atoms. In this report, development of the electrochemistry apparatus is presented.

Figure 1 shows a schematic diagram of the electrochemistry apparatus, which is based on the electrolytic cell [2, 3]. A solution containing the heaviest elements is fed from the inlet, passes through the working electrode made by glassy carbon fibers which are packed into a vycor-glass tube, and flows out of the outlet. The surface of the fibers is chemically modified with a polyelectrolyte material of Nafion perfluorinated ion-exchange resin [4, 5], so that the working electrode works just as the cation-exchange column. Ions are oxidized on the electrode according to their redox potentials, and the resulting oxidized species are separated from non-oxidized species by cation-exchange chromatography.

Test experiments were performed for an oxidation reaction of ^{139}Ce of 10^{10} atoms using the electrochemistry apparatus. Elution behavior of the ^{139}Ce radiotracer from the chemically-modified electrode with applied potentials of 0.2 - 1.0 V versus an Ag-AgCl reference electrode was investigated together with ^{88}Y , ^{88}Zr , and ^{175}Hf in 0.1 M ammonium α -hydroxyisobutyric acid (α -HIB) solution. In the applied potential of 0.2 V, elution of ^{139}Ce followed that of ^{88}Y . This elution behavior of ^{139}Ce shows that Ce is bound in the most stable trivalent state. In higher potentials of 1.0 V, ^{139}Ce was sooner eluted, which is similar to the behavior of ^{88}Zr and ^{175}Hf . It indicates that ^{139}Ce exists as a tetravalent ion. In the middle potentials of 0.6 - 0.8 V, elution behavior of ^{139}Ce was varied from that of Ce^{3+} to that of Ce^{4+} around 0.75 V. The electric potential of 0.75 V is almost equal to that determined by cyclic voltammetry of 0.001 M Ce in 0.1 M α -HIB. These results show that ^{139}Ce in the trivalent state is successfully oxidized to the tetravalent one using the present apparatus on a tracer

¹ The Institute of Physical and Chemical Research (RIKEN)

² Osaka University

scale. Electrochemical oxidation of nobelium will be performed in the near future.

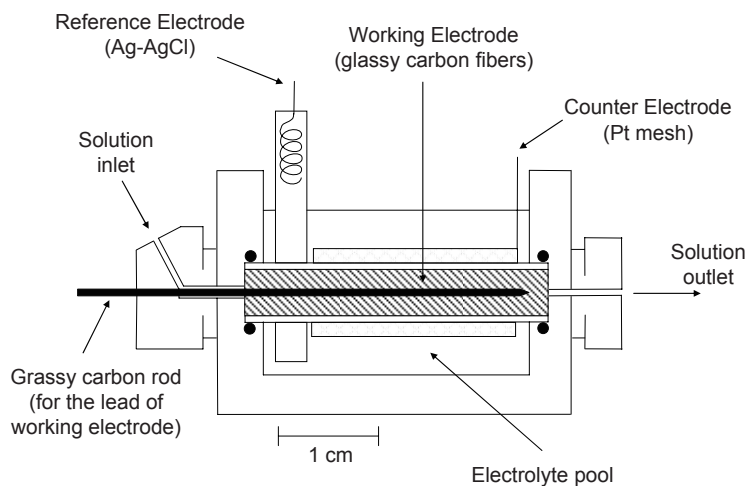


Fig. 1. Schematic diagram of an electrochemistry apparatus developed.

References

- [1] V. Pershina, *Theoretical Chemistry of the Heaviest Elements*, In *The Chemistry of Superheavy Elements*, Ed.M. Schädel, Kluwer Academic publishers, Dordrecht, 2003, p31.
- [2] S. Kihara, Z. Yoshida, H. Muto, H. Aoyagi, Y. Baba and H. Hashitani, *Anal. Chem.* 52 (1980) 1601.
- [3] H. Aoyagi, Z. Yoshida and S. Kihara, *Anal. Chem.* 59 (1987) 400.
- [4] C. R. Martin and H. Freiser, *Anal. Chem.* 53 (1981) 902.
- [5] M. W. Espensheid, A.R. Ghatak-Roy, R.B. Moore III, R.M. Penner, M.N. Szentirmay and C.R. Martin, *J. Chem. Soc., Faraday Trans. 1*, 82 (1986) 1051.

4.3 ELUTION CURVES OF Nb AND Ta IN ANION-EXCHANGE CHROMATOGRAPHY WITH HF/HNO₃ SOLUTIONS

Y. KASAMATSU, A. TOYOSHIMA, K. TSUKADA, M. ASAI, H. HABA¹, Y. ISHII, H. TOUME, I. NISHINAKA, K. AKIYAMA², M. SAKAMA³, H. KIKUNAGA¹, W. SATO⁴, K. OOE⁴, T. KURIBAYASHI⁴, A. SHINOHARA⁴, S. GOTO⁵, T. ISHIKAWA⁵, H. KUDO⁵, N. KINOSHITA⁶, M. ARAI⁶, A. YOKOYAMA⁶, T.K. SATO, K. SUEKI⁷ and Y. NAGAME,

The aqueous phase chemistry of the group-5 elements Nb, Ta, and element 105 (dubnium, Db) has been studied with chromatographic methods, and the similarity of the chemical behavior of Db to those of its lighter homologues has been discussed [1–3]. For a deeper understanding of the chemical property of Db, more detailed chemical studies are required. For systematic investigation of the fluoride complexation of Db as a function of the fluoride ion concentration, we previously studied anion-exchange behavior of the homologues Nb, Ta, and the pseudo homologue Pa in HF/HNO₃ media by a batch method [4]. In the present work, we studied elution curves of Nb and Ta by the on-line anion-exchange technique to find suitable conditions for the experiment of Db.

Niobium-90 and ¹⁷⁸Ta were produced in the ^{nat}Zr(*p*, *xn*) and ^{nat}Hf(*p*, *xn*) reactions, respectively, at the JAEA tandem accelerator. Niobium-88 and ¹⁷⁰Ta were also produced in the ^{nat}Ge(¹⁹F, *xn*) and ^{nat}Gd(¹⁹F, *xn*) reactions, respectively. The reaction products were continuously transported by a He/KCl gas-jet system to the collection site of the automated ion-exchange separation apparatus coupled with the detection system for alpha-spectroscopy (AIDA). After collection for 1–5 min, the products were dissolved in various concentrations of HF/HNO₃ solutions (0.01–5 M HF/0.04–0.6 M HNO₃) and the solution was then fed onto the column ($\phi 1.0 \times 3.5$ mm) filled with the anion-exchange resin MCI GEL CA08Y (particle size of 25 μ m) at a flow rate of 1.2 mL/min. The effluent fractions were collected in 7 polyethylene tubes. Remaining Nb and Ta on the resin were stripped with 0.015 M HF/6 M HNO₃ and collected in another tube. Gamma-ray measurements were performed for the tubes with a Ge detector to observe elution curves of Nb and Ta in the anion-exchange chromatography.

The four product nuclides ^{88, 90}Nb and ^{170, 178}Ta were assigned by the γ -ray spectroscopy on the basis of γ -ray energies and half-lives. The elution curves of Nb and Ta were obtained and those for 0.31 M HF/0.1 M HNO₃ and 0.89 M HF/0.3 M HNO₃ are shown in Fig 1. Distribution coefficients, K_d , were obtained by fitting the Glueckauf equation [5] to the data as shown by the solid elution curves in Fig. 1. The obtained K_d values and their dependence on [F⁻] and [NO₃⁻] agree with those obtained in the previous batch-wise experiments [4] as depicted in Fig. 2. It is found that the anion-exchange behavior of Nb and Ta observed in the

¹Nishina Center for Accelerator Based Science, RIKEN

²Graduate School of Science and Engineering, Tokyo Metropolitan University

³School of Health Sciences, University of Tokushima

⁴Graduate School of Science, Osaka University

⁵Faculty of Science, Niigata University

⁶Graduate School of Natural Science and Technology, Kanazawa University

⁷Graduate School of Pure and Applied Science, University of Tsukuba

batch-wise experiments is well reproduced by the rapid on-line experiments in the studied condition. In the near future, we will perform the rapid anion-exchange experiment in HF/HNO₃ media with ²⁶²Db produced in the ²⁴⁸Cm(¹⁹F, 5n) reaction to study the fluoride complexations of Db.

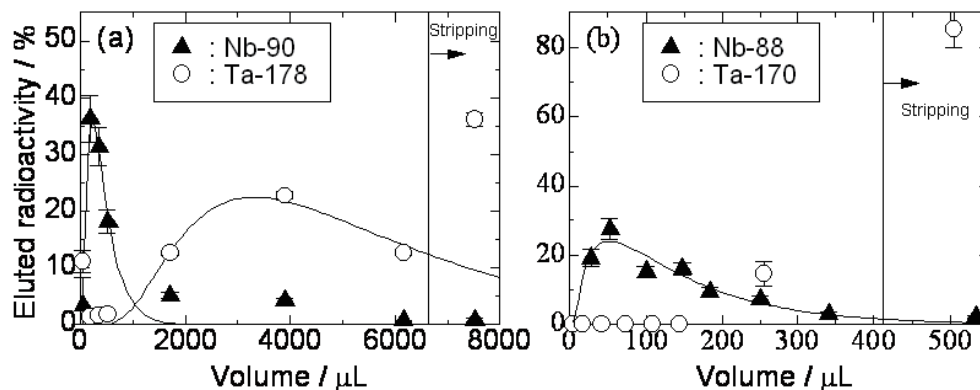


Fig. 1. Elution curves of Nb and Ta in anion-exchange chromatography in (a) 0.31 M HF/0.1 M HNO₃ and (b) 0.89 M HF/0.3 M HNO₃.

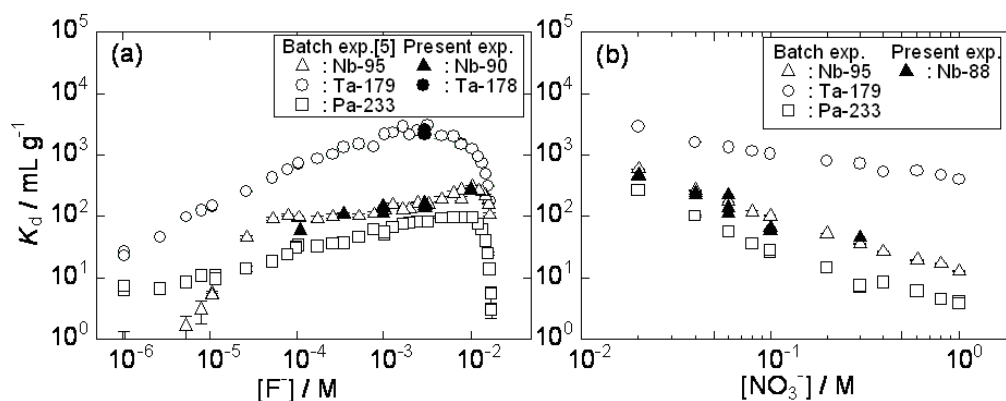


Fig. 2. Variation of the K_d values obtained in the present work and by the batch method as functions of (a) $[F^-]$ ($[NO_3^-] = 0.1$ M) and (b) $[NO_3^-]$ ($[F^-] = 0.0002$ M).

References

- [1] M. K. Guber J. V. Kratz, H. P. Zimmermann, M. Schädel, W. Brüchle, E. Schimpf, K. E. Gregorich, A. Türlér, N. J. Hannink, K. R. Czerwinski, B. Kadkhodayan, D. M. Lee, M. J. Nurmi, D. C. Hoffman, H. Gäggeler, D. Jost, J. Kovacs, U. W. Scherer, and A. Weber, *Radiochim. Acta* 57 (1992) 77.
- [2] H. P. Zimmermann M. K. Guber, J. V. Kratz, M. Schädel, W. Brüchle, E. Schimpf, K. E. Gregorich, A. Türlér, K. R. Czerwinski, N. J. Hannink, B. Kadkhodayan, D. M. Lee, M. J. Nurmi, D. C. Hoffman, H. Gäggeler, D. Jost, J. Kovacs, U. W. Scherer, and A. Weber, *Radiochim. Acta* 60 (1993) 11.
- [3] W. Paulus W. Paulus, J. V. Kratz, E. Strub, S. Zauner, W. Brüchle, V. Pershina, M. Schädel, B. Schausten, J. L. Adams, K. E. Gregorich, D. C. Hoffmann, M. R. Lane, C. Laue, D. M. Lee, C. A. McGrath, D. K. Shaughnessy, D. A. Strellis, and E. R. Sylwester, *Radiochim. Acta* 84 (1999) 69.
- [4] Y. Kasamatsu A. Toyoshima, H. Toume, K. Tsukada, H. Haba, and Y. Nagame, *J. Nucl. Radiochem. Sci.* In press.
- [5] E. Glueckauf, *Trans. Faraday Soc.* 51 (1955) 34.

4.4 PRODUCTION OF RI TRACERS FOR CHEMISTRY OF TRANSACTINIDE ELEMENTS

S. GOTO¹, T. IKEZAWA², M. SAKAMAKI², T. ISHIKAWA², H. KUDO², K. TSUKADA³,
M. ASAI³, A. TOYOSHIMA³ and Y. NAGAME³

Since a transactinide element has a very short life and its production cross-section is very small, only a very little quantity — usually one atom — is handled for a chemistry experiment at a time. To investigate the chemical property of such transactinide element, it is necessary that many repetition experiments in terms of a rapid chemistry method are performed until sufficient statistics are obtained. In other words, it takes very long time to even one experimental condition. Thus, the off-line experiment using a light homologue will be valid for an efficient on-line experiment. The aim of this work is to produce the non-carrier tracer for carrying out the off-line chemical experiments.

For the rapid chemistry experiments of Rf and Db, the radioactive isotopes ^{175}Hf ($T_{1/2} = 70$ d) and ^{95g}Nb ($T_{1/2} = 35$ d) were selected as a tracer in consideration of whether measuring their gamma-ray is possible and whether the half life is long enough. The tracers were produced using the $^{175}\text{Lu}(p, n)^{175}\text{Hf}$ and $^{96}\text{Zr}(p, 2n)^{95g}\text{Nb}$ reactions with JAEA tandem accelerator. The $^{\text{nat}}\text{Zr}$ foil (130 mg cm^{-2}) and the Lu foil (123 mg cm^{-2}) covered with aluminum foils were stacked and placed at the end of the R2 beam line. The Zr target was put on the beam upstream to make the proton energy the optimal to the intended nuclear reactions. The proton beam energies on the Zr and Lu target were about 14 MeV and 9.6 MeV, respectively, according to the energy loss calculation. The irradiation time was 9.5 hours, and the average beam current was about 2.0 μA . The irradiated targets were brought to Niigata University after cooling down the activity of the by-products such as ^{90g}Nb ($T_{1/2} = 14.6$ h), ^{92m}Nb ($T_{1/2} = 10.15$ d), and ^{96}Nb ($T_{1/2} = 23.4$ h). The activities of ^{95g}Nb and ^{175}Hf were 1.4 MBq and 1.2 MBq, respectively, after 14 days from the end of bombardment. Those were enough to perform the experiment for about half year.

Each tracer nuclide was separated from the target material using an anion-exchange method. The tracers have been used in different experiments to develop newer solvent extraction technique for 4th- and 5th-group elements at Niigata University.

¹ Center for Instrumental Analysis, Niigata University

² Faculty of Science, Niigata University

³ Advanced Science Research Center, JAEA

4.5 RADIOISOTOPES INCORPORATION IN FULLERENES BY USING NUCLEAR RECOIL

K. SUEKI¹, K. AKIYAMA², K. TSUKADA, A. TOYOSHIMA,
M. ASAI and Y. NAGAME

We show evidence of Se and Sb-atom-incorporated fullerenes on the collision between a C₆₀ or C₇₀ cages and Se or Sb atoms, which were generated from recoil process following nuclear reactions.

In order to produce Se and Sb atom-incorporated fullerenes, about 60 mg C₆₀ or C₇₀ fullerenes powder was mixed homogeneously with about 60 mg of As₂O₃ or SnO₂ and used to as the target material. Proton irradiation with beam energy of 13 MeV was performed at the TANDEM. Radioisotopes of ⁷⁵Se and ¹²⁴Sb can be produced by the ⁷⁵As(p,n)⁷⁵Se and ¹²⁴Sn(p,n)¹²⁴Sn reactions, respectively. The beam current was typically 0.6 μA and irradiation time was about 3 h. The fullerene samples were dissolved in CS₂ or *o*-dichlorobenzene after being filtrated to remove insoluble materials through a membrane filter (pore size = 0.2 μm). The soluble fraction was injected into a high performance liquid chromatograph (HPLC) equipped with a 5PBB column of 10mm (inner diameter) X 250 nm (length), at a flow rate 1.8 mL/min. The eluted solution was passed through an UV detector, the wavelength of which was adjusted to 340 nm in order to measure the amount of fullerenes and their derivatives. The fraction was collected at 20-sec or 60-sec intervals, and the γ-ray activities of each fraction were measured with an HPGe detector.

Figures (a) and (b), respectively, show the two elution curves of the C₆₀+As₂O₃ and C₇₀+As₂O₃ samples. In figure (a), a strong absorption peaks was observed at retention time of 11-12 min along the elution curve which was measured by a UV detector. This peak indicates the existence of C₆₀. Following the first peak, one peak at around 16-18 min was consecutively observed in the UV chromatogram. Two peaks appeared in the curve of the ⁷⁵Se radioactivities in the radiochromatogram. Aside from a slight delay, the first peak corresponds to the C₆₀ UV absorption peak. The second peak was observed at the retention time 17-20 min. Though there is a delay in the elution peaks of the radioactivites against that of the UV absorption peaks, it seems the elution behavior is similar. The result indicates that the radioactive fullerene monomers and dimmers labeled with ⁷⁵Se. Ohtsuki et al. reported

¹ University of Tsukuba

² Tokyo Metropolitan University

that Se-encapsulated fullerene is reproduced by *ab initio* molecular dynamics simulation[1]. The yield ratios of monomers labeled with radioisotopes were about $1-2 \times 10^{-4}$.

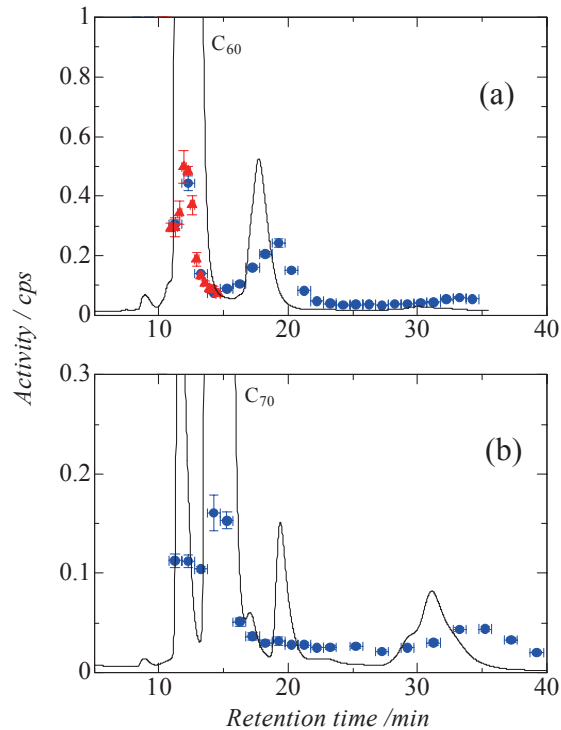


Figure (a) HPLC elution curves of soluble portion of the crude extracted in the proton irradiated sample of C_{60} mixed with As_2O_3 . The horizontal axis indicates retention time, and the vertical axis represents the counting rate of the radioactivities of ^{75}Se in each fraction (solid circle), and the absorbance of UV chromatogram of C_{60} (solid line). (b) HPLC elution curves at the same (a), but for the sample of C_{70} mixed with As_2O_3 .

Reference

[1] T. Ohtuki, K. Ohno, K. Shiga, Y. Kawazoe, H. Yuki, *Phys. Rev. B* 65 (2002) 073402.

This is a blank page

CHAPTER 5

Nuclear Theory

- 5.1 Significance of the Tensor Force in Exotic Nuclei in the SD-PF Shell
- 5.2 Extension of Calculation for Nuclear Potential Energy Surface to Large Deformation
- 5.3 Bulk Properties of Kaonic Nuclei
- 5.4 P-P Scattering Phase Shift in Momentum Space Including the Coulomb and a Short-Range Forces

This is a blank page

5.1 SIGNIFICANCE OF THE TENSOR FORCE IN EXOTIC NUCLEI IN THE SD-PF SHELL

Y. UTSUNO, T. OTSUKA^{1,2}, T. MIZUSAKI³ and M. HONMA⁴

The evolution of the shell structure in exotic nuclei is an intriguing issue and should be clarified by experiment in the near future. The disappearance of the $N=20$ magic number is most likely related to a narrowing $N=20$ shell gap toward smaller proton number, which has been investigated by a large-scale shell-model calculation with the Monte Carlo shell model (MCSM) [1]. It has been recently pointed out [2] that the change of the shell structure, often called shell evolution, is caused by the tensor force. The tensor force is very successful in accounting for the phenomena for spherical nuclei in some regions.

In the present study, we examine whether or not the tensor force leads to an exotic nuclear structure, besides a mere spherical shell evolution, such as an unexpected deformation using the shell model. We focus on persistence or disappearance of the magic structure around $N=28$ in the very neutron-rich region, where the *sd-pf* cross-shell interaction plays a key role. Note that the cross-shell interaction has still some ambiguity compared with the intra-shell interaction. The shell model can treat the deformation and the correlation in a proper way. The numerical calculation was in part performed with the Helios2 cluster system which was installed in JAEA-Tandem in 2006.

To investigate the proper strength of the tensor force as the shell-model effective interaction, we extract the tensor part from the GXPF1 interaction [3] for *pf*-shell nuclei. Since GXPF1 is an interaction that excellently reproduces and predicts many nuclear properties over the region, it should have a reasonable spin/isospin structure. As a result, the monopole centroid of the $T=0$ tensor force in GXPF1 is very similar to that of the $\pi+\rho$ one-boson exchange force and the GT2 interaction [4] that has been newly constructed for the mean-field calculation. Thus, the tensor force in the shell-model interaction seems similar to that of the new mean-field interaction. Since the mean-field calculation is known to work very well over the medium-heavy mass region, the strength of the tensor force in the effective interaction might be quite region-independent.

Based on the above discussion, we construct a new *sd-pf* shell Hamiltonian whose tensor force of the cross-shell part is identical to GT2 (hereafter simply denoted by GT2). As a reference, a Hamiltonian whose cross-shell part is replaced by Millener-Kurath (MK) tensor force [5] is also constructed, and we compare results between them. Note that the tensor force of MK is about one third as weak as that of GT2.

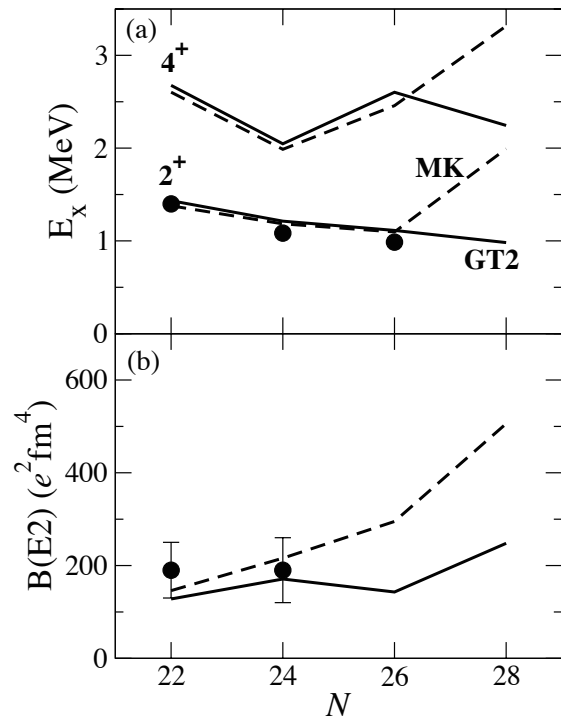
¹Department of Physics and Center for Nuclear Study, University of Tokyo

²Institute of Physical and Chemical Research (RIKEN)

³Institute of Natural Sciences, Senshu university

⁴Center for Mathematical Sciences, University of Aizu

The shell-model calculation shows that GT2 tensor force well reproduces reduction of the $Z=16$ shell gap in moving from $N=20$ to 28, such as the inversion of ordering between $1/2^+_{11}$ and $3/2^+_{11}$ states in ^{42}Si whereas MK does not sufficiently. The tensor force affects the $Z=14$ shell structure relevant nuclear structure, too. Figure 1 shows the low-lying structure of neutron-rich isotopes. The present calculation based on GT2 predicts that the $N=28$ isotope ^{42}Si is a typical magic nucleus due to a narrow $Z=14$ shell gap owing to the tensor force.



different cross-shell interactions MK and GT2.

References

- [1] Y. Utsuno, T. Otsuka, T. Glasmacher, T. Mizusaki, M. Honma, Phys. Rev. C 70 (2004) 044307.
- [2] T. Otsuka, T. Suzuki, R. Fujimoto, H. Grawe, Y. Akaishi, Phys. Rev. Lett. 95 (2005) 232502.
- [3] M. Honma, T. Otsuka, B. A. Brown, T. Mizusaki, Phys. Rev. C 69 (2004) 034335.
- [4] T. Otsuka, T. Matsuo, D. Abe, Phys. Rev. Lett. 97 (2006) 162501.
- [5] D.J. Millener, D. Kurath, Nucl. Phys. A 255 (1975) 315.

5.2 EXTENSION OF CALCULATION FOR NUCLEAR POTENTIAL ENERGY SURFACE TO LARGE DEFORMATION

H. KOURA and S. CHIBA

Nuclear fission is a quite important decay mode in the uranium and transuranium region. We have developed a method of calculating fission barrier heights by using the KUTY (Koura-Uno-Tachibana-Yamada) mass model, which is a kind of macroscopic-microscopic model and is constructed on the spherical-basis consideration [1,2]. A bulk term of this mass model is expressed as a function of proton number Z , neutron number N and mass number A to represent the global feature of atomic masses. Microscopic features including shell and deformation effects are calculated from a modified Woods-Saxon-like single-particle potential [3]. The shell energy of the KUTY method is expressed as

$$E_{\text{sh}}(Z, N, \text{shape}) = \sum_{\text{shape}} \left(\left\langle E_{\text{sh}}^{\text{sph}}(Z, N) \right\rangle_{\text{shape}} + \Delta E_{\text{S}}(Z, N, \text{shape}) - \Delta E_{\text{C}}(Z, N, \text{shape}) - \text{correct.} \right). \quad (1)$$

Here, the first term in the summation is a microscopic shell correction, which is expressed as a weighted sum of spherical shell energies with mixing weights determined by nuclear deformations, and the following two terms correspond to the change of the macroscopic surface and Coulomb energy by the deformations. The surface and Coulomb energies are written as

$$\Delta E_{\text{S}}(Z, N, \text{shape}) = S_0(Z, N) \left[\frac{1}{\pi} \int_{\text{shape}} dS - 1 \right], \quad (2)$$

$$\Delta E_{\text{C}}(Z, N, \text{shape}) = C_0(Z, N) \left[\frac{1}{2} \int_{\text{shape}} d^3r \rho(r) e^2 \int \frac{d^3r'}{|r-r'|} \rho(r') / C_0(Z, N) - 1 \right], \quad (3)$$

where $S_0(Z, N)$ or $C_0(Z, N)$ is a spherical surface or Coulomb energy, respectively. In the previous work, we adopted an explicit expression form with respect to deformation parameters α_2 , α_4 and α_6 up to 6th power as ΔE_{S} and ΔE_{C} as

$$\Delta E_{\text{S}}(Z, N, \text{shape}) = S_0(Z, N) \left[\frac{2}{5} \alpha_2^2 + \alpha_2^4 + \frac{20}{13} \alpha_2^6 - \frac{4}{105} \alpha_2^3 - \frac{66}{175} \alpha_2^4 - \frac{4}{35} \alpha_2^2 \alpha_4 - \dots \right], \quad (4)$$

$$\Delta E_{\text{C}}(Z, N, \text{shape}) = C_0(Z, N) \left[\frac{1}{5} \alpha_2^2 + \frac{5}{27} \alpha_2^4 + \frac{25}{169} \alpha_2^6 - \frac{4}{105} \alpha_2^3 - \frac{51}{245} \alpha_2^4 + \frac{6}{35} \alpha_2^2 \alpha_4 - \dots \right] \quad (5)$$

to reduce a computational time. However this method can be applied only to such a small deformation as near the ground-state shape and, at most, the shape where a neck is formed. In the present work we carry out the numerical integrals of Eqs. (2) and (3) numerically. Regarding a treatment of $1/|r-r'|$ in Eq. (3), we adopt an expansion of the Legendre polynomials of it up to 2^{16} poles determined by considering a numerical error.

Figure 1 shows the potential energy surface for ^{235}U . The open squared area gives the calculated region in the previous work. Though the previous region covers only the second fission barrier in

this nucleus, the present calculation gives the potential energy in the wide deformation area including even the scission point. The present calculation, however, have some problems shown as sudden changes of values, i.e., an arc line near $\alpha_2 \approx 1.0$ and $\alpha_4 \approx 0.5$ and an line near $\alpha_2 \approx 0.0$ and $\alpha_4 \approx -0.3$ etc., due to a numerical error on some conditions for some specific shapes. This is a future problem and we need some mathematical improvements.

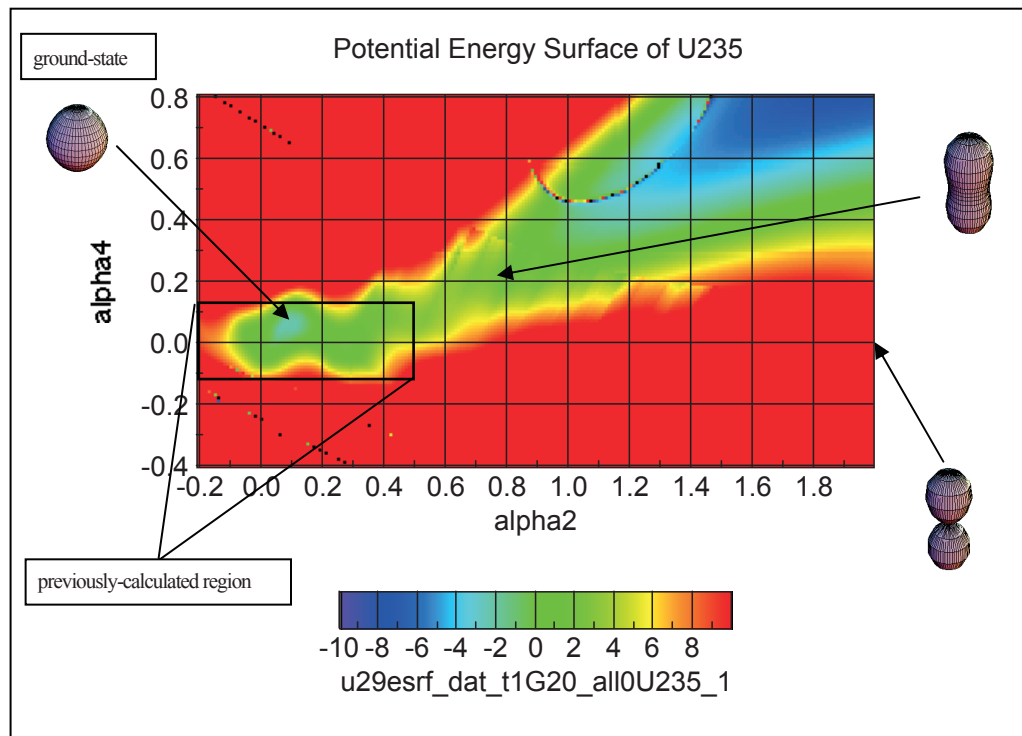


Fig.1. Potential energy surface of ^{235}U

References

- [1] H. Koura, M. Uno, T. Tachibana and M. Yamada, Nucl. Phys. A 674 (2000) 47.
- [2] H. Koura, T. Tachibana, M. Uno and M. Yamada, Prog. Theor. Phys. 113 (2005) 305.
- [3] H. Koura, M. Yamada, Nucl. Phys. , Nucl. Phys. A 671 (2000) 96.

5.3 BULK PROPERTIES OF KAONIC NUCLEI

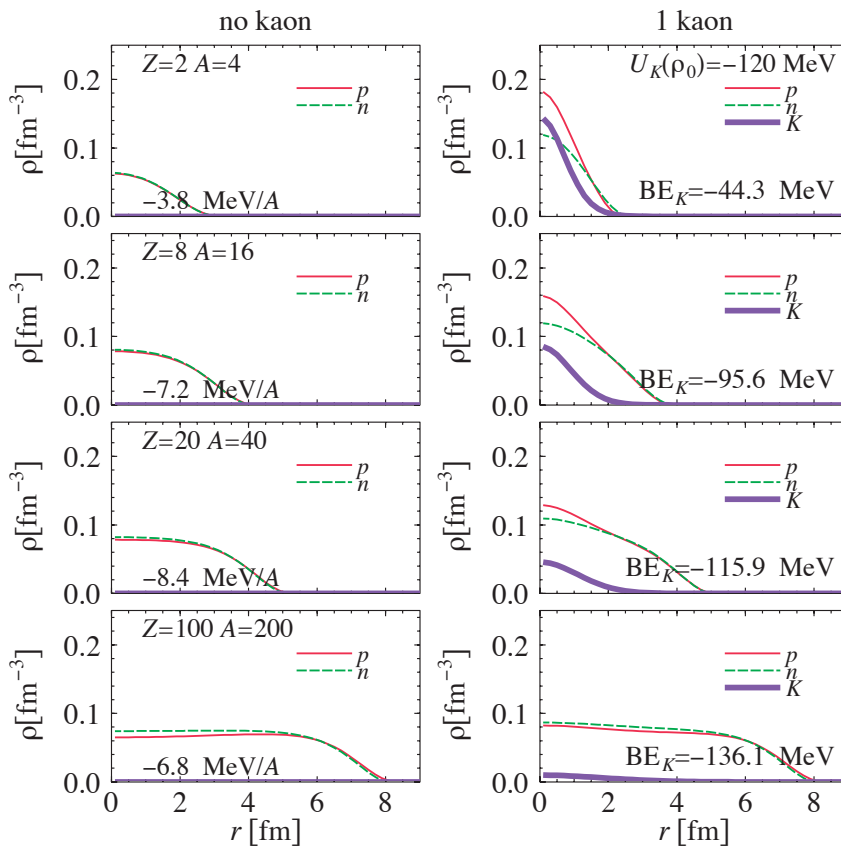
T. MARUYAMA, T. TATSUMI¹ and S. CHIBA

One of the recent topics is the possibility of deeply bound kaonic nuclei. They have observed the missing mass spectra in ${}^4\text{He}(K^-, n)$ [1] and ${}^{16}\text{O}(K^-, n)$ [2] reactions and reported some peaks corresponding to the binding energies of 90 – 170 MeV, while their results are not confirmed yet and there are theoretical controversies about their interpretation [3]. Some theoretical calculations have shown a drastic phenomenon: the central density increases as high as about ten times the normal nuclear density [4]. However, their model has some ambiguities about the nuclear equation of state (EOS) and limited to few-body systems, while this topic should be closely related to kaon condensation in infinite matter [5].

In the present situation it would be meaningful to survey kaonic nuclei in the wide mass number region by using a realistic theoretical model, which can reasonably reproduce EOS of nuclear matter and an empirical KN interaction. Using the relativistic mean field theory and the chiral model for

the KN interaction, we investigate bulk properties of kaonic nuclei such as density profiles and binding energies. Our model is rather simple but has a reliability in the description of nuclear matter and bulk properties of normal nuclei over all range of mass number [5]. We fix the numbers of proton, neutron and kaon and solve the coupled equations for density profiles under the spherical-symmetry approximation.

The figure shows some typical nuclei with and without a kaon. Due



to the strong attraction between kaon and proton, one can see the increase of density at the center, especially the increase of proton density. This feature is similar to that reported by Doté *et al* [4]. However, the highest density is up to two times the normal nuclear density. The effects of a kaon on nuclei is significant for lighter nuclei. The calculated binding energy

¹ Department of Physics, Kyoto University

of kaon for $Z = 8$ system, -95.6 MeV, in the figure seems consistent with the experimentally observed missing mass of ~ 90 MeV [2].

We have also tested a kaon potential with a chiral model and the different choice of kaon optical potential $U_K(\rho_0)$. In both cases the qualitative feature does not change.

As a conclusion, the existence of kaon in a nucleus causes the increase of central density especially the proton density. It is due to the strong attraction between kaon and proton. But the highest density is up to 2 or 3 times of the normal nuclear density in our calculation. Though our calculation is rather simple and includes many limitations, our results include significant information on bulk properties of kaonic nuclei.

References

- [1] T. Suzuki, et al, Nucl. Phys. A754 (2005) 375.
- [2] T. Kishimoto, et al, Nucl. Phys. A754 (2005) 383.
- [3] E. Oset and H. Toki, Phys. Rev. C 74 (2006) 015207.
- [4] A. Doté, H. Horiuchi, Y. Akaishi and T. Yamazaki, Phys. Rev. C 70 (2004) 044313.
- [5] T. Maruyama, T. Tatsumi, D.N. Voskresensky, T. Tanigawa, T. Endo and S. Chiba, Phys. Rev. C 73 (2006) 035802.

5.4 P-P SCATTERING PHASE SHIFT IN MOMENTUM SPACE INCLUDING THE COULOMB AND A SHORT-RANGE FORCES

S. CHIBA, S. NISHINOHARA¹ and S. ORYU¹

Recently, we proposed a new boundary condition model for the three-body Faddeev formalism with the Coulomb interactions [1]. The first numerical test for the two-body Coulomb interaction was done for the energy range larger than keV region successfully [2]. In this work, we would like to apply the method to the proton-proton (p-p) system with a certain NN interaction plus the Coulomb force, and prove the validity of the method for practical uses in scattering problems.

The Lippmann-Schwinger equation for the Coulomb interaction fails by means of the overlapping singularities where the Green's function pole and the logarithmic singularities coincide at on-(the energy)-shell momentum. Therefore, we will start all the interactions with a certain screened Coulomb potential (SCP) with a finite inverse range λ , which should be taken $\lambda \rightarrow 0$ after all other operations are carried out.

With this in mind, we divide a potential (in a partial-wave representation) having the short-range potential V_l^S and a Coulomb potential V_l^C by using a SCP with range R , V_l^R , as

$$V_l^{(C)}(\lambda) = V_l^S + V_l^C(\lambda) = V_l^{(R)}(\lambda) + V_l^\phi(\lambda),$$

where $V_l^{(R)} = V_l^S + V_l^R$, and $V_l^\phi = V_l^C(\lambda) - V_l^R$ is the auxiliary potential (AP). The T-matrix for this potential is given in terms of the two-potential theory as

$$\begin{aligned} T_l^{(C)}(\lambda; z) &= T_l^{(R)\phi}(\lambda; z) + T_l^\phi(\lambda; z) \\ &= \bar{\omega}_l^\phi(\lambda; z) t_l^{(R)\phi}(\lambda; z) \omega_l^\phi(\lambda; z) + T_l^\phi(\lambda; z) \end{aligned}$$

where $t_l^{(R)\phi}$ and the Møller wave operators $\omega_l^\phi, \bar{\omega}_l^\phi$ are given by

$$\begin{aligned} t_l^{(R)\phi}(\lambda; z) &= V_l^{(R)}(\lambda) + V_l^{(R)}(\lambda) G_l^\phi(\lambda; z) t_l^{(R)\phi}(\lambda; z) \\ \bar{\omega}_l^\phi(\lambda; z) &= 1 + T_l^\phi(\lambda; z) G_0(z) \\ \omega_l^\phi(\lambda; z) &= 1 + G_0(z) T_l^\phi(\lambda; z), \end{aligned}$$

with

$$G_l^\phi(\lambda; z) \equiv \frac{1}{z - H_0 - V_l^\phi(\lambda)} = G_0(z) + G_0(z) T_l^\phi(\lambda; z) G_0(z).$$

Furthermore, due to the fact that $V_l^{(R)} = V_l^S + V_l^R$, we can also have the two-potential formalism for $t_l^{(R)\phi}$. We solve this form of the 2-step two-potential theory numerically with the condition that the on-shell value of $T_l^\phi(\lambda)$ vanishes [1, 2]. The phase-shift for $V_l^S + V_l^C$ is obtained finally as a phase of the following quantity:

$$T_l^{(R)\phi}(k, k, \lambda; z) = \int_0^\infty \int_0^\infty \bar{\omega}_l^\phi(k, p'', \lambda; z) t_l^{(R)\phi}(p'', p''', \lambda; z) \omega_l^\phi(p''', k, \lambda; z) dp'' dp'''.$$

¹Tokyo University of Science

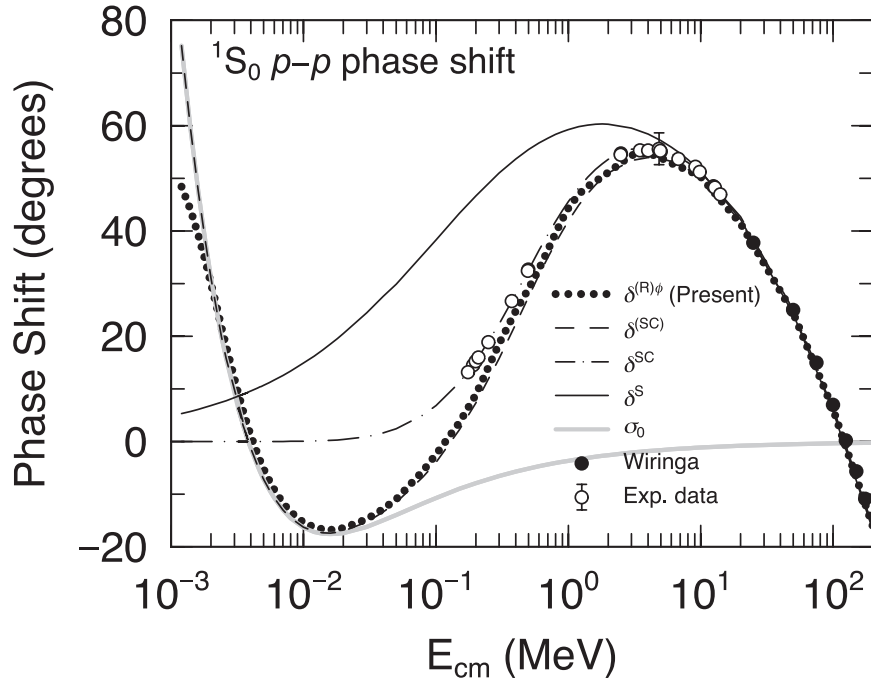


Fig. 1: The 1S_0 -wave proton-proton phase shift $\delta^{(R)\phi}$ by our theory (dots) for the RSC + Coulomb potentials is compared with the r-space result ($\delta^{(SC)}$: dashed-line) from a keV to several hundred MeV. The symbol σ_0 denotes the Coulomb phase shift. The dash-dotted line, $\delta^{SC} = \delta^{(SC)} - \sigma_0$, is obtained as the Coulomb-modified phase shift for the p - p 1S_0 state, which is to be compared with, e.g., experimental data compiled in Ref. [4] and theoretical values given in Ref. [5]. The solid line denotes the phase shift for the RSC potential alone.

Results of the present calculation for 1S_0 p - p system is shown in Fig.1 by a thick dotted curve denoted as $\delta^{(R)\phi}$ (Present). We choose here as V_l^S the Reid Soft Core (RSC) potential [3]. The boundary range parameter R was set to $e^\gamma/2k$, where γ denotes the Euler constant, and k the wave number of the system. Also shown in this figure is a corresponding quantity $\delta^{(SC)}$ calculated in the coordinate space. We notice that the present result agrees quite well with it except for the lowest energy region. Therefore it is numerically shown that the present method based on the auxiliary potential and two-potential theory works well for scattering problems in the short-range + Coulomb forces. Other quantities to be compared with experimental data or other calculations δ^{SC} [4, 5] is related to $\delta^{(SC)}$ by

$$\delta^{SC} = \delta^{(SC)} - \sigma_0$$

and shown with a dash-dotted curve in Fig. 1, where σ_0 is the s-wave Coulomb phase shift (gray line in Fig. 1).

References

- [1] S. Oryu, Phys. Rev. C73 (2006) 054001.
- [2] S. Oryu, S. Nishinohara, N. Shiiki and S. Chiba, Phys. Rev. C 75 (2007) 021001(R).
- [3] R.V. Reid, Ann. of Phys. 50 (1968) 411 (1968).
- [4] J.R. Bergervoet, P.C. van Campen, W.A. van der Sanden and J.J. de Swart, Phys. Rev. C38 (1988) 15.
- [5] R.B. Wiringa, V.G.J. Stoks and R. Schiavilla, Phys. Rev. C51 (1995) 38.

CHAPTER 6

Atomic Physics and Solid State Physics

- 6.1 High-Resolution Zero-Degree Electron Spectroscopy of Neon Ions Passing through Carbon Foils
- 6.2 Measurement of the Diffusion Coefficients in β -LiGa by Using Short-Lived Radiotracer of ^8Li
- 6.3 Charge State Distribution of Sulfur Ions after Penetration of C-Foil Targets (IV)

This is a blank page

6.1 HIGH-RESOLUTION ZERO-DEGREE ELECTRON SPECTROSCOPY OF NEON IONS PASSING THROUGH CARBON FOILS

K. KAWATSURA¹, K. TAKAHIRO¹, M. SATAKA, M. IMAI²,
H. SUGAI, K. OZAKI¹, H. SHIBATA² and K. KOMAKI³

Energy levels of high Rydberg states in highly charged ions and dynamical properties of their collision processes inside a solid target have been one of the major interests in ion-solid interactions. We have been studying mechanisms of electron emission from highly charged ions of 2.0 MeV/u Si, S and Ar passing through gas and solid targets with high-resolution zero-degree electron spectroscopy [1-5]. As for solid target, it has been found that the decays of 3-5 electron systems give a significant contribution in the electron spectrum [1,2,4]. Moreover, we have observed significant difference between the l distributions for the gas and solid targets and dependence of the l distributions on the foil thickness and projectile charge states. In the present work, we have extended our systematic measurements to the lower Z projectile of Ne to study the formation of Rydberg states inside the solid and describe here the results for 0.55 MeV/u Ne^{q+} ($q = 1, 5-7$) ions penetrating carbon foil targets

The experiments were performed at the tandem accelerator facility at the Japan Atomic Energy Agency in Tokai. The details of the experimental set up for high-resolution zero-degree electron spectroscopy have been described in Refs. [1,6]. The primary Ne^{q+} ($q = 1, 5-7$) ion beams were produced by using the ECR ion source installed at the high-voltage terminal of the tandem accelerator. In the present, 0.55 MeV/u Ne^{q+} ions penetrated C-foil targets of 1-10 $\mu\text{g}/\text{cm}^2$. The measurements of ejected electrons at zero degrees in the beam direction were performed using a tandem-type zero-degree electron spectrometer. Figure 1 shows the observed electron spectra in the laboratory frame for 0.55 MeV/u Ne^{q+} ions ($q = 1, 5-7$) through a C-foil target of 10 $\mu\text{g}/\text{cm}^2$. The spectra are dominated by the cusp peak at around 0.3 keV. A series of Coster-Kronig (C-K) electron peaks is superposed on the low and high energy wings of the cusp.

Figure 2 shows the C-K spectra for the forward ejected electrons, corresponding to the high energy wing of the cusp, which were obtained by converting data points into the projectile rest frame from the laboratory frame. An intense series of Coster-Kronig transitions from $\text{Ne}^{6+} 1s^2 2p(^2P)nl - 1s^2 2s(^2S)\ell'$ ($n = 7-10$) has been observed for $q = 1, 5$ and 6, but a weak series is observed for $q = 7$. Only a weak series of C-K transitions from $\text{Ne}^{5+} 1s^2 2s 2p(^3P)nl - 1s^2 2s(^1S)\ell'$ ($n = 7-10$) is observed for $q = 1, 5$ and 6, which is different from the case for Ar projectiles [5]. It is explained by the fact that the fraction ratio emerging from a carbon foil for $\text{Ne}^{6+}/\text{Ne}^{7+}$ is 0.55 for this incident energy, 0.55 MeV/u Ne ions, while that for $\text{Ar}^{14+}/\text{Ar}^{15+}$ is 2.0 for 2.0 MeV/u Ar ions [7].

¹ Kyoto Institute of Technology

² Kyoto University

³ National Center for University Entrance Examinations

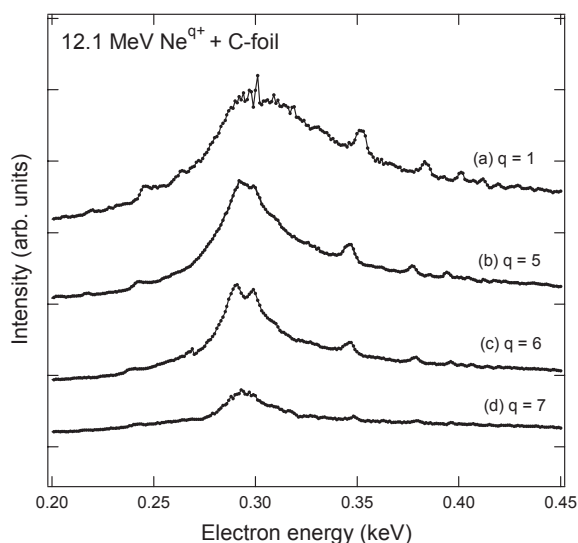


Fig. 1. Electron spectra measured at 0° in collisions of $0.55 \text{ MeV/u Ne}^{q+}$ on C foil ; (a) $q = 1$, (b) 5, (c) 6, and (d) 7, respectively.

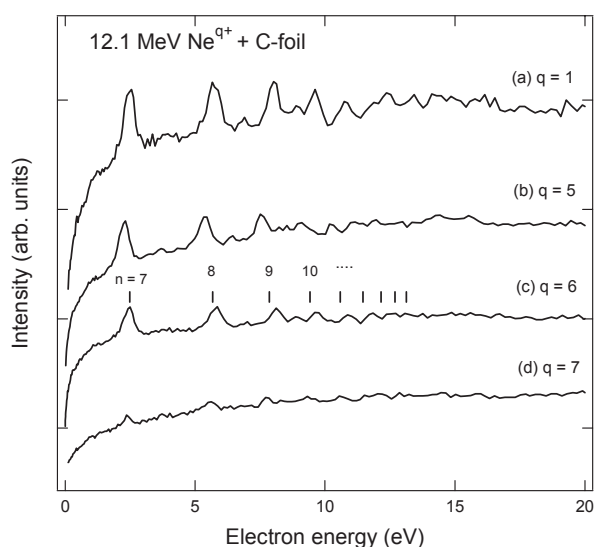


Fig. 2. High-resolution Coster-Kronig electron spectra ejected at 0° from the moving projectile in collisions of $0.55 \text{ MeV/u Ne}^{q+}$ on C foil; (a) $q = 1$, (b) 5, (c) 6, and (d) 7, respectively.

References

- [1] K. Kawatsura, M. Sataka, H. Naramoto, M. Imai, K. Komaki, Y. Yamazaki, K. Kuroki, Y. Kanai, T. Kambara, Y. Awaya, J. E. Hansen, I. Kadar and N. Stolterfoht, Nucl. Instrum. Methods Phys. Res. B53 (1991) 421.
- [2] M. Imai, M. Sataka, Y. Yamazaki, K. Komaki, K. Kawatsura and Y. Kanai, Physica Scripta T73 (1997) 93.
- [3] M. Sataka, M. Imai, K. Kawatsura, K. Komaki, H. Tawara, A. Vasilyev and U. I. Safronova, J. Phys. B35 (2002) 267.
- [4] M. Sataka, M. Imai, K. Kawatsura, K. Komaki, H. Tawara, A. Vasilyev and U. I. Safronova, Phys. Rev. A65 (2002) 052704.
- [5] M. Imai, M. Sataka, K. Kawatsura, K. Takahiro, K. Komaki and H. Shibata, Braz. J. Phys. 36 (2006) 541.
- [6] K. Kawatsura, M. Sataka, Y. Yamazaki, K. Komaki, Y. Kanai, H. Naramoto, K. Kuroki, T. Kambara, Y. Awaya, Y. Nakai and N. Stolterfoht, Nucl. Instrum. Methods Phys. Res. B48 (1990) 103.
- [7] K. Shima, N. Kuno, M. Yamanouchi and H. Tawara, At. Data Nucl. Data Tables, 51 (1992) 173.

6.2 MEASUREMENT OF THE DIFFUSION COEFFICIENTS IN β -LiGa BY USING SHORT-LIVED RADIOTRACER OF ^8Li

S.C. JEONG¹, I. KATAYAMA¹, H. KAWAKAMI¹, H. ISHIYAMA¹, Y. WATANABE¹,
N. IMAI¹, Y. HIRAYAMA¹, H. MIYATAKE¹, M. SATAKA, S. OKAYASU, H. SUGAI,
S. ICHIKAWA, K. NISHIO, T. NAKANOYA, S. MITSUOKA, Takashi HASHIMOTO,
Takanori HASHIMOTO², M. YAHAGI², K. TAKADA³, M. WATANABE³,
T. ISHIKAWA⁴ and A. IWASE⁵

For β -LiAl and LiIn, iso-structural with β -LiGa, the Li diffusion coefficients have been measured by a pulsed field gradient nuclear magnetic resonance (PFG-NMR) method [1], where the coefficients decrease monotonically with increasing lithium content with a minor modification due to the coexistence of vacancies on the Li atomic site (V_{Li}) and Li anti-structure atoms on the A site (Li_A), where A stands for Al or In. The monotonic behavior is supposed to be associated with the vacancy concentration (single vacancy diffusion) that decreases with increasing lithium content. However, the motion of Li is slightly suppressed or assisted depending on the kinds of anti-site atoms; Li diffusion rather slows down in β -LiAl, while becomes rather faster in β -LiIn around the stoichiometric composition, as compared to what would be expected when mediated by a single kind of vacancies (Li atomic vacancy). Such a slight modification in the monotonic behavior of Li diffusion has suggested the possibility of an interaction between vacancies and lithium anti-structure atoms; the interaction must be attractive in LiAl and repulsive in LiIn. The difference in the interactions has been understood by the atomic size effect [1, 2]: The Li_{Al} in β -LiAl produces compressional strain (expanded lattice), since the radius for the Li ion (0.68 Å) in a closed shell configuration [3] is larger than that for the Al ion (0.50 Å), while the Li_{In} in β -LiIn induces dilatational strain (contracted lattice) because of ionic radius for In (0.8 Å) larger than that for the substitutional Li ion. On the other hand, the vacancy, V_{Li} always produces dilatational strain.

Based on the atomic size effect, the interaction between V_{Li} and Li_{Ga} in β -LiGa is supposed to be attractive as in β -LiAl, because the radius for Ga ion (0.62 Å) is slightly small than that for Li ion. And its strength can be considered to be weaker than observed in β -LiAl and LiIn, since the radii for the constituent ions are quite close to each other. In addition, the concentration of

¹ Institute of Particle and Nuclear Studies, KEK

² Aomori University

³ National Institute of Materials Science (NIMS)

⁴ Tokyo University of Science

⁵ Osaka Prefecture University

the V_{Li} defect in β -LiGa is much (almost three times) larger in the Li-deficient content as compared to the case in β -LiAl and LiIn studied so far, even though there is just little difference in the concentration of Li anti-structure atoms. Of special interest is how the Li diffusion in β -LiGa depends on the Li content, consequently the concentration of the V_{Li} defect.

The diffusion coefficients of Li in β -LiGa with different Li content are compared in Fig.1.

As shown in Fig.1, what observed in the present measurement is much different from those for β -LiAl and LiIn; the Li diffusion around the stoichiometric composition is faster than in the Li-excess and Li-deficient compositions, demonstrating that the motion of the vacancies on the Li atomic site in β -LiGa, supposedly the carriers of Li atom, seems to be strongly promoted by the coexistence of V_{Li} and Li_{Ga} .

This suggests that the interaction between V_{Li} and Li_{Ga} would be unexpectedly large and quite repulsive than observed in β -LiAl and LiIn, on the one hand. On the other hand, it is also suggested

that the motion of Li ion for the Li-deficient composition could be quenched by the formation of the multiple complex defects such as the $V_{\text{Li}}\text{-Li}_{\text{Ga}}\text{-}V_{\text{Li}}$ and/or $V_{\text{Li}}\text{-}V_{\text{Li}}$, since the concentration of V_{Li} defects is much (almost three times) larger in the Li-deficient side as compared to the case in β -LiAl and LiIn, even though there is just little difference in the concentration of Li anti-structure atoms. It should be noted that the number of vacant Li sites in a unit cell volume (8 for Li and 8 for Ga) is about two for the most Li-deficient β -LiGa, i.e 44 at. % Li, whereas there exist about one vacant Li site in every two unit cells for the most Li-deficient β -LiAl and LiIn by assuming the random distribution of the vacancies over the entire volume. Further studies are going on to verify the above assumption.

References

- [1] J.C. Tarczon et al., Mater. Sci. Eng. A101 (1988) 99.
- [2] K. Kuriyama et al., Phys. Rev. B 54 (1996) 6-15.
- [3] C. Kittel, Introduction to Solid State Physics, 8th ed. (Wiley, New York, 2005) p71.

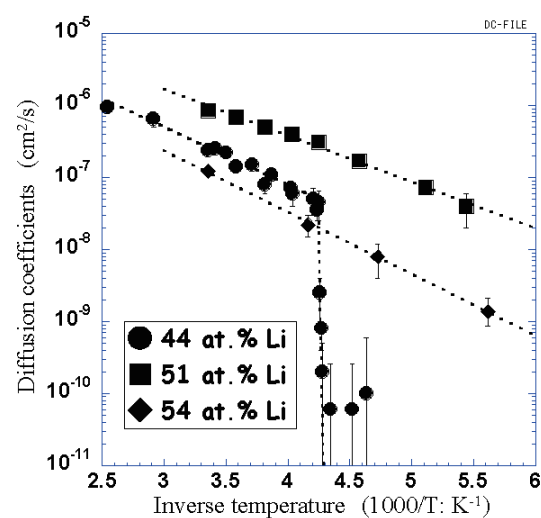


Fig.1 Temperature dependence of diffusion coefficients in b-LiGa with different Li content as indicated.

6.3 CHARGE STATE DISTRIBUTION OF SULFUR IONS AFTER PENETRATION OF C-FOIL TARGETS (IV)

M. IMAI¹, M. SATAKA, K. NISHIO, H. SUGAI, K. KAWATSURA²,
K. TAKAHIRO², K. KOMAKI³, and H. SHIBATA¹

Charge state is one of the most important aspects to study ion-solid interactions. Various interactions, such as electron capture, ionization and excitation of projectile and/or target electrons, and the consequent phenomena like energy deposition into the target, i.e. stopping of projectile, are closely related with the projectile charge state and its evolution in the target. Equilibrium charge state distributions for various collision systems after passing gaseous or solid target have been extensively investigated and compiled [1], although the charge state distribution somewhat changes upon exiting the target foil. As has been presented in the previous annual reports [2], we measured the exit charge state distributions for penetrations of S^{10+} , S^{11+} and S^{13+} ions through C-foil targets of $0.9 - 10 \mu\text{g}/\text{cm}^2$ in thickness and performed calculations by ETACHA code [3] to succeed in reproducing the experimental results sufficiently, although ETACHA has been designed for higher energy ($>10\text{MeV}/\text{u}$) region [4]. We have also started another simulation for S^{q+} ion fractions, in which the electron transfer cross sections $\sigma_{qq'}$ are calculated with codes applicable to the present collision energy [5]. In this report, results of our extensive measurements, deriving charge state evolution for $2.0 \text{ MeV}/\text{u}$ S ions of all the initial charge states between $6+$ and $14+$ are presented.

The present experiments were performed at the LIR1–3 beam line of the 20UR Tandem Accelerator Facility. A beam of $2.0 \text{ MeV}/\text{u}$ (64 MeV) S^{6+} , S^{7+} or S^{8+} ions was provided from the tandem accelerator within 0.1% of energy accuracy, using a calibrated energy analyzing magnet. A post-stripper C-foil of $\sim 20 \mu\text{g}/\text{cm}^2$ in thickness was placed after the energy analyzing magnet to produce higher charge state projectile ions. The energy losses at the post-stripper foil were estimated to be at most 0.7% by our separate measurement of cusp electron energies with zero-degree electron spectroscopy [6]. The primary S^{q+} ($q = 6-8$) or post-stripped S^{q+} ($q = 9-14$) ion beam was directed by a switching magnet to a self-support carbon target foil of $0.9, 1.1, 1.5, 2.0, 3.0, 4.7, 6.9$ and $10 \mu\text{g}/\text{cm}^2$ in thickness. The charge state distributions after foil penetration were measured using the heavy ion magnetic spectrometer ENMA and a position-sensitive gas chamber detector. The vacuum condition inside the spectrometer was maintained below 10^{-6} Pa to eliminate the background charge exchange collisions with residual gas, which was confirmed by measurements without target foil.

Measured charge state fractions for $2.0 \text{ MeV}/\text{u}$ S^{q+} ($q = 6-9, 12, 14$) ion incidences are shown in Fig. 1. The statistical errors are less than 1% for almost all the points, except for S^{q+} ($q = 6-8$) ion fractions of S^{6+} projectile. Typical total error values are estimated as 20% for the smallest fractions around 1.0×10^{-5} and less than 0.5% for the largest fractions around 0.3 . It can be seen that the fractions do not completely flat off in the measured foil thickness range, and the mean charge states and the widths still

¹ Department of Nuclear Engineering, Kyoto University

² Department of Chemistry and Materials Technology, Kyoto Institute of Technology

³ National Center for University Entrance Examinations

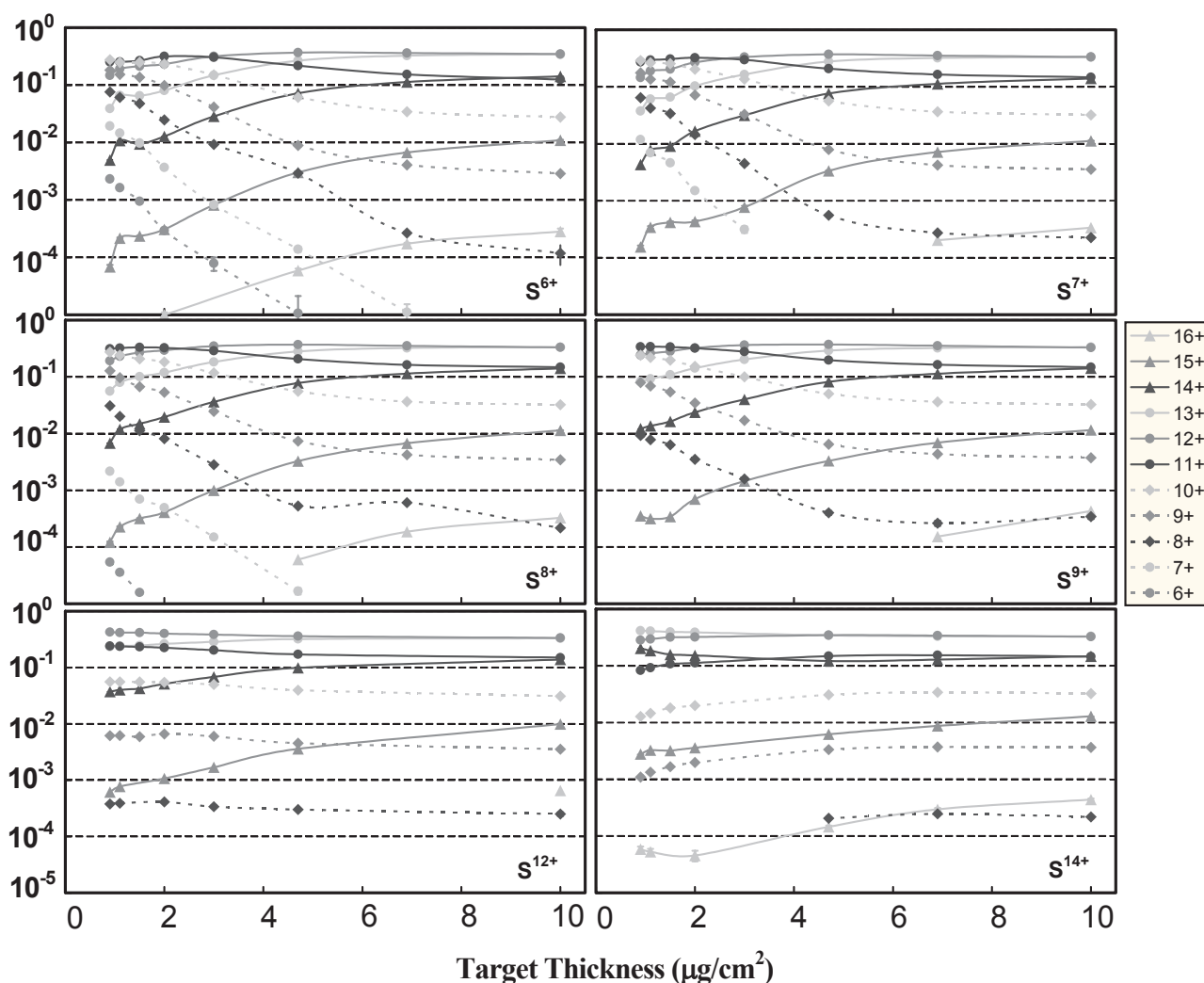


Fig. 1 Charge state evolution for 2.0 MeV/u S^{6+} , S^{7+} , S^{8+} , S^{9+} , S^{12+} and S^{14+} projectiles penetrated through C-foil targets of 0.9, 1.1, 1.5, 2.0, 3.0, 4.7, 6.9 and 10 $\mu\text{g}/\text{cm}^2$ in thickness. Error bars account only for the statistical error and those for $S^{(15-9)+}$ fractions are less than the symbol size for all the data points. Charge state evolution for S^{10+} , S^{11+} and S^{13+} ions has already been presented in the previous annual reports [2].

increasing creepily respectively around 12.4 and 1.06, expectedly to reach the equilibrium value of 12.62 and 1.10 [1], for all the initial charge states.

References

[1] A. B. Wittkower and H. D. Betz, *At. Data Nucl. Data Tables* 5 (1973) 5; K. Shima *et al.*, *At. Data Nucl. Data Tables* 51 (1992) 173; K. Shima *et al.*, *Nucl. Instrum. and Method* B33 (1988) 212.
 [2] M. Imai *et al.*, *JAEA-Review* 2005-004 (2006) 65; *JAEA-Review* 2006-029 (2006) 77.
 [3] J. P. Rozet *et al.*, *J. Phys.* B22 (1989) 33; *Nucl. Instrum. and Method* B107 (1996) 67.
 [4] M. Imai *et al.*, *Nucl. Instrum. Method* B230 (2005) 63.
 [5] M. Imai *et al.*, *Nucl. Instrum. Method* B256 (2007) 11.
 [6] M. Sataka *et al.*, *Phys. Rev.* A65 (2002) 052704; M. Imai *et al.*, *Nucl. Instrum. Method* B67 (1992) 142.

CHAPTER 7

Radiation Effects in Materials

- 7.1 Microstructure and Ion Configuration of Spinel Compound Irradiated with Swift Heavy Ions
- 7.2 Effects of Accumulation of Ion Tracks and Pre-Implantation of Xe Ions on Microstructure Changes in CeO₂
- 7.3 A Trial Usage of Microprobes for Improvement of a Scanning SQUID Microscope
- 7.4 Study on Irradiation-Induced Magnetic Transition in FeRh Alloys by Using X-Ray Magnetic Circular Dichroism
- 7.5 Electronic Sputtering of Nitrides and Oxides by High-Energy Heavy Ions
- 7.6 X-Ray Diffraction Study of CeO₂ Irradiated with High-Energy Heavy Ions
- 7.7 Swift Heavy Ion Induced Structural Modifications in Single Crystalline α -Al₂O₃
- 7.8 Hardness Modification in FeCu Alloys by Using Radiation Enhanced Segregation

This is a blank page

7.1 MICROSTRUCTURE AND ION CONFIGURATION OF SPINEL COMPOUND IRRADIATED WITH SWIFT HEAVY IONS

K. YASUDA¹, T. YAMAMOTO¹, S. KAWASOE¹, S. MATSUMURA¹ and
N. ISHIKAWA

Considerable attention has been devoted to magnesium aluminate spinel as a host of inert matrix fuels in light water reactors and a transmutation target for minor actinides and/or long life fission products. Radiation damage by fission products is one of the major concerns under these radiation environments, under which ion tracks formation will occur in these materials due to the high density electronic excitation [1-3].

In the present study, atomic resolution transmission electron microscopy (TEM) observations and analyses have been undertaken on single crystals of magnesium aluminate spinel ($\text{MgO}\cdot n\text{Al}_2\text{O}_3$) with stoichiometric and non-stoichiometric composition, to understand the structure of ion tracks induced by swift heavy ions. Swift heavy ions of 200 MeV Xe and 350 MeV Au were irradiated at the Tandem Accelerator Facility of JAEA-Tokai at an ambient temperature to fluence from 1×10^{15} to 4×10^{17} ions/m². A combination of TEM techniques, which includes high-resolution (HR) and bright-field (BF) imaging, and high angular resolution electron channeling spectroscopy (HARECXS) analysis, was utilized. The electronic stopping powers for Xe and Au ions were 25 and 35 keV/nm, respectively, at the surface region of specimens where TEM observations and analyses were performed.

Figure 1 shows HRTEM images of $\text{MgO}\cdot 1.1\text{Al}_2\text{O}_3$ irradiated with 350 MeV Xe ions to a fluence of 3×10^{15} ions/m². Traces of 350 MeV Au ions were seen as dark contrasts, indicating that considerable lattice strain was induced around the ion tracks. In the magnified image of Figure 1, lattice images with half lattice spacing are seen at the core region of ion tracks. This suggests that high-density electronic excitation by 350 MeV Au ions causes the preferential occupation of cations at octahedral sites than tetrahedral ones [2]. Figure 2 shows BF images of $\text{MgO}\cdot 1.1\text{Al}_2\text{O}_3$ taken under justfocus, underfocus and overfocus conditions. Strings of black/white reverse contrast were seen at overfocus/underfocus conditions in specimens irradiated with 350 MeV Au ions. The formation of these phase contrast suggests the decrease in atomic density at the core region of ion tracks [2,3] and might be related to the preferential occupation of cations at octahedral sites.

¹ Department of Applied Quantum Physics and Nuclear engineering, Kyushu University

The present study includes the result of ‘Study on radiation damage in oxide ceramics for the transmutation of long life radio isotopes’ entrusted to Kyushu University by the Ministry of Education, Culture, Sports, Science and Technology of Japan (MEXT).

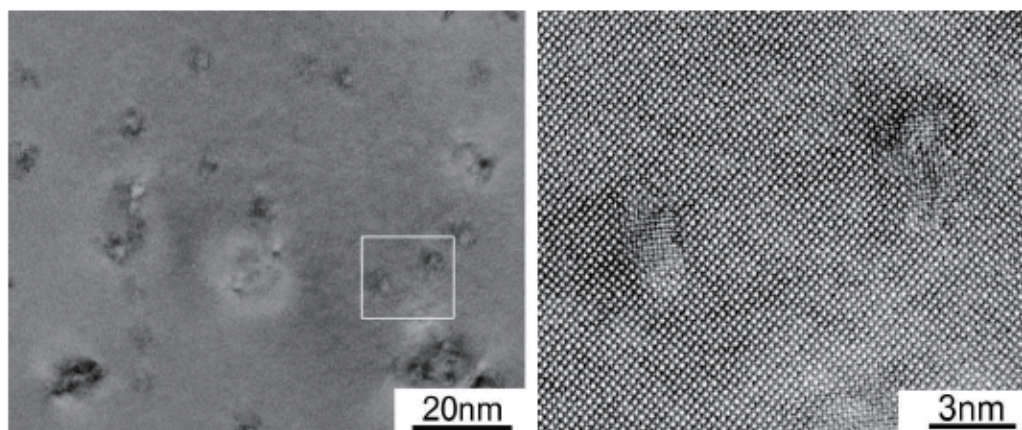


Figure 1 High-resolution electron micrographs of $\text{MgO}\cdot 1.1\text{Al}_2\text{O}_3$ irradiated with 350 MeV Au ions. The right side micrograph is the magnified image of the inside of a frame in the left side micrograph.

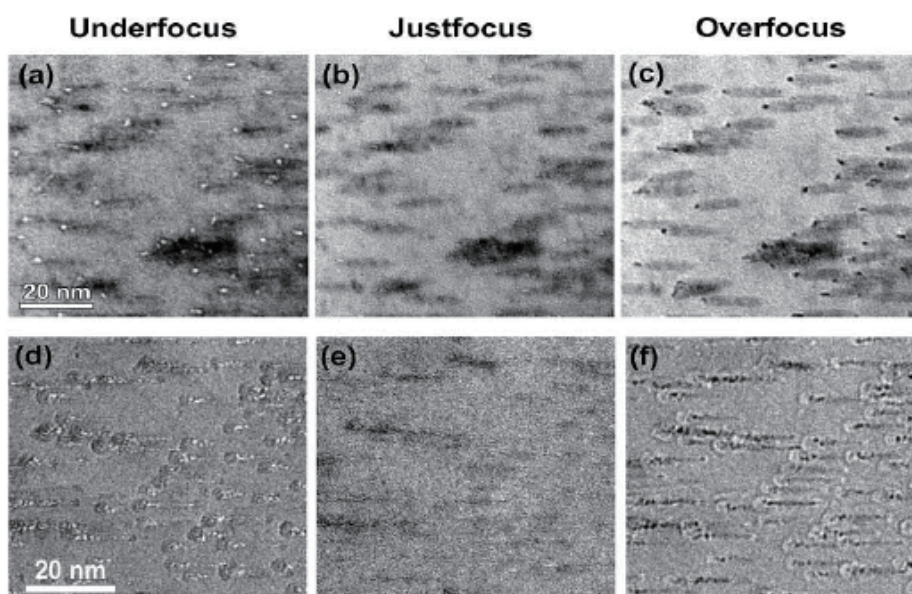


Figure 2 Bright-field images of $\text{MgO}\cdot 1.1\text{Al}_2\text{O}_3$ irradiated with 200 MeV Xe ions ((a) to (c)) or 350 MeV Au ions ((d) to (f)) taken with a kinematical diffraction condition under justfocus, underfocus and overfocus conditions. Micrographs were taken with inclining specimens to show their traces. The directions of incident ions are from left side to right side.

References

- [1] T. Yamamoto, M. Shimada, K. Yasuda, S. Matsumura, Y. Chimi and N. Ishikawa, Nucl. Instr. and Meth. Phys. Res., B, 245 (2006) 235.
- [2] K. Yasuda, T. Yamamoto, M. Shimada, S. Matsumura, Y. Chimi and N. Ishikawa, Nucl. Instr. and Meth. Phys. Res., B, 250 (2006) 238.
- [3] Kazuhiro Yasuda, Tomokazu Yamamoto and Syo Matsumura, JOM, April (2007) 27.

7.2 EFFECTS OF ACCUMULATION OF ION TRACKS AND PRE-IMPLANTATION OF Xe IONS ON MICROSTRUCTURE CHANGES IN CeO₂

T. SONODA¹, N. ISHIKAWA, M. SATAKA, K. YASUNAGA², M. KINOSHITA¹ and A. IWASE³

In order to extend the burnup of LWR fuels, formation and growth mechanism of a crystallographic re-structuring in the periphery region of high burnup fuel pellets, namely “rim structure” [1] should be clarified. This structure is characterized by the existence of highly dense small sub-grains whose size is approximately 200 nm, and the accumulation of small pores with average size around 1 μm. The structure can be formed by the accumulation and mutual interactions of radiation damages, fission products (FPs) and electronic excitations deposited partially by nuclear fissions [2,3].

In order to clarify the effects of accumulation of ion tracks that are formed by highly dense electronic excitation, 210 MeV Xe ions irradiation examinations on CeO₂, as a simulation of fluorite ceramics of UO₂, have been done at JAEA-Tandem accelerator facility. Moreover, in order to simulate the retained FP gas in high burnup fuels, 240 keV Xe ions are pre-implanted in CeO₂ by use of ion implanter with ECR ion source. Microstructure evolutions in the irradiated samples are observed in a FE-SEM (JSM-6340F) and a FE-TEM (HF-3000) at CRIEPI. This study was financially supported by the Budget for Nuclear Research of the Ministry of Education, Culture, Sports, Science and Technology, based on the screening and counseling by the Atomic Energy Commission.

Fig.1 (a) - (d) shows the typical SEM images of irradiated surfaces in CeO₂ under irradiation with 210 MeV Xe⁺¹⁴ at 300 °C to a fluence of (a) 1×10^{13} ions/cm², (b) 3×10^{14} ions/cm², (c) 1×10^{15} ions/cm² and (d) 2×10^{15} ions/cm². This figure indicates that the drastic change of the surface condition is occurred between (b) 3×10^{14} ions/cm² and (c) 1×10^{15} ions/cm². High magnification image of the surface roughness in the sample (d), as shown in Fig. 1 (e), has similar morphology of small sub-divided grains that are observed in inner surfaces of coarsened bubbles (size : ~1μm) in high burnup fuels[2]. A cross-sectional TEM image of the sample (d) is indicated in Fig. 1 (f). In this figure, the grain boundaries are observed at around 100nm depth from the irradiated surface whose morphology is changed. This result suggests a possibility that the surface roughness is caused by sub-divided grains. Several irradiation examinations whose irradiation temperature up to 800 °C confirm that the drastic change of surface morphology in all irradiated area is caused at a fluence to over 5×10^{14} ions/cm². These results clarify that the overlapping of ion tracks is needed for the drastic change of surface morphology.

For the simulation of high burnup fuels, high fluence implantation of 240 keV Xe ions (~ 1×10^{16} ions/cm²) at room temperature are prepared before irradiation with 210 MeV Xe ions. Fig. 2 indicates the typical SEM image of irradiated surface in CeO₂ under irradiation with (a) 210 MeV Xe⁺¹⁴ to a fluence of 2×10^{14} ions/cm² at 600 °C, (b) 240 keV Xe⁺¹² to a fluence of 1×10^{16} ions/cm² at R. T. + 210 MeV Xe⁺¹⁴ to a fluence of 1×10^{14} ions/cm² at 300 °C, (c) 240 keV Xe⁺¹² to a fluence of 1×10^{16} ions/cm² at R. T. + 210 MeV Xe⁺¹⁴ to a fluence of 3×10^{14} ions/cm² at 300 °C, and (d) 320 keV Xe⁺¹⁶ to a fluence of 2×10^{15} ions/cm² at R. T. + 210 MeV Xe⁺¹⁴ to a fluence of 1×10^{14} ions/cm² at 500 °C. Fig. 2 (a) and (b) suggest that the formation of surface roughness tends to be accelerated by the

¹ Sector, Nuclear Power Generation Technology, Nuclear Technology Research Laboratory, Central Research Institute of Electric Power Industry (CRIEPI)

² Department of Applied Quantum Physics and Nuclear Engineering, Kyushu University

³ Department of Materials Science, Osaka Prefecture University

pre-implantation of Xe ions. Moreover, Fig. 2 (b)-(d) also shows the possibility of temperature effects on the acceleration of the surface modification.

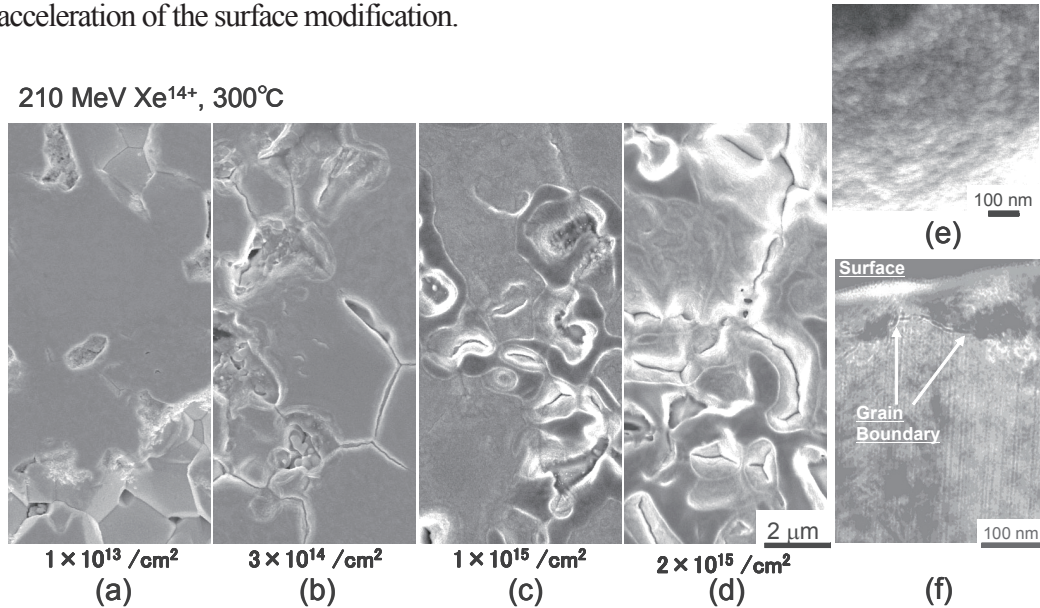


Fig. 1 SEM images of irradiated surfaces in CeO₂ under irradiation with 210 MeV Xe⁺¹⁴ to a fluence of (a) $1 \times 10^{13} / \text{cm}^2$, (b) $3 \times 10^{14} / \text{cm}^2$, (c) $1 \times 10^{15} / \text{cm}^2$ and (d) $2 \times 10^{15} / \text{cm}^2$, at 300 °C. The image of (e) and (f) is the high magnification SEM image and the cross-sectional TEM image of the sample (d), respectively.

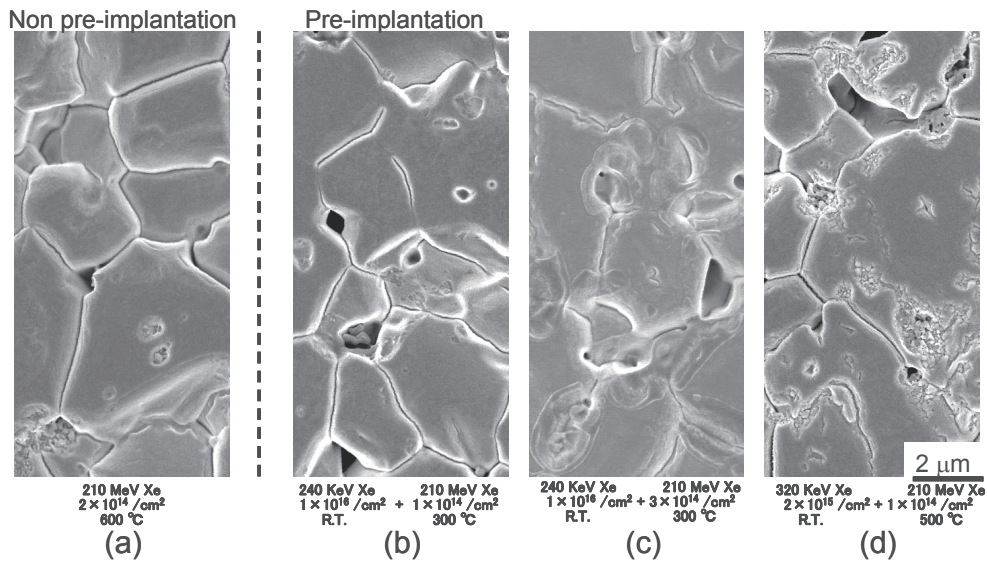


Fig. 2 SEM image of irradiated surface in CeO₂ under irradiation with (a) 210 MeV Xe⁺¹⁴ to a fluence of $2 \times 10^{14} / \text{cm}^2$ at 600 °C, (b) 240 keV Xe⁺¹² to a fluence of $1 \times 10^{16} / \text{cm}^2$ at R. T. + 210 MeV Xe⁺¹⁴ to a fluence of $1 \times 10^{14} / \text{cm}^2$ at 300 °C, (c) 240 keV Xe⁺¹² to a fluence of $1 \times 10^{16} / \text{cm}^2$ at R. T. + 210 MeV Xe⁺¹⁴ to a fluence of $3 \times 10^{14} / \text{cm}^2$ at 300 °C, and (d) 320 keV Xe⁺¹⁶ to a fluence of $2 \times 10^{15} / \text{cm}^2$ at R. T. + 210 MeV Xe⁺¹⁴ to a fluence of $1 \times 10^{14} / \text{cm}^2$ at 500 °C.

References

- [1] J. O. Barner, M. E. Cunningham, M. D. Freshley, and D. D. Lanning, HBEP-61, 1990, Battelle Pacific Northwest Laboratories.
- [2] T. Sonoda, M. Kinoshita, I.L.F. Ray, T. Wiss, H. Thiele, D. Pellottiero, V.V. Rondinella and HJ. Matzke, Nucl. Instr. and Meth. B 191 (2002) 622.
- [3] T. Sonoda, M. Kinoshita, Y. Chimi, N. Ishikawa, M. Sataka, A. Iwase, Nucl. Instr. Meth. B (2006), B 250 (2006) 254-258.

7.3 A TRIAL USAGE OF MICROPROBES FOR IMPROVEMENT OF A SCANNING SQUID MICROSCOPE

S. OKAYASU, M. SATAKA, I.KAKEYA¹ and N. KOKUBO²

A scanning SQUID microscope is a powerful tool for direct observations of vortices (fluxoid quantum) [1,2]. We have been investigating the relation between the vortices and columnar defects introduced by heavy ion irradiation in high T_c superconductors. A small pickup-coil connected a SQUID device scans on the surface of the sample, and local magnetizations are measured. Magnetic sensitivity of this tool is high enough, but spatial resolution is limited by the size of pickup coils. To improve the spatial resolution, a trial usage of microprobe on the pickup coil was achieved. Obtained images are expanded about 4 times the sizes of the original images without the microprobe, and the attached microprobe acts as a magnetic lens.

All images are obtained by a commercial scanning SQUID microscope (SQM-2000, SII NanoTechnology) with a standard 10 μm diameter pickup coil. All measured temperatures are below 4 K in a residual magnetic field (~1 μT). A commercial cantilever for MFM (SI-MF3N, SII) was used as a small magnetic guide rod. Under a microscope, the apical end of the cantilever with a sharp exploring needle was placed on the standard scanning device. The needle was settled on the center of the coil. The settled needle was fixed with GE varnish. For detailed preparation, see fig.1. The evaluation of this modified scanning device was achieved by usual two shipping inspections, one vortex observation on niobium film and the other meander line detection. For usual usage, the pickup coil is scanned just on the sample surface to maintain the highest spatial resolution (contact scan mode, CS mode). For measurements in this study, on the other hand, the modified pickup coil is adjusted and its position is just above the surface without contacting the sample during the scanning (no contact scan mode, NCS mode) to avoid scratching the sample surface by the needle.

Figure 2 shows some snap shots of vortex arrangement of the sample of niobium film. The scanned area was 315 μm x 315 μm with a 5 μm step. The boundary between bright and dark regions of the upper part in fig.2 is the edge of niobium. In fig.2, approximately 30 vortex images can be observed. The contrast of each vortex is not high enough. Within a square shown in the figure, the integrated value of vortex is almost the same to the quantized vortex Φ_0 ($=2.07 \times 10^3 \mu\text{T} \mu\text{m}^2$) for fig.2-(a). On the other hand, the integrated value of the same region is $0.3\Phi_0$ for fig.2-(b) in spite of almost the same measurement conditions. The quantitative certainty or reproducibility for the measurement is not guaranteed. The impedance of the pickup coil circuit changed due to the addition of the cantilever, and the SQUID tuning deviated from an optimum condition.

¹Univ. of Tsukuba, Tsukuba, Ibaraki 305-8571, Japan

²Kyushu Univ., Fukuoka-city, Fukuoka 810-8560, Japan

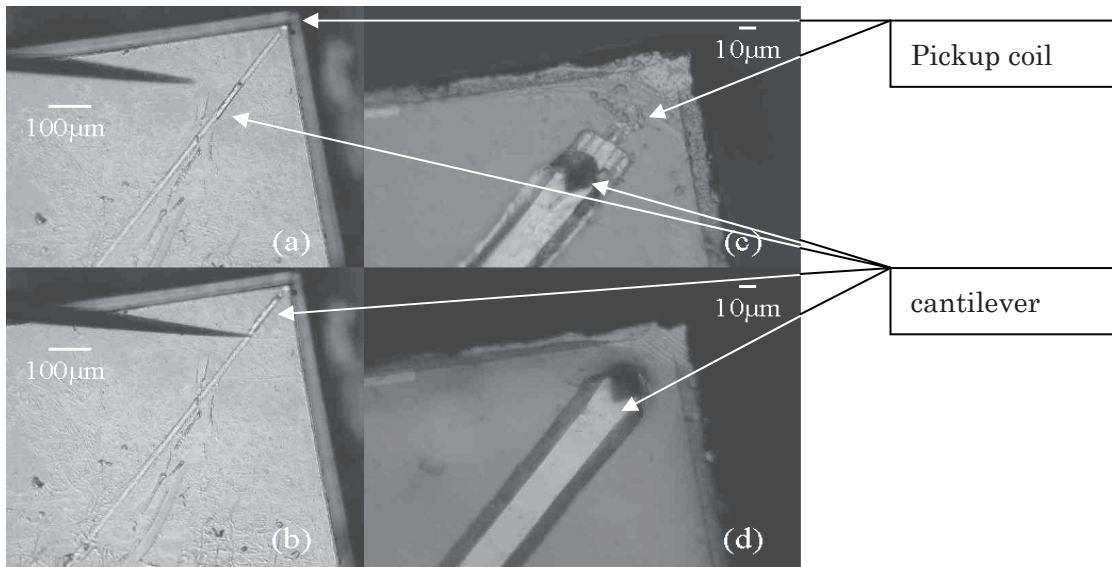


Fig.1 Microprobe preparation on the pickup coil of the scanning SQUID microscope. (a) A cantilever of MFM is settled on the SQUID device. The pickup coil is located at upper right end. (b) The cantilever is slid with a needle on the device. (c) The cantilever near the pickup coil. (d) The cantilever is settled on the coil. After this, the cantilever is fixed with GE varnish

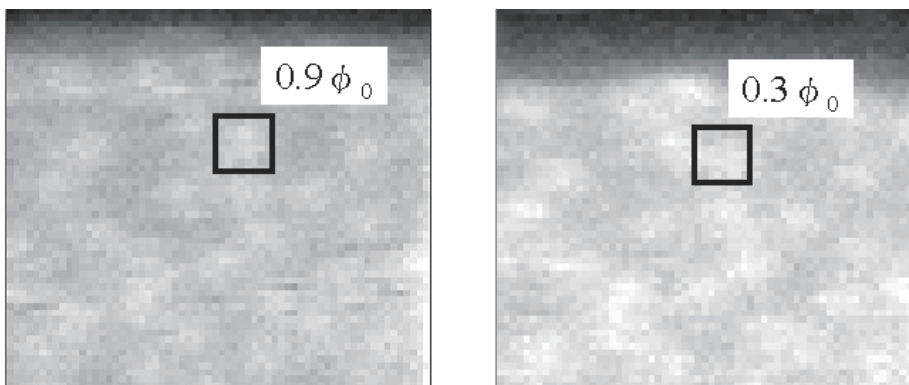


Fig.2 Vortex images for the sample of niobium film taken with the modified pickup coil. Scanned range is $315 \mu\text{m} \times 315 \mu\text{m}$ with a $5 \mu\text{m}$ step. The measured temperature is 4.2K. Almost 30 vortices can be observed in both viewgraphs. The diameter of each vortex is larger than the standard pickup coil case. In spite of almost the same experimental conditions between (a) and (b), the integrated values within a square shown in the figure are different, $0.9\Phi_0$ for (a) and $0.3\Phi_0$ for (b). The quantitative certainty is not guaranteed for the measurements by using the microprobe.

References

- [1] S. Okayasu, T. Nishio, M. Ono, T. Mashimo, Y. Tanaka, A. Iyo, *Physica C* 437-438 (2006) 239.
- [2] Y. Hata, J. Suzuki, I. Kakeya, K. Kadowaki, S. Nakayama, S. A. Nagata, A. Odawara, K. Chinone, *Physica C* 378-381 (2002) 420.

7.4 STUDY ON IRRADIATION-INDUCED MAGNETIC TRANSITION IN FeRh ALLOYS BY USING X-RAY MAGNETIC CIRCULAR DICHROISM

A. IWASE¹, M. FUKUZUMI¹, Y. ZUSHI¹, M. SUZUKI², M. TAKAGAKI², N. KAWAMURA²,
Y. CHIMI, N. ISHIKAWA, J. MIZUKI and F. ONO³

Recently, we have found that swift heavy ion irradiation induces the ferromagnetism in Fe-50% Rh alloy at low temperatures. To study the details of the ion-induced ferromagnetism, we have used the X-ray Magnetic Circular Dichroism (XMCD). Specimens used in the present study were Fe-50 at.%Rh alloy sheets, dimension of which was 5.0 x 5.0 x 0.2 mm³. The specimens were irradiated at room temperature with ¹³⁶Xe ions using the tandem accelerator at JAEA-Tokai. For ion-irradiated Fe-50%Rh specimens, the XMCD measurement at 20 K under the external magnetic field of 0.6 T near the Fe K-edge (7.11 keV) was carried out using a helicity-modulation method on the beam line 39XU of SPring-8 synchrotron facility. As the specimens were not thin films but thick sheets, we used the fluorescence method.

Figure 1 shows the ion-fluence variation of the XMCD spectrum at the Fe K-edge for 200 MeV ¹³⁶Xe irradiation. The XMCD spectra for ion-irradiated specimens are characterized by a dispersion type profile with a positive peak, labeled “A” around 7.112 keV with a negative peak “B” around 7.119 keV. In addition, another positive peak “C” appears around 7.122 keV. As can be seen in Fig.1, XMCD intensities at peaks A and B vary systematically with increasing the ion-fluence. The experimental result shows that the swift heavy ion irradiation definitely induces the ferromagnetism in Fe-50at.%Rh alloy at 20 K, and the ferromagnetic state develops with increasing the ion-fluence. The intensity of XMCD is proportional to the mean magnetic moment of the specified element (in the present case, Fe), which is projected onto the direction of the incident x-rays. Therefore, we have adopted the intensity difference between the height of positive peak A and that of negative peak B as a measure of the mean magnetic moment of Fe in the ion-irradiated Fe-50at.%Rh. To study which energy deposition process mainly contributes to the enhancement of the magnetic moment in Fe-50at.%Rh alloy, the magnetic moment induced per unit-fluence is plotted as a function of nuclear stopping power, S_n , and electronic stopping power, S_e , in Fig. 2. Since the attenuation length of the X-ray is about 2.5 μm , values of S_n and S_e for irradiating ions can be used as a parameter of energy deposition in the specimen. The figure indicates that the ion-irradiation induced magnetic moment is well correlated both with S_n and with S_e . The magnetic moment is nearly proportional to $S_n^{0.6}$ and to $S_e^{1.8}$. Up to the present, we cannot decide which process is dominant for the enhancement of Fe magnetic moment, and the physical meaning of its power dependence on S_e and S_n still remains uncertain.

1 Osaka Prefecture University

2 Japan Synchrotron Research Institute (JASRI)

3 Okayama University

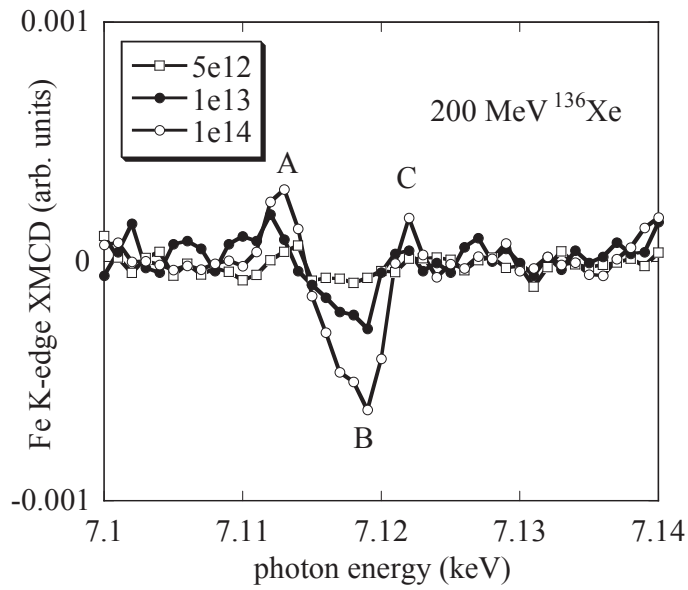


Fig.1. Ion-fluence variation of Fe K-edge XMCD spectra for Fe-50%Rh irradiated with 200 MeV Xe ions to the fluences of 5×10^{12} , 1×10^{13} and $1 \times 10^{14}/\text{cm}^2$.

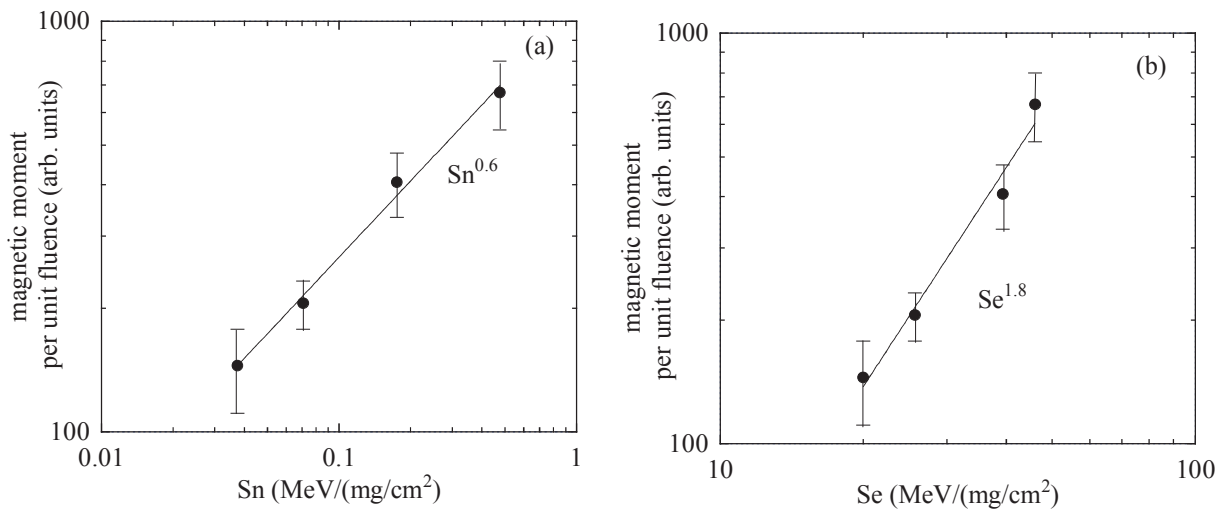


Fig. 2. (a) S_n dependence of Fe magnetic moment and (b) S_e dependence of Fe magnetic moment.

7.5 ELECTRONIC SPUTTERING OF NITRIDES AND OXIDES BY HIGH-ENERGY HEAVY IONS

N. MATSUNAMI¹, M. SATAKA², S. OKAYASU² and M. TAZAWA³

We have extended measurements of the electronic sputtering yields to nitrides (Si₃N₄ and AlN) and oxides (Y₂O₃ and ZrO₂) for a better understanding of the electronic sputtering, i.e., energy transfer mechanism from the electronic system to lattice [1]. It will be shown that the present data fits to the suggested bad-gap dependence, indicating again the importance of the band-gap in the electronic sputtering [2] and supporting the multi-exciton model [3].

The sputtering yields Y , obtained by carbon-film collector method, are fitted to power dependence on the electronic stopping power S_e : $Y=(BS_e)^n$. The results are summarized in Table 1. The sputtering yields are much larger than the calculated sputtering yields Y_c based on the elastic collisions. The sputtering yields at $S_e=15$ keV/nm vs the band-gap E_g are plotted in Fig. 1. So far, the suggestion [2] holds for twelve oxides and two nitrides that the sputtering yields at a given electronic stopping power take the upper limit.

In Fig. 1, one notices that the sputtering yields of MgO and Al₂O₃ are much smaller than those of SiO₂, though they have a similar band-gap of ~8 eV. It is known [4, 5] that self-trapped-exciton (STX), i.e., localized-excited state exists in both amorphous (a)- and crystalline (c)-SiO₂, does not in MgO and ZnO, and probably does not in Al₂O₃. Existence of STX is unknown for other materials in Table 1. Hence its existence is unlikely a sole factor determining the electronic sputtering yields and the multi-exciton model [3] has been suggested independent of existence of STX.

Table 1 Summary of electronic sputtering yields (Y) and relevant parameters, band-gap (E_g) and difference in the electronegativity ($\Delta\chi$).

Sample	$Y=(BS_e)^n$		$Y(S_e=15\text{keV/nm})$	Y/Y_c	E_g (eV)	$\Delta\chi$
	B	n				
c-SiO ₂	0.58	3	660	2E3	8.9	1.76
a-SiO ₂	0.58	3	660	2E3	8.3	1.76
SCO	0.8	2.2	240	1.5E3	7.5	
Al ₂ O ₃	0.25	1.4	6.4	200	8.8	2.03
MgAl ₂ O ₄	0.13	1.8	3.3	100	7.0	
MgO	0.075	3	1.4	40	7.7	2.27
Si ₃ N ₄	0.68	2	104	1.2E3	5.7	1.33
AlN	0.86	1.5	46	1E3	6.0	1.6
Y ₂ O ₃	0.24	3	47	150	5.5	2.39
ZrO ₂	0.052	2	1.8	30	4.9	2.28
SrTiO ₃	0.14	3.6	14	200	3.4	
CeO ₂	0.12	4	10	100	3.4	2.42
TiO ₂	0.18	2.5	12	350	3.2	2.18
ZnO	0.15	1.8	4.1	30	3.2	1.84

¹ Division of Energy Science, EcoTopia Science Institute, Nagoya University

² Japan Atomic Energy Agency (JAEA)

³ National Institute of Advanced Industrial Science and Technology (AIST)

The evaporation yield Y_t for SiO_2 is estimated to be ~ 0.01 for $S_e=20$ keV/nm, assuming the thermal spike model [6] and it is far smaller than the experimental sputtering yields of 1.6×10^3 [1]. This indicates that the thermal spike model is unsound for the electronic sputtering. Furthermore, covalency can be estimated based on the difference in the electronegativity $\Delta\chi$ (see Table 1) and we have examined whether the suggestion [7] that materials characterized by covalent bond is more sensitive to radiation than ionic bond is effective for the electronic sputtering or not. The suggestion seems to work for SiO_2 , MgO and Al_2O_3 . For other cases, no simple relation between the covalency and the electronic sputtering yields is found [1].

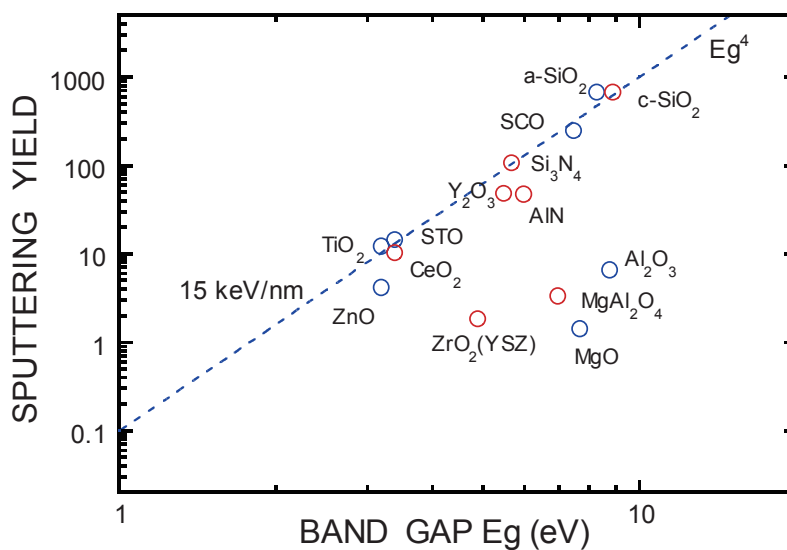


Fig. 1 Sputtering yields at $S_e=15$ keV/nm as a function of the band-gap E_g . Dashed line indicates E_g^4 -dependence for the upper limits of the sputtering yields. An estimated error is 20 %.

References

- [1] N. Matsunami, M. Sataka, S. Okayasu, M. Tazawa, Nucl. Instr. Meth. B256 (2007) 333.
- [2] N. Matsunami, M. Sataka, A. Iwase, S. Okayasu, Nucl. Instr. Meth. B209 (2003) 288.
- [3] N. Matsunami, O. Fukuoka, T. Shimura, M. Sataka, S. Okayasu, Nucl. Instr. Meth. B230 (2005) 507.
- [4] N. Itoh, A. M. Stoneham, Materials Modification by Electronic Excitation, Cambridge, 2001.
- [5] P. Martin, S. Guizard, Ph. Daguzan, G. Petite, P. D'Oliveira, P. Meynadier, M. Perdrix, Phys. Rev. B55(1997)5799.
- [6] M. Toulemonde, W. Assmann, C. Trautmann, F. Gruner, H. D. Mieskes, H. Kucal, Z. G. Wang, Nucl. Instr. Meth. B 212 (2003) 346.
- [7] K. Trachenko, J. Phys.: Condens. Matter 16 (2004) R1491.

7.6 X-RAY DIFFRACTION STUDY OF CeO₂ IRRADIATED WITH HIGH-ENERGY HEAVY IONS

N. ISHIKAWA, Y. CHIMI, O. MICHIKAMI¹, Y. OHTA¹, M. LANG² and R. NEUMANN²

Nuclear fuels in light water reactors (LWR) are subjected to various high-energy particles such as neutrons and fission fragments (Xe, Kr, etc.). It is known that high-energy fission products create serious damage in the UO₂ crystal structure, leading to swelling and degradation of thermal properties. Cerium dioxide, CeO₂, is one of the ceramics which have the same structure (fluorite structure) as UO₂ and also a similar melting temperature. In order to investigate the damage process of UO₂ fuel ceramics, the simulation material CeO₂ is irradiated with high-energy projectiles, such as 2.7-GeV U, 200-MeV Au, and 230-MeV Xe.

Thin films of CeO₂ were prepared on sapphire substrates by dc sputtering. The film thickness was about 300 nm. The films were irradiated at room temperature with 2.7-GeV U from the UNILAC accelerator at GSI and with 200-MeV Au and 230-MeV Xe from the tandem accelerator at Tokai Research and Development Centre, Japan Atomic Energy Agency (JAEA-Tokai). In order to investigate the degradation of the crystal structure, X-ray diffraction (XRD) patterns were measured before and after the irradiation. The XRD peaks corresponding to (002) and (004) reflections are observed before irradiation. In this study irradiation-induced change of the (002) peak intensity is investigated. The electronic stopping power is calculated by the SRIM-2003 code.

By 2.7-GeV U irradiation the intensity of the (002) XRD peak monotonically decreases as a function of ion fluence. It is known that in most ceramic materials a high-energy heavy ion creates a track along its path. The ion-track has typically a diameter of several nanometers. The crystal structure inside the track can be amorphous or have a disordered lattice depending on ion mass, ion energy, and target material. It is expected that, if the interior of the track is sufficiently damaged, the track does not contribute to X-ray diffraction and the XRD intensity decreases exponentially as a function of fluence. By using a simple Poisson rule, the decrease in the XRD intensity can be written as

$$I(\Phi) = I_0 \exp(-A\Phi), \quad (1)$$

where $I(\Phi)$ is the intensity of XRD peak as a function of ion-fluence Φ , I_0 the $I(\Phi=0)$, and A the area of a single track.

¹Iwate University

²GSI(Gesellschaft für Schwerionenforschung)

As shown in Fig. 1, equation (1) holds only for 2.7-GeV U irradiation. From the above formula, a track diameter of 15 nm can be derived for 2.7-GeV U irradiation. For 200-MeV Au and 230-MeV Xe irradiations, however, equation (1) is not valid, and the decrease in XRD intensity tends to saturate in the high-fluence region. It is already known that for 210-MeV Xe irradiation [1], ion tracks are formed, but the crystal lattice inside the track is maintained. Based on this finding, the XRD peak behavior for 200-MeV Au and 230-MeV Xe irradiations can be explained as follows. Even if ion tracks cover the whole sample, they do not completely destroy the crystal structure, and the lattice order is maintained. This leads to saturation of the intensity decrease. The degree of damage in the high-fluence region is higher for 200-MeV Au than for 230-MeV Xe. The electronic stopping powers for 2.7-GeV U, 200-MeV Au, and 230-MeV Xe irradiations are 57.3 keV/nm, 32.0 keV/nm, and 28.6 keV/nm, respectively. The degree of damage increases with increasing electronic stopping power as demonstrated in Fig 1.

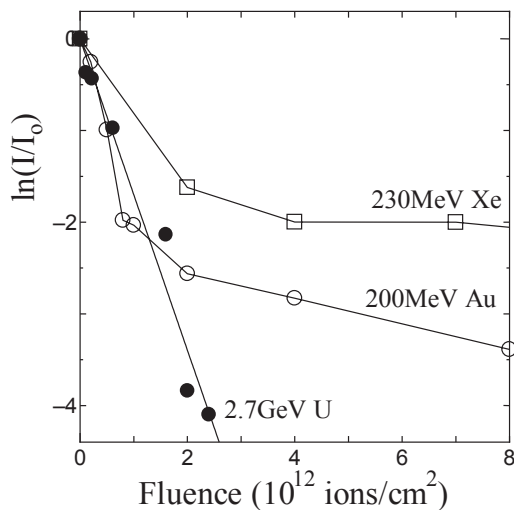


Fig.1 Logarithm of normalized XRD intensity as a function of fluence for the irradiations with 230-MeV Xe, 200-MeV Au, and 2.7-GeV U.

Reference

- [1] T. Sonoda, M. Kinoshita, Y. Chimi, N. Ishikawa, M. Sataka, A. Iwase, Nucl. Instrum. Methods Phys. Res. B 250 (2006) 254.

7.7 SWIFT HEAVY ION INDUCED STRUCTURAL MODIFICATIONS IN SINGLE CRYSTALLINE α -Al₂O₃

N. OKUBO, T. NAKAZAWA, T. ARUGA, M. SATAKA and S. JITSUKAWA

Aluminum oxide (α -Al₂O₃) is expected as functional materials in a field of nuclear energy e.g. an insulating material and window used for plasma diagnosis in a fusion reactor and an inert matrix material of geological disposal of high level radioactive waste. Recently, amorphization in ceramics such as α -Al₂O₃, which affects the physical and mechanical properties, is attracted as a phenomenon induced by high energy ion irradiations [1]. In previous studies, we have reported that amorphous phase is caused in polycrystalline aluminum oxide by ion irradiation with high-density electronic energy depositions (S_e), although lattice structure of the aluminum oxide is stable against nuclear energy depositions (S_n) [2]. The amorphization behaviors caused by high-density S_e indicated dependences on the specimen depth and grain orientation around the amorphized-crystalline region. We reported that new lattice planes, which meant lattice distorted, formed in the early stage of irradiation around the fluence of 5.0×10^{13} ions/cm² for single crystalline α -Al₂O₃ irradiated with 160 MeV-Xe ions [3]. Moreover, the amorphization appeared to take place by the irradiation above the fluence of 1.0×10^{14} ions/cm². Detailed mechanism of the amorphization induced by ion irradiation has not been clearly understood. In this study, we reported energy dependence of structural modifications leading to amorphization in crystalline α -Al₂O₃ irradiated by swift heavy ions.

Single crystalline α -Al₂O₃ specimens with (0001) surface were irradiated with several energies of Xe ions at ambient temperature, by using the Tandem Accelerator of JAEA. The irradiation energy was from 160 to 68 MeV by using aluminum foil energy degrader. The specimens used were 10×10 mm² plates with 0.5 mm thickness. The fluence was 2.0×10^{14} ions/cm². The electronic energy deposition (S_e), nuclear energy deposition (S_n) at the surface and projected range (R_p) of the Xe ions in the α -Al₂O₃ were calculated with the SRIM2000 [4] (See Table 1). X-ray diffractometry (XRD) for the specimens before and after irradiations were conducted in the range of 20 to 110 degree for 2θ . The accumulative time and step angle were 2.0 second and 0.004 degree, respectively, and the specimen was rotated parallel to c axis. The specimen was covered by Au film with 10 μ m thickness and 3mm ϕ hole to eliminate XRD signals from the unirradiated region.

The XRD patterns of the specimens before and after irradiations at various energies are shown in the range of 41 to 42.5 degree for 2θ in Fig. 1. A strong peak is observed at 41.7 degree in the XRD pattern for the specimen before irradiation. The peak is due to Al₂O₃ (0006) plane. The XRD intensities of the irradiated specimens were normalized to that of the pristine Al₂O₃ (0006) peak. After the irradiation, new two peaks appear around 41.4 (peak 1) and 41.6 (peak 2) degree as shown by arrows in the figure. Each angle of peak 1 and 2 did not changed in this energy range, while the peaks shifted depending on ion fluence [3]. The intensities of the peak

2 are almost equal, though the peak 1 decreases gradually as decreasing the energy below 100 MeV. Though origins of the two peaks have not been identified yet, interplanar spacing in the irradiated specimens expands by the irradiations and does not depend on the ion energy in this study. Threshold S_e value of track formation in Al_2O_3 is about 20 keV/nm [5]. The energy of 20 keV/nm corresponds to the 100 MeV irradiation in this study. Then, the decrease of peak1 is considered to decreasing of ion track formation and their overlapping leading to amorphization.

In summary, energy dependence on structural modification was examined in single crystalline $\alpha-Al_2O_3$ irradiated by swift heavy ions. The XRD results indicate that the swift heavy ion irradiation causes the lattice expansion and the structural modification leading to amorphization progresses above the energy of 100 MeV in this study. Elucidation of mechanism on the amorphization is in progress by cross sectional TEM measurements.

Table 1
Irradiation conditions in $\alpha-Al_2O_3$

Energy (MeV)	dE/dx (keV/nm)		Rp (μm)
	S_e	S_n	
68	18	0.20	6.5
100	21	0.15	8.2
130	23	0.12	9.5
160	25	0.10	10.7

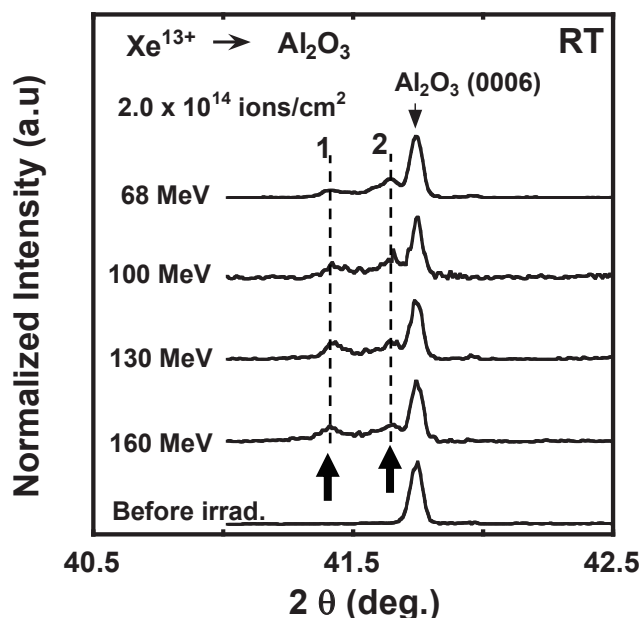


Fig. 1 XRD patterns of Al_2O_3 specimens irradiated by various energy Xe ions. Total fluence was constant at 2.0×10^{14} ions/cm².

References

- [1] G. Szenes, J. Nucl. Mater. 336 (2005) 81-89.
- [2] T. Aruga, Y. Katano, T. Ohmichi, S. Okayasu, Y. Kazumata, Nucl. Instr. and Meth. B 166-167 (2000) 913-919.
- [3] N. Okubo, T. Nakazawa, Y. Chimi, N. Ishikawa, T. Aruga and S. Jitsukawa, JAERI Tandem Annual Reports, JAEA-REVIEW 2005-004, 2005, p. 90.
- [4] J.F. Ziegler, J.P. Biersack, U. Littmark, The Stopping and Range of Ions in Solids, (Pergamon Press, New York, 1985), Chap 8.
- [5] S. M. M. Ramas, N. Bonardi, B. Canut, S. Bouffard and S. Della-Negra, Nucl. Instr. and Meth. B 143 (1998) 319-332.

7.8 HARDNESS MODIFICATION IN FeCu ALLOYS BY USING RADIATION ENHANCED SEGREGATION

S. NAKAGAWA¹, F. HORI¹, Y. CHIMI, N. ISHIKAWA, M. KITAGAWA², R. OSHIMA²,
T. TOBITA, R. TANIGUCHI¹, M. SUZUKI and A. IWASE¹

When supersaturated alloys are irradiated with high energy particles, point defects are produced and they enhance the diffusion of supersaturated atoms and their segregation. This phenomenon is called radiation enhanced segregation. This segregation under irradiation leads to some changes in structures and properties of alloys. For Fe-based Cu alloys, as Cu-precipitates act as obstacles against the dislocation motion, energetic particle irradiation causes the increase in hardness of the alloys. The amount of hardness increase in FeCu alloys depends on irradiation dose, dose rate, irradiation temperature and so on [1,2]. Therefore, there exist some possibilities of local modification of structures and properties of supersaturated alloys using the radiation enhanced segregation because the segregation of supersaturated atoms is expected to occur only in the irradiated region. In this study, we use the swift heavy ion irradiation for the local modification of hardness in FeCu alloys [3].

A supersaturated alloy, Fe-1.2 wt.% Cu was selected for this experiment. Specimens were solution-annealed at 850 °C and then were quenched into the water. In this process, Cu atoms were dissolved supersaturatedly in the matrix. The specimens were irradiated at 250 °C with 200 MeV Au and Xe ions using a 20 MV tandem accelerator at JAEA-Tokai. During the irradiation, about a half area of each specimen was covered with a thick copper plate to produce a straight boundary of irradiated and unirradiated regions. For some specimens, masking plate with a circular hole was put on each specimen during the irradiation, which restricted the ion-irradiation to the circular region. Changing loads and indents intervals, Vickers microhardness was measured near the boundary of irradiated and unirradiated regions after the irradiation. Using the result of some experiments, we determined the suitable conditions for the two-dimensional mapping of hardness change in the specimens which had been covered with a masking plate with a circular hole during irradiation.

Fig. 1 shows the indent-depth dependence of the change in Vickers microhardness for Fe-1.2 wt.% Cu specimens irradiated with Xe and Au ions to the fluence of $1 \times 10^{13}/\text{cm}^2$ at 250 °C. The data for an unirradiated specimen is also plotted. The Vickers microhardness for unirradiated specimen does not depend on the indent depth, meaning that the hardness is constant over the observed depth. For the irradiated specimens, the hardness decreases monotonically with increasing indent depth. This result indicates that the hardness only near the surface layer about several – several tens μm thick increases by the irradiation. Next, we discuss the hardness change in Xe-irradiated specimens near the boundary of irradiated and unirradiated regions. Vickers microhardness was measured from unirradiated region to the irradiated region at a regular interval on a straight line perpendicular to the boundary. If the load is so large or the indentation interval is so small, the hardness increases during the sequential indentations because of the work-hardening. Fig. 2 shows the relationship between Vickers microhardness and the measuring positions for the combination of applied load 50 gf and indentation interval 0.25 mm. A dashed line in the figure presents the boundary of

¹ Osaka Prefecture University

² Osaka Nuclear Science Association (ONSA)

unirradiated (left) and irradiated (right) regions. Using this indentation condition, Vickers microhardness is constant in both regions and we can measure correctly the spatial distribution of hardness. Fig. 3 shows the spatial distribution of hardness for a Xe-irradiated specimen. The hardness measurement was performed over an area of 5 mm × 5 mm with 20 × 20 data points. As the masking plate has a circular hole, the hardness only in the irradiated circular region increases. The present experiment implies that swift heavy ion irradiation can be used for the local modification of hardness in supersaturated alloys.

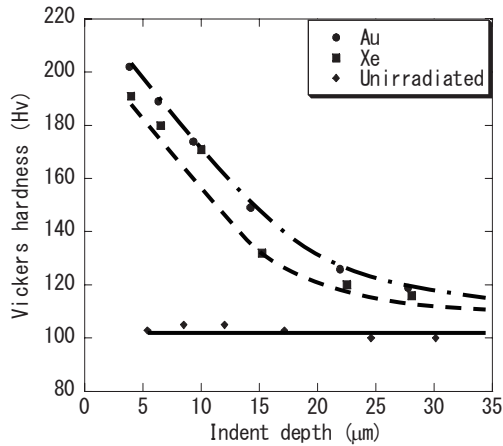


Fig. 1 Indent-depth dependence of Vickers microhardness for 200 MeV Xe irradiation and 200 MeV Au irradiation. For comparison, data for an unirradiated specimen are also plotted.

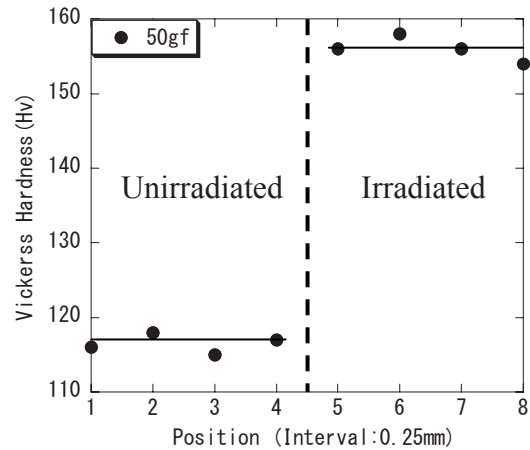


Fig. 2 Vickers microhardness measured ranging over the irradiated and unirradiated regions at a regular interval.

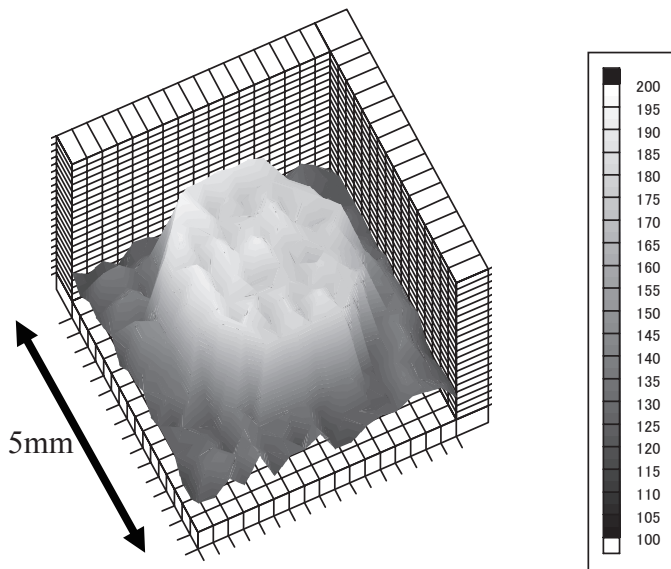


Fig. 3 Two-dimensional hardness mapping for Xe ion irradiated specimen. During irradiation, the specimen is covered with a thick copper masking plate having a circular hole. Vickers microhardness is measured at 20 × 20 data points.

References

[1] T. Tobita, M. Suzuki, A. Iwase and K. Aizawa, J. Nucl. Mater. 299 (2001) 267-270.
 [2] K. Morita, S. Ishino, T. Tobita, Y. Chimi, N. Ishikawa and A. Iwase, J. Nucl. Mater. 304 (2002) 153-160.
 [3] Shou Nakagawa, F. Hori, Y. Chimi, N. Ishikawa, M. Kitagawa, R. Oshima, T. Tobita, R. Taniguchi, M. Suzuki and A. Iwase, Nucl. Instr. and Meth. B 257 (2007) 397-401.

CHAPTER 8

Publication in Journal and Proceedings, and Contribution to Scientific Meetings

- 8.1 Accelerator Operation and Development
- 8.2 Nuclear Structure
- 8.3 Nuclear Reaction
- 8.4 Nuclear Chemistry
- 8.5 Nuclear Theory
- 8.6 Atomic Physics and Solid State Physics
- 8.7 Radiation Effects in Materials

This is a blank page

8.1 Accelerator Operation and Development

Journal/Proceedings

M. Matsuda et al.

Status Report of the JAEA-Tokai Tandem Accelerator

Proc. of the 19th Workshop of the Tandem Accelerator and their Associated Technology, Gunma, Paleo Labo Co.,Ltd. (July. 1-2, 2006) 9-12.

S. Hanashima

Update scheme of 180° bending magnet in the terminal of JAEA Tandem Accelerator

Proc. of the 19th Workshop of the Tandem Accelerator and their Associated Technology, Gunma, Paleo Labo Co.,Ltd. (July. 1-2, 2006) 50-53.

K. Kutsukake, M. Nakamura, M. Matsuda, S. Hanashima and K. Horie

Troubleshooting for JAEA Tandem Accelerator

Proc. of the 19th Workshop of the Tandem Accelerator and their Associated Technology, Gunma, Paleo Labo Co.,Ltd. (July. 1-2, 2006) 92-94.

M. Matsuda et al.

Present status of JAEA-Tokai tandem accelerator

Proc. of the 3rd Annual Meeting of Particle Accelerator Society of Japan and the 31th Linear Accelerator Meeting in Japan, Sendai (Aug. 2-4, 2006) 275-277.

H. Kabumoto, S. Takeuchi, M. Makoto, A. Iijima, T. Yoshida, T. Usami and S. Hida

Development of Superconducting Twin Quarter Wave Resonator for Acceleration of Low Velocity Heavy Ions

Proc. of the 3rd Annual Meeting of Particle Accelerator Society of Japan and the 31th Linear Accelerator Meeting in Japan, Sendai (Aug. 2-4, 2006) 819-821.

A. Osa for the TRIAC Collaboration

Status of JAEA-KEK Radioactive Ion Beam facility, TRIAC

Proc. of the 19th International Conference on the Application of Accelerators in Research and Industry, Fort Worth, Texas USA (Aug. 20-25, 2006)

Nucl. Instrum. Methods Phys. Res., B 261 (2007) 1048-1052.

Y.X. Watanabe et al.

TOKAI RADIOACTIVE ION ACCELERATOR COMPLEX (TRIAC)

Proceedings of the Seventh International Conference on "Radioactive Nuclear Beams" (RNB7), Cortina d'Ampezzo, Italy (July 3-7, 2006).

Meetings

T.K. Sato, A. Osa, K. Tsukada, M. Asai and S. Ichikawa

Development of A Thick Target For Ion Source of On-Line Mass Separation Of Heavy Actinide Isotopes

The 6th International Symposium on Advanced Science Research (ASR2006), Ibaraki, Japan (Oct. 26-27, 2006).

A. Osa for the TRIAC Collaboration

Status of JAEA-KEK Radioactive Ion Beam facility, TRIAC

The 6th International Symposium on Advanced Science Research (ASR2006), Ibaraki, Japan (Oct. 26-27, 2006).

A. Osa, T. K. Sato and S. Ichikawa

Development of Ion source for JAEA-ISOL-I

The 50th Symposium on Radiochemistry, Ibaraki, Japan (Oct. 26-27, 2006).

T. K. Sato, A. Osa and S. Ichikawa

Development of Ion source for JAEA-ISOL-II

The 50th Symposium on Radiochemistry, Ibaraki, Japan (Oct. 26-27, 2006).

8.2 Nuclear Structure

Journal/Proceedings

M. Asai, K. Tsukada, S. Ichikawa, M. Sakama, H. Haba, I. Nishinaka, Y. Nagame, S. Goto, Y. Kojima, Y. Oura and M. Shibata
 α decay of ^{238}Cm and the new isotope ^{237}Cm
 Phys. Rev., C 73 (2006) 067301-1-4.

M. Koizumi, Y. Toh, A. Osa, A. Kimura, Y. Utsuno, M. Oshima, T. Hayakawa, Y. Hatsukawa, J. Katakura, M. Matsuda, T. Shizuma, A. Seki, T. Morikawa, M. Sugawara, H. Kusakari, J. Goto, T. Czosnyka and M. Zielinska
Coulomb Excitation Experiments at JAEA Tandem Facility for The Study of Nuclear Structure
 Proceedings of the International Workshop on Quark Nuclear Physics 2006, Pusan National University Press ISBN (978-89-7316-270-3) 245-251.

Y.H. Zhang, X.H. Zhou, J.J. He, Z. Liu, Y.D. Fang, W.T. Guo, X.G. Lei, Y.X. Guo, M.M. Ndontchueng, L. Ma, M. Oshima, Y. Toh, M. Koizumi, A. Osa, A. Kimura, Y. Hatsukawa, H. Hayakawa, T. Shizuma, J. Katakura, M. Matsuda, G. De Angelis, N. Marginean, A. Gadea, D.R. Napoli, M. Axiotis, C. Rusu, T. Martinez, T. Morikawa, M. Sugawara, H. Kusakari and F.R. Xu
Search for signature inversion in the $\pi i_{13/2} \otimes \nu i_{13/2}$ bands in $^{182, 184, 186}\text{Au}$
 Int. J. Mod. Phys., E 15 (2006) 1437.

Y.H. Zhang, S. Guo, X.H. Zhou, L. MA, W.T. Guo, M. Oshima, Y. Toh, M. Koizumi, A. Osa, A. Kimura, Y. Hatsukawa, M. Sugawara and H. Kusakari
Identification of a new band and its signature inversion in ^{174}Re
 Chin. Phys. Lett. Vol.24, No.5 (2007) 1203.

T. Shizuma, T. Ishii, H. Makii, T. Hayakawa, S. Shigematsu, M. Matsuda, E. Ideguchi, Y. Zheng, M. Liu, T. Morikawa, P.M. Walker and M. Oi
Excited states in neutron-rich ^{188}W produced by an ^{18}O -induced 2-neutron transfer reaction
 Eur. Phys. J., A 30 (2006) 391.

X.H. Zhou, L. Ma, Y.B. Xing, Y.H. Zhang, Y.X. Guo, X.G. Lei, C.Y. Xie, M. Oshima, Y. Toh, M. Koizumi, A. Osa, Y. Hatsukawa, M. Sugawara and M.M. Ndontchueng
Observation of a $\pi h_{9/2} \otimes \nu i_{13/2}$ oblate band in ^{188}Tl
 Eur. Phys. J., A 28 (2006) 271.

L. Ma, X.H. Zhou, Y.B. Xing, Y.H. Zhang, Y.X. Guo, X.G. Lei, C.Y. Xie, M. Oshima, Y. Toh, M. Koizumi, A. Osa, Y. Hatsukawa and M. Sugawara

Properties of the $\pi h_{9/2} \otimes \nu i_{13/2}$ Oblate Band in ^{188}Tl

Chin. Phys. Lett. 23 (2006) 1727.

X.H. Zhou, Y.B. Xing, M.L. Liu, Y.H. Zhang, Y.X. Guo, L. Ma, X.G. Lei, W.T. Guo, M. Oshima, Y. Toh, M. Koizumi, A. Osa, Y. Hatsukawa, F.R. Xu and M. Sugawara

Band properties of the transitional nucleus ^{187}Pt

Phys. Rev., C 75 (2007) 034314.

T. Ishii, S. Shigematsu, H. Makii, M. Asai, K. Tsukada, A. Toyoshima, M. Matsuda, A. Makishima, T. Shizuma, J. Kaneko, I. Hossain, H. Tome, M. Ohara, S. Ichikawa, T. Kohno and M. Ogawa

Ground-state band of the neutron-rich transuranium nucleus $^{250}\text{Cm}_{154}$

J. Phys. Soc. Jpn. 75 (2006) 043201.

A.N. Andreyev, S. Antalic, D. Ackermann, S. Franchoo, F.P. Hessberger, S. Hofmann, M. Huyse, I. Kojouharov, B. Kindler, P. Kuusiniemi, S.R. Leshner, B. Lommel, R. Mann, G. Munzenberg, K. Nishio, R.D. Page, J.J. Ressler, B. Streicher, S. Saro, B. Sulignano, P. Van Duppen, D.R. Wiseman

α -decay spectroscopy of the new isotope ^{192}At

Phys. Rev., C 73 (2006) 024317-1-11.

A.N. Andreyev, S. Antalic, D. Ackermann, S. Franchoo, F.P. Hessberger, S. Hofmann, M. Huyse, I. Kojouharov, B. Kindler, P. Kuusiniemi, S.R. Leshner, B. Lommel, R. Mann, G. Munzenberg, K. Nishio, R.D. Page, J.J. Ressler, B. Streicher, S. Saro, B. Sulignano, P. Van Duppen, D. Wiseman, R. Wyss

α -decay of the new isotope ^{187}Po : Probing prolate structures beyond the neutron mid-shell at $N = 104$

Phys.Rev., C 73 (2006) 044324-1-8.

F.P. Hessberger, S. Hofmann, D. Ackermann, S. Antalic, B. Kindler, I. Kojouharov, P. Kuusiniemi, M. Leino, B. Lommel, R. Mann, K. Nishio, A.G. Popeko, B. Sulignano, S. Saro, B. Streicher, M. Venhart, A.V. Yeremin

Alpha-gamma decay studies of ^{251}No

Eur. Phys. J., A 29 (2006) 165 - 173.

F.P. Hessberger, S. Hofmann, D. Ackermann, S. Antalic, B. Kindler, I. Kojouharov, P.

Kuusiniemi, M. Leino, B. Lommel, R. Mann, K. Nishio, A.G. Popeko, B. Sulignano, S. Saro, B. Streicher, M. Venhart, A.V. Yeremin
Alpha-gamma decay studies of ^{255}Rf , ^{251}No and ^{247}Fm
 Eur. Phys. J., A 30 (2006) 561 - 569.

P. Kuusiniemi, F.P. Hessberger, D. Ackermann, S. Antalic, S. Hofmann, K. Nishio, B. Sulignano, I. Kojouharov, R. Mann
Studies of $^{213g, m}\text{Ra}$ and $^{214g, m}\text{Ra}$ by α and γ decay
 Eur. Phys. J., A 30 (2006) 551- 560.

Meetings

M. Asai
Gamma-ray spectroscopy for superheavy elements
 Discussion Meeting on the Production and Spectroscopy for Superheavy Elements, Wako (Nov. 1-2, 2006).

M. Asai
Spectroscopy of superheavy elements
 The Specialists' Meeting on the Nuclear Science of Heavy Elements, KURRI, Kumatori (Feb. 5-6, 2007).

T. Morikawa, E. Ideguchi, M. Liu, Y. Zheng, M. Nakamura, T. Sugimitsu, S. Mitarai, H. Kusakari, M. Oshima, M. Koizumi, Y. Toh, A. Kimura, A. Osa, H. Harada, K. Furutaka, S. Nakamura, F. Kitatani, Y. Hatsukawa and M. Sugawara
Study of largely deformed states and high-spin shell structure in $A\sim 30$ nuclei
 Material Science Symposium 'Heavy Ion Science in Tandem Energy Region', Tokai (Dec. 12, 2006).

T. Morikawa, M. Nakamura, T. Sugimitsu, H. Kusakari, S. Mitarai, M. Ohsima, Y. Toh, Y. Hatsukawa, J. Katakura, M. Koizumi, A. Osa, A. Kimura, J. Goto, E. Ideguchi, M. Liu, Y. Zheng and M. Sugawara
High-spin yrast levels in neutron-rich ^{33}P nucleus
 Spring Meeting of Physical Society of Japan, Hachioji (Mar. 26, 2007).

Y. Hirayama
Beta-delayed Neutron Detectors

International Collaboration Workshop on Experiments at the RIBF, RIKEN, Wako, Saitama, Japan (Nov. 6-9, 2006).

M. Koizumi, Y. Toh, A. Osa, A. Kimura, M. Oshima, Y. Hatsukawa, H. Kusakari, M. Sugawara, T. Morikawa, T. Czosnyka, M. Zielinska and Y. Kojima
Nuclear structure study with Coulomb excitation experiments
JUSTIPEN (Japan-US Theory Institute for Physics with Exotic Nuclei) meeting on gamma deformation of nuclear systems with Prof. P. Moller, Wako (Dec. 11, 2006).

M. Koizumi, Y. Toh, M. Oshima, A. Osa, A. Kimura, Y. Hatsukawa, H. Harada, F. Kitatani, S. Nakamura, K. Furutaka, K. Hara, M. Ohta, M. Sugawara, T. Morikawa, H. Kusakari, Y. Kojima and T. Czosnyka
Study of the low-lying ^{132}Xe structure with Coulomb excitation experiment
Spring Meeting of the Physical Society of Japan (Mar. 26, 2007).

T. Shizuma, T. Ishii, H. Makii, T. Hayakawa, M. Matsuda, E. Ideguchi, Y. Zheng, M. Liu, T. Morikawa, S. Mitarai and M. Fujiwara
Nuclear structure of nuclei in the $A=180$ region using transfer reactions
Tandem Workshop, JAEA, Tokai (Dec. 2006).

T. Shizuma
Studies of nuclear isomers by γ -ray spectroscopy
RCNP Workshop, Osaka University (Feb. 2007).

T. Shizuma, T. Ishii, H. Makii, T. Hayakawa, S. Shigematsu, M. Matsuda, E. Ideguchi, Y. Zheng, M. Liu, T. Morikawa, P.M. Walker, and M. Oi
Spectroscopy on neutron-rich ^{187}W and ^{188}W produced in neutron transfer reactions
Spring Meeting of the Physical Society of Japan, Tokyo (Mar. 2007).

H. Iimura
Plan of Gas-Cell Laser Spectroscopy at JAEA Tandem Accelerator
Workshop on Laser Experiment at Next Generation Accelerator Facility, Wako (Dec. 1, 2006).

T. Ishii, S. Shigematsu, H. Makii, M. Asai, K. Tsukada, A. Toyoshima, M. Matsuda, A. Makishima, T. Shizuma, J. Kaneko, I. Hossain, H. Tome, M. Ohara, S. Ichikawa, T. Kohno, and M. Ogawa
In-beam γ -ray study of the neutron-rich nuclei of ^{240}U , ^{246}Pu and ^{250}Cm

Int. Conf. on Nuclear Structure and Related Topics, Dubna (Jun. 13-17, 2006).

T. Ishii

In-beam γ -ray spectroscopy of the neutron-rich nuclei in the uranium region produced by the heavy-ion transfer reaction

Autumn Meeting of the Physical Society of Japan, Nara (Sep. 20-23, 2006).

H. Makii, T. Ishii, M. Asai, K. Tsukada, A. Toyoshima, M. Matsuda, A. Makishima, J. Kaneko, H. Tome, S. Ichikawa, S. Shigematsu, T. Kohno and M. Ogawa

In-beam γ -ray measurement of the neutron-rich nucleus ^{246}Pu

Autumn Meeting of the Physical Society of Japan, Nara (Sep. 20-23, 2006).

T. Ishii, H. Makii, M. Asai, S. Shigematsu, K. Tsukada, A. Toyoshima, M. Matsuda, A. Makishima, J. Kaneko, H. Tome, I. Hossain, T. Shizuma, S. Ichikawa, T. Kohno and M. Ogawa

In-beam γ -ray spectroscopy of the neutron-rich ^{236}Th and ^{242}U produced by the (^{18}O , ^{20}Ne) reaction

Spring Meeting of the Physical Society of Japan, Tokyo (Mar. 25-28, 2007).

M. Asai, K. Tsukada, H. Haba, A. Toyoshima, T. Ishii, Y. Nagame, I. Nishinaka, T. Ichikawa, Y. Kojima and K. Sueki

α - γ Spectroscopy of ^{255}No

2006 Autumn Meeting of the Physical Society of Japan, Nara (Sep. 21, 2006).

M. Asai

γ -ray Spectroscopy of the Heaviest Elements at JAEA

ASR2006: the 6th International Symposium on Advanced Science Research, Frontiers of Nuclear and Radiochemistry, Ibaraki (Oct. 26, 2006).

8.3 Nuclear Reaction

Journal/Proceedings

H. Ishiyama, T. Hashimoto, T. Ishikawa, Y.X. Watanabe, S.K. Das, H. Miyatake, Y. Mizoi, T. Fukuda, M-H. Tanaka, Y. Fuchi, N. Yoshikawa, Y. Hirayama, S.C. Jeong, T. Nomura, I. Katayama, S. Mitsuoka, K. Nishio, M. Matsuda, P.K. Saha, S. Ichikawa, H. Ikezoe, T. Furukawa, H. Izumi, T. Shimoda and K. Nakai

A New Measurement of the astrophysical ${}^8\text{Li}(\alpha, n){}^{11}\text{B}$ reaction

Phys. Lett., B 640 (2006) 82.

K. Nishio, S. Hofmann, F.P. Hessberger, D. Ackermann, S. Antalic, V.F. Comas, Z. Gan, S. Heinz, J.A. Heredia, H. Ikezoe, J. Khuyagbaatar, B. Kindler, I. Kojouharov, P. Kuusiniemi, B. Lommel, R. Mann, M. Mazzocco, S. Mitsuoka, Y. Nagame, T. Ohtsuki, A.G. Popeko, S. Saro, H.J. Schött, B. Sulignano, A. Svirikhin, K. Tsukada, K. Tsuruta and A.V. Yeremin

Measurement of evaporation residue cross-sections of the reaction ${}^{30}\text{Si} + {}^{238}\text{U}$ at subbarrier energies

Eur. Phys. J., A 29 (2006) 281.

H. Ishiyama, Y.X. Watanabe, N. Imai, Y. Hirayama, H. Miyatake, M-H. Tanaka, N. Yoshikawa, S.C. Jeong, Y. Fuchi, I. Katayama, T. Nomura, T. Ishikawa, K. S.K. Das, Y. Mizoi, T. Fukuda, T. Hashimoto, K. Nishio, S. Mitsuoka, H. Ikezoe, M. Matsuda, S. Ichikawa and T. Shimoda

Study of astrophysical (α, n) reactions on light neutron-rich nuclei using low-energy radioactive nuclear beams

American Institute of Physics Conference Proceedings 847 (2006) 249.

S.K. Das, T. Fukuda, Y. Mizoi, H. Ishiyama, H. Miyatake, Y.X. Watanabe, Y. Hirayama, M-H. Tanaka, N. Yoshikawa, S.C. Jeong, Y. Fuchi, I. Katayama, T. Nomura, T. Ishikawa, K. Nakai, T. Hashimoto, S. Mitsuoka, K. Nishio, P.K. Saha, M. Matsuda, S. Ichikawa, H. Ikezoe, T. Furukawa, H. Izumi, T. Shimoda and T. Sasaqui

A New measurement of the ${}^8\text{Li}(\alpha, n){}^{11}\text{B}$ Reaction for Astrophysical Interest

American Institute of Physics Conference Proceedings 847 (2006) 374.

H. Ikezoe, S. Mitsuoka, K. Nishio, K. Tsuruta, Y. Watanabe, S.C. Jeong and K. Satou

Barrier distributions for cold fusion reactions

AIP Conference Proceedings Volume 853, FUSION06:Reaction Mechanisms and Nuclear Structure at the Coulomb Barrier, Venezia, Italy (Mar. 19-23, 2006).

K. Nishio, H. Ikezoe, M. Asai, K. Tsukada, S. Mitsuoka, K. Tsuruta, K. Satou, C.J. Lin and T. Ohsawa

Evidence of Complete Fusion in the Subbarrier $^{16}\text{O} + ^{238}\text{U}$ Reaction

Proceedings of the National Conference on Nuclear Physics “Frontiers in the Physics of Nucleus” St. Petersburg State University, Russia (Jun. 28–Jul. 1, 2005).

Phys. Atomic Nuclei 69 (2006) 1399.

K. Nishio, S. Hofmann, F.P. Hessberger, D. Ackermann, S. Antalic, V.F. Comas, Z. Gan, S. Heinz, J.A. Heredia, H. Ikezoe, J. Khuyagbaatar, B. Kindler, I. Kojouharov, P. Kuusiniemi, B. Lommel, R. Mann, M. Mazzocco, S. Mitsuoka, Y. Nagame, T. Ohtsuki, A.G. Popeko, S. Saro, H.J. Schött, B. Sulignano, A. Svirikhin, K. Tsukada, K. Tsuruta and A.V. Yeremin

Measurement of evaporation residue cross-sections of the reaction $^{30}\text{Si} + ^{238}\text{U}$ at subbarrier energies

Tours Symposium on Nuclear Physics VI, Torus, France (Sep. 5-8, 2006).

AIP Conference Proceedings, 891 (2007) 71-79.

Meetings

H. Miyatake, H. Ishiyama, Y.X. Watanabe, Y. Hirayama, N. Imai, M-H. Tanaka, N. Yoshikawa, S.C. Jeong, Y. Fuchi, T. Nomura, I. Katayama, H. Kawakami, T. Ishikawa, S.K. Das, Y. Mizoi, T. Fukuda, T. Hashimoto, K. Nishio, S. Mitsuoka, H. Ikezoe, M. Matsuda, S. Ichikawa, P.K. Saha, A. Sato, T. Shimoda and T. Sasaqui

Direct measurement of astrophysical nuclear reaction rates on light-neutron rich nuclei at TRIAC and JAEA-RMS

The 7th international conference on Radioactive Nuclear Beams, Cortina d’Ampezzo, Italy (Jul. 3–7, 2006).

K. Nishio, S. Hofmann, H. Ikezoe, F.P. Hessberger, D. Ackermann, S. Antalic, V.F. Comas, Z. Gan, S. Heinz, J.A. Heredia, J. Khuyagbaatar, B. Kindler, I. Kojouharov, P. Kuusiniemi, B. Lommel, R. Mann, M. Mazzocco, S. Mitsuoka, Y. Nagame, T. Ohtsuki, A.G. Popeko, S. Saro, H.J. Schött, B. Sulignano, A. Svirikhin, K. Tsukada, K. Tsuruta and A.V. Yeremin

Measurement of evaporation residue and fission cross-sections of the reaction $^{30}\text{Si} + ^{238}\text{U}$ at subbarrier energies

The 6th International Symposium on Advanced Science Research, Frontiers on Nuclear and radiochemistry (ASR2006), Tokai, Japan (Oct. 26-27, 2006).

I. Nishinaka, M. Tanikawa, Y. Nagame, M. Asai, K. Tsukada, A. Toyoshima and T. Ichikawa

Correlation between fission and α -particle emission in the $^{18}\text{O} + ^{244}\text{Pu}$ Reaction

The 6th Int. Symp. on Advanced Science Research, Tokai (Oct. 26-27, 2006).

S. Hofmann, D. Ackermann, S. Antalic, H.G. Burkhard, R. Dressler, F.P. Hessberger, B. Kindler, I. Kojouharov, P. Kuusiniemi, M. Leino, B. Lommel, R. Mann, G. Munzenberg, K. Nishio, A.G. Popeko, S. Saro, H.J. Schoett, B. Streicher, B. Sulignano, J. Uusitalo and A.V. Yeremin

Studies of SHE at SHIP

EXON 2006, International Symposium on exotic nuclei, Khanty-Mansiysk (Jul.17-22, 2006).

Y. Watanabe

Study of isotope dependence of fusion process

International Collaboration Workshop 2006, RIKEN (Nov. 6-9, 2006).

T. Hashimoto, H. Ishiyama, Y. Hirayama, Y.X. Watanabe, N. Imai, H. Miyatake, M-H. Tanaka, N. Yoshikawa, Y. Fuchi, T.K. Sato, A. Osa, S. Ichikawa, S. Mitsuoka, K. Nishio, H. Ikezoe, M. Matsuda, Y. Mizoi, S.K. Das, T. Fukuda, A. Sato and S. Shimoda

Direct measurement of the $^8\text{Li}(d, t)$, (d, p) , (d, α) reaction cross sections

Autumn Meeting of the Physical Society of Japan, Nara (Sep. 20-23, 2006).

S. Mitsuoka, H. Ikezoe, K. Nishio, S.C. Jeong and Y. Watanabe

Barrier distribution of quasi-elastic backward scattering in $^{70}\text{Zn} + ^{208}\text{Pb}$, ^{209}Bi

Autumn Meeting of the Physical Society of Japan, Nara (Sep. 20-23, 2006).

K. Nishio, S. Hofmann, F.P. Hessberger, D. Ackermann, S. Antalic, V.F. Comas, Z. Gan, S. Heinz, J.A. Heredia, H. Ikezoe, J. Khuyagbaatar, B. Kindler, I. Kojouharov, P. Kuusiniemi, B. Lommel, R. Mann, M. Mazzocco, S. Mitsuoka, Y. Nagame, T. Ohtsuki, A.G. Popeko, S. Saro, H.J. Schött, B. Sulignano, A. Svirikhin, K. Tsukada, K. Tsuruta and A.V. Yeremin

Production of Sg isotopes in the fusion reaction $^{30}\text{Si} + ^{238}\text{U}$

Autumn meeting of the Physical Society of Japan, Nara (Sep. 20-23, 2006).

I. Nishinaka, M. Tanikawa, Y. Nagame, M. Asai, K. Tsukada, A. Toyoshima and T. Ichikawa

Correlation between fission fragments and α -particles in the $^{18}\text{O} + ^{244}\text{Pu}$ Reaction

The 50th Symp. on Radiochemistry, Mito (Oct. 24-27, 2006).

S. Mitsuoka, H. Ikezoe, K. Nishio, S.C. Jeong and Y. Watanabe

Measurement of fusion barrier distribution for cold fusion reactions

RCNP Workshop on Heavy-ion Reaction Dynamics of Fusion and Fission for Super-Heavy Synthesis, Osaka (Jul. 13-14, 2006).

8.4 Nuclear Chemistry

Journal/Proceedings

R.A. Gherghescu and Y. Nagame

Isobaric cold-fusion channels for synthesis of $^{276}114$, $^{286}114$, and $^{290}114$
 Phys. Rev., C 74 (2006) 014611-1-12.

R.A. Gherghescu, D.N. Poenaru, W. Greiner and Y. Nagame

Synthesis of $^{286}114$ and $^{290}114$ using low-energy fusion channels
 J. Phys. G: Nucl. Phys. 32 (2006) L73-L84.

Y. Nagame, M. Asai, H. Haba, H. Hirata, Y. Ishii, I. Nishinaka, A. Toyoshima and K. Tsukada

Aqueous chemistry of the transactinide element, rutherfordium (Rf)
 Lecture Series on Computer and Computational Sciences, 7 (2006) 927-930.

J. Dovrak, W. Bröchle, M. Chelnokov, R. Dressler, Ch.E. Düllmann, K. Eberhardt, V. Gorshokov, E. Jüger, R. Krücken, A. Kuznetsov, Y. Nagame, F. Nebel, Z. Novackova, Z. Qin, M. Schädel, B. Schausten, E. Schimpf, A. Semchenkov, P. Thörler, A. Türler, M. Wegrzecki, B. Wierczinski, A. Yakushev and A. Yeremin

Doubly magic $^{270}_{108}\text{Hs}_{162}$
 Phys. Rev. Lett. 97 (2006) 242501-1-4.

Y. Nagame, K. Akiyama, M. Asai, S. Goto, H. Haba, M. Hirata, Y. Ishii, I. Nishinaka, H. Tome, A. Toyoshima and K. Tsukada

Chemical studies of the transactinide elements at JAEA
 Proceedings of the 6th China-Japan Joint Nuclear Physics Symposium -Nuclear Physics Trends-, Shanghai, China (May 16-20, 2006).
 AIP Conference Proceedings, Vol. 865 (2006) 165-172.

H. Haba, K. Tsukada, M. Asai, A. Toyoshima, Y. Ishii, H. Toume, T. Sato, I. Nishinaka, T. Ichikawa, S. Ichikawa, Y. Nagame, W. Sato, K. Matsuo, Y. Kitamoto, Y. Tashiro, A. Shinohara, J. Saito, M. Ito, T. Ikezawa, M. Sakamaki, S. Goto, H. Kudo, H. Kikunaga, M. Arai, S. Kamataki, A. Yokoyama, K. Akiyama, K. Sueki, Y. Oura, M. Schädel, W. Bröchle and J.V. Kratz

Extraction behavior of rutherfordium into tributylphosphate from hydrochloric acid
 Radiochim. Acta 95 (2007) 1-6.

Meetings

Y. Nagame

Chemistry of superheavy elements

RCNP symposium - Dynamics of heavy-ion fusion and fission -, Suita (Jun. 13-14, 2006).

I. Nishinaka

Partition of mass and total excitation energy between fragment pairs in low energy fission

RCNP symposium - Dynamics of heavy-ion fusion and fission -, Suita (Jun. 13-14, 2006).

Y. Nagame

Elements at the upper most end of the periodic table

The 50th Symp. on Radiochemistry, Mito-Tokai (Oct. 24-27, 2006).

I. Nishinaka, M. Tanikawa, Y. Nagame, M. Asai, K. Tsukada, A. Toyoshima and T. Ichikawa

Correlation between fission fragments and α -particles in the $^{18}\text{O} + ^{244}\text{Pu}$ reaction

The 50th Symp. on Radiochemistry, Mito-Tokai (Oct. 24-27, 2006).

Y. Ishii, H. Tome, A. Toyoshima, M. Asai, I. Nishinaka, K. Tsukada, Y. Nagame, S. Miyashita, T. Mori, H. Suganuma, Y. Tashiro, A. Shinohara, M. Sakamaki, S. Goto, H. Kudo, H. Haba, K. Akiyama and Y. Oura

Cation-exchange behavior of Rf in HNO_3/HF mixed solution (II)

The 50th Symp. on Radiochemistry, Mito-Tokai (Oct. 24-27, 2006).

A. Toyoshima, Y. Kasamatsu, K. Tsukada, H. Haba, A. Shinohara and Y. Nagame

Development of an electrochemistry apparatus for atom-at-a-time chemistry

The 50th Symp. on Radiochemistry, Mito-Tokai (Oct. 24-27, 2006).

A. Toyoshima, Y. Kasamatsu, K. Tsukada, H. Haba, M. Asai, Y. Ishii, H. Toume, T. K. Sato, I. Nishinaka, Y. Nagame, S. Goto, T. Ishikawa, M. Sakamaki, H. Kudo, K. Akiyama, Y. Oura, H. Kikunaga, K. Ooe, T. Kuribayashi, A. Shinohara, K. Sueki and A. Yokoyama

TOPO-reversed phase extraction behavior of rutherfordium in HCl solutions

The 50th Symp. on Radiochemistry, Mito-Tokai (Oct. 24-27, 2006).

Y. Kasamatsu, A. Toyoshima, H. Toume, K. Tsukada, H. Haba and Y. Nagame

Adsorption of Nb, Ta, and Pa on anion exchangers in diluted HF media

The 50th Symp. on Radiochemistry, Mito-Tokai (Oct. 24-27, 2006).

K. Akiyama, H. Haba, K. Tsukada, M. Asai, A. Toyoshima, T. Yaita, K. Sueki and Y. Nagame
EXAFS study for complexation of Zr and Hf with TBP in HCl solution
The 50th Symp. on Radiochemistry, Mito-Tokai (Oct. 24-27, 2006).

Y. Ishii

Cation-exchange behavior of element 104, rutherfordium (Rf)

The Specialists' Meeting on the Nuclear Science of Heavy Elements, KURRI, Kumatori (Feb. 5-6, 2007).

A. Toyoshima

Oxidation of nobelium

The Specialists Meeting on the Nuclear Science of Heavy Elements, KURRI, Kumatori (Feb. 5-6, 2007).

A. Toyoshima, Y. Kasamatsu, Y. Kitatsuji, K. Tsukada, Y. Ishii, H. Toume, M. Asai, H. Haba, K. Akiyama, K. Ooe, W. Sato, A. Shinohara and Y. Nagame

Electrochemical oxidation of nobelium

The 87th Spring Meeting of the Chemical Society of Japan, Kansai Univ., Suita (Mar. 25-28, 2007).

Y. Ishii, H. Tome, A. Toyoshima, M. Asai, I. Nishinaka, K. Tsukada, Y. Nagame, S. Miyashita, T. Mori, H. Suganuma, Y. Tashiro, A. Shinohara, M. Sakamaki, S. Goto, H. Kudo, H. Haba, K. Akiyama and Y. Oura

Fluoride complex formation of Rf in HNO₃/HF mixed solution

The 87th Spring Meeting of the Chemical Society of Japan, Kansai Univ., Suita (Mar. 25-28, 2007).

Y. Kasamatsu, A. Toyoshima, H. Toume, K. Tsukada, H. Haba and Y. Nagame

Anion-exchange behavior of Nb, Ta, and Pa in HF/HNO₃ media for chemical investigation of Db

The 87th Spring Meeting of the Chemical Society of Japan, Toyonaka (Mar. 25-28, 2007).

H. Toume, Y. Kasamatsu, A. Toyoshima, Y. Ishii, K. Tsukada, H. Haba, N. Shinohara and Y. Nagame

Cation exchange behavior of Nb and Ta in mixed HF/HNO₃ solutions - Model experiment for chemical study of element 105 (Db)

The 87th Spring Meeting of the Japan Chemical Society, Suita (Mar. 25-28, 2007).

Y. Nagame

Nuclear chemistry of the heaviest elements at JAEA

2006 Spring Meeting of the Korean Physical Society, Pyungchang, Korea (Apr. 20-21, 2006)

Y. Nagame

Chemical studies of the transactinide elements at JAEA

The 6th China-Japan Joint Nuclear Physics Symposium, Shanghai, China (May 16-20, 2006).

A. Toyoshima

Fluoride complexation study of rutherfordium at JAEA

Workshop on the Atomic Properties of the Heaviest Elements, Abtei Frauenwörth im Chiemsee, Germany (Sep. 25-27, 2006).

K. Tsukada

Chemical studies of the heaviest elements at JAEA

ASR2006: the 6th International Symposium on Advanced Science Research - Frontiers of Nuclear and Radiochemistry -, Tokai, Japan (Oct. 26-27, 2006).

Y. Nagame

Aqueous chemistry of the transactinide element, rutherfordium (Rf)

International Conference of Computational Methods in Sciences and Engineering 2006 (ICCMSE 2006), Chania, Crete, Greece (Oct. 27- Nov. 1, 2006).

I. Nishinaka, M. Tanikawa, Y. Nagame, M. Asai, K. Tsukada, A. Toyoshima and T. Ichikawa

Correlation between fission and α -particle emission in the $^{18}\text{O} + ^{244}\text{Pu}$ reaction

ASR2006: the 6th International Symposium on Advanced Science Research - Frontiers of Nuclear and Radiochemistry -, Tokai, Japan (Oct. 26-27, 2006).

Y. Ishii, H. Toume, A. Toyoshima, M. Asai, I. Nishinaka, K. Tsukada, Y. Nagame, Y. Tashiro, A. Shinohara, M. Sakamaki, S. Goto, H. Kudo, K. Akiyama, H. Haba, Y. Oura, S. Miyashita, T. Mori and H. Suganuma

A cation-exchange study of fluoride complexation of rutherfordium (Rf) in HNO_3/HF mixed solution system

ASR2006: the 6th International Symposium on Advanced Science Research - Frontiers of Nuclear and Radiochemistry -, Tokai, Japan (Oct. 26-27, 2006).

Y. Kasamatsu, A. Toyoshima, H. Toume, K. Tsukada, H. Haba and Y. Nagame
Adsorption of Nb, Ta and Pa on anion exchangers in HF/HNO₃ media - Model experiments for the chemical study of dubnium (Db) -
ASR2006: the 6th International Symposium on Advanced Science Research - Frontiers of Nuclear and Radiochemistry -, Tokai, Japan (Oct. 26-27, 2006).

A. Toyoshima, Y. Kasamatsu, K. Tsukada, H. Haba, M. Asai, Y. Ishii, H. Toume, T. K. Sato, I. Nishinaka, Y. Nagame, S. Goto, T. Ishiyama, M. Sakamaki, H. Kudo, K. Akiyama, Y. Oura, H. Kikunaga, K. Ooe, T. Kuribayashi, A. Shinohara and A. Yokoyama
TOPO reversed-phase extraction behavior of rutherfordium in HCl solutions
ASR2006: the 6th International Symposium on Advanced Science Research - Frontiers of Nuclear and Radiochemistry -, Tokai, Japan (Oct. 26-27, 2006).

A. Toyoshima, Y. Kasamatsu, K. Tsukada, H. Haba, A. Shinohara and Y. Nagame
Development of an electrochemistry apparatus for an atom-at-a-time chemistry
ASR2006: the 6th International Symposium on Advanced Science Research - Frontiers of Nuclear and Radiochemistry -, Tokai, Japan (Oct. 26-27, 2006).

Y. Nagame
Rapid ion-exchange apparatus AIDA for heavy element chemistry
233rd American Chemical Society National Meeting, Chicago, USA (Mar. 25-29, 2007).

8.5 Nuclear Theory

Journal/Proceedings

Y. Akimura, T. Maruyama, N. Yoshinaga and S. Chiba

Properties of Baryon and Quark Matter Studied with a Molecular Dynamics
Acta Phys. Hung., A 27 (2006) 355.

T. Maruyama, T. Tatsumi, T. Endo and S. Chiba

Pasta Structures in Compact Stars
Recent Developments in Physics 7 (2006) 1.

N.T. Okumucsoglu, F.K. Gorur, J. Birchall, E.Sh. Soukhovitskii, R. Capote, J.M. Quesada and S. Chiba

Angular Distributions of Protons Scattered by ^{40}Ar Nuclei with Excitation of the 2^+ (1.46 MeV) and 3^- (3.68 MeV) Collective Levels for Incident Energies of 25.1, 32.5 and 40.7 MeV
Phys. Rev., C 75 (2007) 034616.

S. Oryu, S. Nishinohara, N. Shiiki and S. Chiba

Coulomb Phase Shift Calculation in Momentum Space
Phys. Rev., C 75 (2007) 021001(R).

T. Hayakawa, S. Miyamoto, Y. Hayashi, K. Kawase, K. Horikawa, S. Chiba, K. Nakanishi, H. Hashimoto, T. Ohta, M. Kando, T. Mochizuki, T. Kajino and M. Fujiwara

Half-life of ^{184}Re Populated by the (γ, n) Reaction from Laser Compton Scattering γ -rays at the Electron Storage Ring NewSUBARU
Phys. Rev., C 74 (2006) 065802.

K. Sumiyoshi, S. Yamada, H. Suzuki and S. Chiba

Neutrino Signals from the Formation of Black Hole : A Probe of Equation of State of Dense Matter
Phys. Rev. Lett. 97 (2006) 091101.

T. Suzuki, S. Chiba, T. Yoshida, T. Kajino and T. Otsuka

Neutrino Nucleus Reactions based on New Shell Model Hamiltonians
Phys. Rev., C 74 (2006) 034307.

Michael Smith, Eric J. Lingerfelt, Jason P. Scott, Caroline D. Nesaraja, Kyungyuk Chae,

Hiroyuki Koura, W. Raphael Hix, Luke F. Roberts, Daniel W. Bardayan and Jeffery C. Blackmon

New Features in the Computational Infrastructure for Nuclear Astrophysics

Nuclei in the Cosmos IX (Proceedings of Science, SISSA, Italy, 2006), POS(NIC-IX) 180, 1-5.

Michael S. Smith, Eric J. Lingerfelt, Jason P. Scott, Caroline D. Nesaraja, W. Raphael Hix, Kyungyuk Chae, Hiroyuki Koura, Richard A. Meyer, Daniel W. Bardayan, Jeffery C. Blackmon and Michael W. Guidry

Computational Infrastructure for Nuclear Astrophysics

Origin of Matter and Evolution of Galaxies(OMEG05), (AIP Conference Proceedings 847, 2006) 470-472.

K. Morita, K. Morimoto, D. Kaji, T. Akiyama, S. Goto, H. Haba, E. Ideguchi, R. Kanungo, K. Katori, H. Kikunaga, H. Koura, H. Kudo, T. Ohnishi, A. Ozawa, N. Sato, T. Suda, K. Sueki, F. Tokanai, H. Xu, T. Yamaguchi, A. Yoneda, A. Yoshida and Y.L. Zhao

Experiments on Synthesis of the Heaviest Element at RIKEN

TOURS Symposium on Nuclear Physics VI, ed. M. Arnould et al., (AIP Conf. Proc. 891, 2007) 3-9.

S. Tatsuta, K. Hashizume, T. Wada, M. Ohta, K. Sumiyoshi, K. Otsuki, T. Kajino, H. Koura, S. Chiba and Y. Aritomo

Fission fragment mass distribution for nuclei in the r-process region

TOURS Symposium on Nuclear Physics VI, ed. M. Arnould et al., (AIP Conf. Proc. 891, 2007) 423-426.

Y. Utsuno, T. Otsuka, T. Mizusaki, and M. Honma

Structure of exotic nuclei in the sd-pf shell region and its relation to the effective interaction

Proc. Int. Symposium "Structure of Exotic Nuclei and Nuclear Forces", J. Phys., Conf. Ser. Vol. 49 (2006) 126.

Y. Utsuno, T. Otsuka, T. Mizusaki, and M. Honma

Structure of exotic nuclei by large-scale shell model calculations

Proc. 6th China-Japan Joint Nuclear Physics Symposium "Nuclear Physics Trends", AIP Conf. Proc. Vol. 865 (2006) 101.

V. Tripathi, S.L. Tqabor, C.R. Hoffman, M. Wiedeking, A. Volya, P.F. Mantica, A.D. Davies, S.N. Liddick, W.F. Mueller, A. Stolz, B.E. Tomlin, T. Otsuka and Y. Utsuno

β -delayed γ spectroscopy of neutron rich $^{27, 28, 29}\text{Na}$

Phys. Rev., C 73 (2006) 054303.

A. Ozawa, K. Matsuda, T. Nagatomo, M. Mihara, K. Yamada, T. Yamaguchi, T. Ohtsubo, S. Momota, T. Izumikawa, T. Sumikama, Y. Nakashima, H. Fujiwara, S. Kumashiro, R. Matsumiya, M. Ota, D. Shinojima, H. Tanaka, T. Yasuno, S. Nakajima, T. Suzuki, K. Yoshida, K. Muranaka, T. Maemura, A. Chiba, Y. Utsuno, M. fukuda, K. Tanaka, I. Tanihata, Y. Nojiri, T. Minamisono, J.R. Alonso, G.F. Krebs and T.J.M. Symons

Measurement of the spin and magnetic moment of ^{23}Al

Phys. Rev., C 74 (2006) 021301(R).

J.R. Terry, D. Bazin, B.A. Brown, C.M. Campbell, J.A. Church, J.M. Cook, A.D. Davies, D-C. Dinca, J. Enders, A. Gade, T. Glasmacher, P.G. Hansen, J.L. Lecouey, T. Otsuka, B. Pritychenko, B.M. Sherrill, J.A. Tostevin, Y. Utsuno, K. Yoneda and H. Zwahlen

Direct evidence for the onset of intruder configurations in neutron-rich Ne isotopes

Phys. Lett., B 640 (2006) 86.

Meetings

T. Maruyama, T. Tatsumi and S. Chiba

Bulk properties of Kaonic Nuclei Obtained by a RMF model

KEK Conference on modern physics of nuclei, diversifying and progressing pictures of nuclei, Tsukuba (Aug. 1-3, 2006).

T. Maruyama, T. Tatsumi, J.H. Shulze and S. Chiba

Quark-hyperon Mixed Phase in Compact Stars

Autumn Meeting of the Physical Society of Japan, Nara (Sep. 20-23, 2006).

H. Koura

Systematical study of decay modes and half-lives for superheavy nuclei

The RCNP workshop “Reaction mechanism of heavy-ion fusion-fission and dynamics on synthesis of super-heavy nuclei”, Ibaraki, Osaka (Jul. 4-5, 2006).

H. Koura and S. Chiba

Estimation of Calculation for nuclear potential energy surfaces to large deformations

2006 Autumn Meeting of the Atomic Energy Society of Japan, Sapporo, Hokkaido (Sep. 27-29, 2006).

H. Koura and S. Chiba

Systematical properties of spontaneous fission for superheavy nuclei and a limit of existence of nuclei

The 6th International Symposium on Advanced Science Research -Frontiers of Nuclear and Radiochemistry- (ASR06), Tokai, Ibaraki (Oct. 26-27, 2006).

H. Koura

Nuclear shape evolution on the spherical-basis method and some predictions from the KTUY mass formula

JUSTIPEN (Japan-US Theory Institute for Physics with Exotic Nuclei) meeting on mass formula and gamma deformation of nuclear systems with Prof. P. Moller, Wako, Saitama (Dec. 11, 2006).

M. Takano, T. Tachibana and H. Koura

Consideration of the synthesis of superheavy nuclei based on nuclear data

H. 18 Symposium on Heliosphere and Annual meeting of the Solar Terrestrial Environment Laboratory, Nagoya, Aichi (Jan. 29, 2007).

H. Koura

Systematical study of nuclear fission in the heavy and superheavy nuclidic region related to the r-process nucleosynthesis

Mini-workshop on "Nuclear data for fission cycle in the r-process nucleosynthesis", Mitaka, Tokyo (Mar. 23, 2007).

H. Koura, T. Tachibana and S. Chiba

Estimation of limit of stability of nuclei considering spontaneous fission in the heavy and super-heavy, nuclidic region II

Spring Meeting of the Physical Society of Japan, Hachioji (Mar. 25-28, 2007).

K. Oyamatsu, K. Iida and H. Koura

Masses of unstable nuclei and the Equation of State of Asymmetric Nuclear Matter

Spring Meeting of the Physical Society of Japan, Hachioji (Mar. 25-28 2007).

S. Chiba, H. Koura and S. Kunieda

Collective level structure and neutron cross sections of Actinides by SRM-CC

2006 Autumn Meeting of the Atomic Energy Society of Japan, Sapporo, Hokkaido (Sep. 27-29, 2006).

S. Chiba, H. Koura, T. Maruyama, T. Hayakawa, T. Kawano and T. Kajino

Calculation of neutron capture cross sections by direct/semi-direct model

2007 Annual Meeting of the Atomic Energy Society of Japan, Nagoya, Aichi (Mar. 27-29, 2007).

S. Chiba, H. Koura, T. Maruyama, M. Ohta, S. Tatsuda, T. Wada, T. Tachibana, T. Kajino, K. Sumiyoshi and K. Otsuki

R-process abundance pattern including fission

Mini-workshop on “Nuclear data for fission cycle in the r-process nucleosynthesis”, Mitaka, Tokyo (Mar. 23, 2007).

Y. Utsuno,

Structure of exotic nuclei by large-scale shell model calculations

The 6th China-Japan Joint Nuclear Physics Symposium (invited), Shanghai, China (May 16-20, 2006).

Y. Utsuno, T. Otsuka, T. Mizusaki, and M. Honma

Structure of unstable nuclei in the sd-pf shell region by shell model with proper tensor force

The Seventh International Conference on Radioactive Nuclear Beams (RNB7), Cortina d'Ampezzo, Italy (Jul. 3-7, 2006).

Y. Utsuno, T. Otsuka, T. Mizusaki, and M. Honma,

Evolution of shell- and nuclear-structure in unstable nuclei studied by large-scale shell-model calculation

Opening meeting of Japan-US Theory Institute for Physics with Exotic Nuclei, Wako, Japan (Jul. 10-11, 2006).

Y. Utsuno

Shell evolution in exotic nuclei and exotic nuclear structure

KEK Workshop “Modern Nuclear Physics –Diversifying and Evolving Picture of Nuclei” (invited), Tsukuba (Aug. 1-3, 2006).

Y. Utsuno

Shell-model approach to the island of inversion and beyond

5th CNS International Summer School (CISS06) (invited lecture), Wako, Japan (Aug. 24-29, 2006).

Y. Utsuno, T. Otsuka, T. Mizusaki and M. Honma

Systematic calculation of unstable nuclei around $N=28$ by the shell model
Autumn Meeting of the Physical Society of Japan, Nara (Sep. 20-23, 2006).

Y. Utsuno, T. Otsuka, T. Mizusaki and M. Honma

Significance of tensor force in the structure of exotic nuclei around $N=28$
2nd German-Japanese Workshop on Nuclear Structure and Astrophysics (invited talk), Wako, Japan (Oct. 4-7, 2006).

Y. Utsuno, T. Otsuka, T. Mizusaki and M. Honma

Present status and future of the sd - pf shell region by the shell model
RIBF Mini Workshop “Gamma-ray experiment by RIBF II”, Wako (Oct. 16-17, 2006).

Y. Utsuno

Nuclear radii in the “island of inversion” region from the structure viewpoint
RIBF Mini Workshop “Nuclear Structure Probed by Reaction Cross Section”, Wako (Nov. 17-18, 2006).

Y. Utsuno, T. Otsuka, T. Mizusaki and M. Honma

Shell model calculation of unstable nuclei and effective interaction
YITP Workshop “Theory of Effective Interaction and Nuclear Model”, Kyoto (Feb. 5-7, 2007).

8.6 Atomic Physics and Solid State Physics

Journal/Proceedings

M. Imai, M. Sataka, K. Kawatsura, K. Takahiro, K. Komaki and H. Shibata
High Resolution Zero Degree Electron Spectroscopy of Argon Ions through Carbon Foil
Braz. J. Phys. 36 (2006) 541.

S.C. Jeong and TRIAC collaboration
Diffusion experiment by using the short-lived radiotracer of ^8Li
AIP-CP865 (2006) 338-343.

M. Imai, M. Sataka, K. Kawatsura, K. Takahiro, K. Komaki, H. Shibata, H. Sugai and K. Nishio
Charge state evolution of 2 MeV/u sulfur ion passing through thin carbon foil
Nucl. Instrum. Methods Phys. Res., B 256 (2007) 11.

Meetings

K. Kawatsura, K. Takahiro, K. Ozaki, M. Sataka, M. Imai, H. Sugai, H. Shibata and K. Komaki
Ejected Electron Spectra from Rydberg States of Ne Ions Passing through C Foils
22th International Conference on Atomic Collisions in Solids, Berlin Germany (Jul. 21-26, 2006).

8.7 Radiation Effects in Materials

Journal/Proceedings

K. Yasuda, T. Yamamoto, M. Shimada, S. Matsumura, Y. Chimi and N. Ishikawa
Atotic structure and disordering induced by 350 MeV Au ions in MgAl₂O₄
 Nucl. Instrum. Methods Phys. Res., B 250 (2006) 238.

T. Yamamoto, M. Shimada, K. Yasuda, S. Matsumura, Y. Chimi and N. Ishikawa
Microstructure and atomic disordering of magnesium aluminate spinel irradiated with swift heavy ions
 Nucl. Instrum. Methods Phys. Res., B 245 (2006) 235.

K. Yasuda, T. Yamamoto M. Shimada and S. Matsumura
Structure and Disordering Processes of Ion Tracks in Spinel Compounds
 Kenbikyō 41 (2006) 150 (in Japanese).

T. Sonoda, M. Kinoshita, Y. Chimi, N. Ishikawa, M. Sataka, and A. Iwase
Electronic excitation effects in CeO₂ under irradiations with high-energy ions of typical fission products
 Nucl. Instrum. Methods Phys. Res., B 250 (2006) 254-258.

A. Iwase, M. Fukuzumi, Y. Zushi, M. Suzuki, M. Takagaki, N. Kawamura, Y. Chimi, N. Ishikawa, J. Mizuki and F. Ono
Study on Irradiation-Induced Magnetic Transition in FeRh Alloy by means of Fe K-edge XMCD Spectroscopy
 Nucl. Instrum. Methods Phys. Res., B 256 (2007) 429-433.

Y. Zushi, M. Fukuzumi, Y. Chimi, N. Ishikawa and A. Iwase
Ion-Species dependence of swift heavy ion induced ferromagnetism of FeRh at low temperatures
 Nucl. Instrum. Methods Phys. Res., B 256 (2007) 434-437.

N. Matsunami, M. Sataka, S. Okayasu and M. Tazawa
Electronic Sputtering of Nitrides by High-Energy Ions
 Nucl. Instrum. Methods Phys. Res., B 256 (2007) 333.

O. Fukuoka, N. Matsunami, M. Tazawa, T. Shimura, M. Sataka, H. Sugai and S. Okayasu

Irradiation Effects with 100 MeV Xe Ions on Optical Properties of Al-doped ZnO Films
Nucl. Instrum. Methods Phys. Res., B 250 (2006) 295.

H. Sugai, N. Matsunami, O. Fukuoka, M. Sataka, T. Kato, S. Okayasu and T. Shimura
M. Tazawa, Electrical Conductivity Increase of Al-doped ZnO Films Induced by High-Energy-Heavy Ions

Nucl. Instrum. Methods Phys. Res., B 250 (2006) 291.

N. Ishikawa, S. Yamamoto and Y. Chimi

Structural Changes in Anatase TiO₂ Thin Films Irradiated with High-Energy Heavy Ions

Nucl. Instrum. Methods Phys. Res., B 250 (2006) 250.

S. Nakagawa, F. Hori, Y. Chimi, N. Ishikawa, M. Kitagawa, R. Oshima, T. Tobita, R. Taniguchi, M. Suzuki and A. Iwase

Local Modification of Hardness in FeCu Alloys by Using Swift Heavy Ion Irradiation
Nucl. Instrum. Methods Phys. Res., B 257 (2007) 397.

Meetings

K. Yasuda

Structure and Ion Configuration in and around Ion Tracks in Spinel Compounds

Workshop on Materials under Radiation Field, Japan Institute of Metals, Niigata (Sep. 2006).

S. Matsumura, T. Yamamoto, K. Yasuda, Y. Chimi and N. Ishikawa

Atomic Resolution Transmission Electron Microscope Analysis of Disordered Ion Tracks Formed in Magnesium Aluminate Spinel by Swift Heavy Ions
Materials Science and Technology 2006, Cincinnati, USA (Oct. 2006).

S. Matsumura, K. Yasuda, K. Yasunaga, K. Shiyama, T. Sonoda, H. Abe, T. Iwai, M. Sataka, N. Ishikawa, Y. Chimi, S. Okubo, A. Iwase and M. Kinoshita

New Cross-Over Project; New engineering to control materials behaviour at high energy and high fluence irradiation (V)- Microstructure observation and analysis of

irradiated ceramic compounds with the fluorite crystal structure-

2006 Autumn Meeting of the Atomic Energy Society of Japan, Hokkaido Univ. (Sep. 27, 2006).

T. Sonoda, Y. Chimi, N. Ishikawa, M. Sataka, and A. Iwase

Formation and Accumulation Effects of Ion Tracks on the Microstructural Evolution in CeO₂

Materials Science & Technology 2006 Conference and Exhibition (MS&T'06), Cincinnati, USA (Oct. 18, 2006).

K. Yasunaga, K. Yasuda, S. Matsumura, T. Sonoda, Y. Chimi, and N. Ishikawa

Microstructure Change Induced by Swift Heavy Ions in CeO₂ Pre-Implanted with Xe Ions

Materials Science & Technology 2006 Conference and Exhibition (MS&T'06), Cincinnati, USA (Oct. 18, 2006).

T. Sonoda, S. Matsumura, K. Yasuda, K. Yasunaga, K. Shiyama, M. Sataka, N. Ishikawa, Y. Chimi, S. Okubo, H. Abe, T. Iwai, A. Iwase and M. Kinoshita

Review of Experimental Approach of NXO Project

New Cross-over Project Workshop-3 -Recovery cycles and restructuring of fission-energy driven ceramics-, Tokyo (Dec. 12, 2006).

S. Okayasu, N. Kokubo and I. Takeya

International Symposium on Superconductivity 2006

Nagoya (Oct. 25, 2006).

N. Matsunami, M. Sataka, S. Okayasu and M. Tazawa

Electronic Sputtering of Nitrides by High-Energy Ions

6th Int. Conf. Atomic Collisions in Solids (ICACS)2006, Berlin, Germany (Jul. 21-26, 2006).

N. Matsunami, O. Fukuoka, M. Tazawa, T. Shimura, M. Sataka, H. Sugai and S. Okayasu

Modifications of Al-doped ZnO Properties by High-Energy Ions

Autumn Meeting of the Physical Society of Japan, Chiba (Sep. 2006).

N. Ishikawa, Y. Chimi, O. Michikami, Y. Ohta, M. Lang and R. Neumann

Irradiation Damage of Oxide Materials

JAEA-GSI Meeting, Takasaki (Mar.12, 2007).

S. Nakagawa, Y. Chimi, N. Ishikawa, M. Kitagawa, R. Oshima, T. Tobita, R. Taniguchi,
M. Suzuki and A. Iwase

Local Modification of Hardness in FeCu Alloys by Using Swift Heavy Ion Irradiation

15th International Conference on Ion Beam Modification of Materials (IBMM 2006),
Taormina, Italy (Sep. 18, 2006).

S. Nakagawa, F. Hori, A. Iwase, N. Ishikawa, Y. Chimi, T. Tobita, M. Suzuki, M.
Kitagawa and R. Oshima

Swift Heavy Ion Induced Cu Segregation in FeCu Alloys

2006 Autumn Meeting of the Atomic Energy Society of Japan, Hokkaido (Sep. 28,
2006).

This is a blank page

CHAPTER 9

Personnel and Committee

- 9.1 Personnel
- 9.2 Research Planning and Assessment Committee

This is a blank page

9.1 Personnel

Department of Research Reactor and Tandem Accelerator

Fumio	Sakurai	Director (Apr.-Dec.)
Kiyonobu	Yamashita	Director (Jan.-)
Suehiro	Takeuchi	Deputy Director
Shigeru	Mori	Manager of Administration Section

Department of Research Reactor and Tandem Accelerator

Tandem Accelerator Section (* General Manager)

Scientific Staff

Suehiro	Takeuchi*	(Apr.-Sep.)
Masao	Sataka*	(Oct.-)
Susumu	Hanashima	
Akihiko	Osa	
Makoto	Matsuda	

Technical Staff

Yoshihiro	Tsukihashi	
Shin-ichi	Abe	
Nobuhiro	Ishizaki	
Hidekazu	Tayama	(Apr.-Sep.)
Takamitsu	Nakanoya	
Hiroshi	Kabumoto	
Masahiko	Nakamura	
Ken-ichi	Kutsukake	
Yoshinori	Otokawa	
Katsuzo	Horie	(Apr.-Sep.)
Isao	Ohuchi	

Entrusted Operators

Akihiko	Iijima	
Takahiro	Yoshida	
Takahiro	Usami	
Tetsusi	Hida	(Apr.-Sep.)
Takayuki	Ishiguro	(Jun.-)
Kazushi	Yamaguchi	(Oct.-)
Hisashi	Sakurayama	
Hikaru	Nisugi	
Nobuo	Seki	
Teruo	Onodera	

Entrusted Assistant

Kenjiro	Obara	
---------	-------	--

Department of Radiation Protection

Facility Radiation Control Section I

Kenji	Yamane
Takashi	Nakazawa
Katsuji	Yasu
Takehisa	Ohkura
Hayato	Hiraga

Advanced Science Research Center

Yoshihiko Hatano	Director
Hiroshi Ikezoe	Deputy Director

Advanced Science Research Center

Research Group for Shell Structure and Reaction Properties of Heavy Nuclei far from Stability

(Group Leader)*

Hiroari Miyatake*	
Tetsuro Ishii	
Shin-ichi Ichikawa	
Satoshi Chiba	
Toshiki Maruyama	
Shin-ichi Mitsuoka	
Katsuhisa Nishio	
Hiroyuki Koura	
Yutaka Utsuno	
Tetsuya Sato	
Takashi Hashimoto	(Post Doc.)
Hiroyuki Makii	(Post Doc.)

Advanced Science Research Center

Research Group for Nuclear chemistry of the Heaviest Elements (* Group Leader)

Yuichiro Nagame*	
Kazuaki Tsukada	
Ichiro Nishinaka	
Masato Asai	
Atsushi Toyoshima	(Post Doc.)
Yoshitaka Kasamatsu	(Post Doc.)
Yasuo Ishii	(Student)
Hayato Toume	(Student)

Advanced Science Research Center

Mega Gravity Research Group

Satoru Okayasu

Nuclear Science and Engineering Directorate

***Innovative Nuclear Science Research Group* (* Group Leader)**

Masumi	Oshima*	
Hideo	Harada	Sub Leader (Oct.-Mar.)
Hideki	Iimura	
Mitsuo	Koizumi	
Kazuyoshi	Furutaka	
Yuichi	Hatsukawa	
Fumito	Kitatani	
Shoji	Nakamura	
Yosuke	Toh	
Atsushi	Kimura	
Kaoru	Hara	(Post Doc.)
Masayuki	Ohta	(Post Doc.)
Tadahiro	Kin	(Post Doc.)

Nuclear Science and Engineering Directorate

***Research Group for Irradiation Field Materials* (* Group Leader)**

Shiro	Jitsukawa*
Masao	Sataka
Hiroyuki	Sugai
Nariaki	Okubo
Teruo	Kato
Norito	Ishikawa
Takeo	Aruga
Daijyu	Yamaki

Quantum Beam Science Directorate

Laser Accelerator Group

Takehito	Hayakawa
Toshiyuki	Shizuma

High Energy Accelerator Research Organization (KEK)

Institute of Particle and Nuclear Studies – Radioactive Nuclear Beams Project Group

(Group Leader)*

Physics Division IV

Hiroari Miyatake*
Sun-Chan Jeong
Masahiko Tanaka
Hironobu Ishiyama
Yutaka Watanabe
Nobuaki Imai
Yoshikazu Hirayama
Yoshihide Fuchi
Michihiro Oyaizu
Ichiro Katayama
Hirokane Kawakami
Nobuharu Yoshikawa

Physics Division I

Shoji Suzuki

High Energy Accelerator Research Organization (KEK)

Accelerator Laboratory

Accelerator Division I

Shigeaki Arai
Masashi Okada

9.2 Research Planning and Assessment Committee

<i>Chairman</i>	Shigeru Kubono	(Professor, The University of Tokyo)
<i>Vice Chairman</i>	Ken-ichiro Komaki	(Professor, The University of Tokyo)
<i>Member</i>	Tadashi Kambara	(Senior Scientist, RIKEN)
	Kenji Kimura	(Professor, Kyoto University)
	Noriaki Matsunami	(Associate Professor, Nagoya University)
	Tetsuo Noro	(Professor, Kyushu University)
	Tsutomu Ohtsuki	(Associate Professor, Tohoku University)
	Tadashi Shimoda	(Professor, Osaka University)
	Kazuhiro Yabana	(Associate Professor, Tsukuba University)
	Yuichi Hatsukawa	(Quantum Beam Science Directorate, JAEA)
	Shiro Jitsukawa	(Nuclear Science and Engineering Directorate, JAEA)
	Motoharu Mizumoto	(Quantum Beam Science Directorate, JAEA)
Kazumasa Narumi	(Advanced Science Research Center, JAEA)	
<i>Organizer</i>	Hiroshi Ikezoe	(Deputy Director, Advanced Science Research Center, JAEA)
	Suehiro Takeuchi	(Deputy Director, Dep. Research Reactors and Accelerator, JAEA)
<i>Secretary</i>	Akihiko Osa	(Tandem Accelerator Section, JAEA)
	Susumu Hanashima	(Tandem Accelerator Section, JAEA)
	Masao Sataka	(Tandem Accelerator Section, JAEA)

This is a blank page

CHAPTER 10

Cooperative Researches , and Common Use Program in JAEA

- 10.1 Cooperative Researches List
- 10.2 Common Use Program in JAEA

This is a blank page

10.1 Cooperative Researches List

Title	Contact Person & Organization
1. Dynamic behavior of heavy ions in material	Kiyoshi KAWATSURA Kyoto Institute of Technology
2. Process of irradiation damage in nuclear reactor materials with Fe base alloys	Akihiro IWASE Osaka Prefecture University
3. Process of structural change in light-water reactor fuel with irradiation damage by fission products	Takeshi SONODA Central Research Institute of Electric Power Industry
4. Study of secondary ion emission from heavy ion-solid collision	Tsuguhisa SEKIOKA University of Hyogo
5. Study of nuclear structure in the region of A=180 nuclei by the transfer reaction	Mamoru FUJIWARA Osaka University
6. In-beam gamma-ray spectroscopy in the trans-uranium region by the transfer reaction	Masao OGAWA Tokyo Institute of Technology
7. Production heavy elements by heavy-ion fusion reaction using actinide targets and measurement of the decay properties	Tutomu OHTSUKI Tohoku University
8. Measurement of spectroscopic factor and spin-parity on $^{62}\text{Ni}(d, p)^{63}\text{Ni}^*$ reaction in inverse kinematics	Sun-Chan JEONG High Energy Accelerator Research Organization
9. Experimental study of fusion barrier distribution for super-heavy element synthesis	Sun-Chan JEONG High Energy Accelerator Research Organization
10. Study of element synthesis in the universe via short-lived nuclei	Hiroari MIYATAKE High Energy Accelerator Research Organization
11. Study of super-deformed state and high-spin shell structure in A=30 region	Eiji IDEGUCHI University of Tokyo
12. Study of nuclear deformation by Coulomb excitation and lifetime measurement	Masahiko SUGAWARA Chiba Institute of Technology
13. Coulomb excitation on neutron-rich Xe nuclei of fission products	Hiroari MIYATAKE High Energy Accelerator Research Organization
14. Gamma-ray spectroscopy for super-heavy nuclei	Keisuke SUEKI University of Tsukuba

10.1 Cooperative Researches List (contd.)

Title	Contact Person & Organization
15. Aqueous chemistry of super-heavy elements Rf and Db	Hisaaki KUDO Niigata University
16. Development of electrochemical apparatus for single atom chemistry	Atsushi SHINOHARA Osaka University
17. Study of nuclear fission from excited states of heavy-actinide nuclei	Akihiko YOKOYAMA Kanazawa University
18. Nuclear spectroscopy using lasers for refractory element isotope in Re region	Takayoshi HORIGUCHI Hiroshima International University
19. Decay study on neutron-rich nuclei of fission products of ^{238}U using the on-line mass separator JAEA-ISOL	Michihiro SHIBATA Nagoya University
20. Ion source development for the JAEA on-line isotope separator	Sun-Chan JEONG High Energy Accelerator Research Organization
21. Diffusion study in super-ionic conducting materials using the short-lived nuclei	Sun-Chan JEONG High Energy Accelerator Research Organization
22. Study of the nuclear synthesis under an explosive condition in the universe by using ^8Li radioactive nuclei beam	Hironobu ISHIYAMA High Energy Accelerator Research Organization
23. β -decay spectroscopy of nuclear spin polarized nuclei in the region of ^{132}Sn	Yoshikazu HIRAYAMA High Energy Accelerator Research Organization
24. Generation of polarized In, Cs and Ba isotope by using tilted-foil method and measurement of nuclear magnetic moment	Kensaku MATSUTA Osaka University

10.2 Common Use Program in JAEA

Title	Contact Person & Organization
1. Radiation-induced magnetic transition in FeRh alloys	Akihiro IWASE Osaka Prefecture University
2. Study on electronic structure and processes for highly charged heavy-ions by zero-degree electron spectroscopy	Kiyoshi KAWATSURA Kyoto Institute of Technology
3. Synthesis of water-soluble radioisotope-metallofullerenes	Keisuke SUEKI University of Tsukuba
4. Systematic study of signature inversion and shape coexistence in high-spin states of A=170-190 nuclei	Yu.Hu. Zhang Institute of Modern Physics Chinese Academy of Science
5. Electronic excitation effects on non-metals by high energy heavy ions	Noriaki MATSUNAMI Nagoya University
6. Production of radioactive-isotope tracers for chemistry of heavy and super heavy elements	Shinichi GOTO Niigata University
7. Atomic structure and ion distribution in ion tracks in spinel irradiated with swift heavy ions	Kazuhiro YASUDA Kyushu University
8. Effect of neutron transfer in heavy-ion fusion reaction	Yutaka WATANABE High Energy Accelerator Research Organization

This is a blank page

国際単位系 (SI)

表1. SI 基本単位

基本量	SI 基本単位	
	名称	記号
長さ	メートル	m
質量	キログラム	kg
時間	秒	s
電流	アンペア	A
熱力学温度	ケルビン	K
物質の量	モル	mol
光度	カンデラ	cd

表2. 基本単位を用いて表されるSI組立単位の例

組立量	SI 基本単位	
	名称	記号
面積	平方メートル	m ²
体積	立方メートル	m ³
速度	メートル毎秒	m/s
加速度	メートル毎秒毎秒	m/s ²
波数	毎メートル	m ⁻¹
密度 (質量密度)	キログラム毎立方メートル	kg/m ³
質量体積 (比体積)	立方メートル毎キログラム	m ³ /kg
電流密度	アンペア毎平方メートル	A/m ²
磁界の強さ (物質量の) 濃度	アンペア毎メートル	A/m
輝度	モル毎立方メートル	mol/m ³
屈折率	カンデラ毎平方メートル (数 の) 1	cd/m ² 1

表5. SI 接頭語

乗数	接頭語	記号	乗数	接頭語	記号
10 ²⁴	ヨタ	Y	10 ⁻¹	デシ	d
10 ²¹	ゼタ	Z	10 ⁻²	センチ	c
10 ¹⁸	エクサ	E	10 ⁻³	ミリ	m
10 ¹⁵	ペタ	P	10 ⁻⁶	マイクロ	μ
10 ¹²	テラ	T	10 ⁻⁹	ナノ	n
10 ⁹	ギガ	G	10 ⁻¹²	ピコ	p
10 ⁶	メガ	M	10 ⁻¹⁵	フェムト	f
10 ³	キロ	k	10 ⁻¹⁸	アト	a
10 ²	ヘクト	h	10 ⁻²¹	ゼプト	z
10 ¹	デカ	da	10 ⁻²⁴	ヨクト	y

表3. 固有の名称とその独自の記号で表されるSI組立単位

組立量	SI 組立単位			
	名称	記号	他のSI単位による表し方	SI基本単位による表し方
平面角	ラジアン ^(a)	rad		m ² ・m ⁻¹ =1 ^(b)
立体角	ステラジアン ^(a)	sr ^(c)		m ² ・m ⁻² =1 ^(b)
周波数	ヘルツ	Hz		s ⁻¹
力	ニュートン	N		m ² ・kg ² ・s ⁻²
圧力, 応力	パスカル	Pa	N/m ²	m ⁻² ・kg ² ・s ⁻²
エネルギー, 仕事, 熱量	ジュール	J	N・m	m ² ・kg ² ・s ⁻²
工率, 放射束	ワット	W	J/s	m ² ・kg ² ・s ⁻³
電荷, 電気量	クーロン	C		s・A
電位差 (電圧), 起電力	ボルト	V	W/A	m ² ・kg ² ・s ⁻³ ・A ⁻¹
静電容量	ファラド	F	C/V	m ⁻² ・kg ⁻¹ ・s ⁴ ・A ²
電気抵抗	オーム	Ω	V/A	m ² ・kg ⁻³ ・s ⁻³ ・A ⁻²
コンダクタンス	ジーメン	S	A/V	m ⁻² ・kg ⁻¹ ・s ³ ・A ²
磁束	ウェーバ	Wb	V・s	m ² ・kg ² ・s ⁻² ・A ⁻¹
磁束密度	テスラ	T	Wb/m ²	kg ² ・s ⁻² ・A ⁻¹
インダクタンス	ヘンリー	H	Wb/A	m ² ・kg ² ・s ⁻² ・A ⁻²
セルシウス温度	セルシウス度 ^(d)	°C		K
光度	ルーメン	lm	cd・sr ^(c)	m ² ・m ⁻² ・cd=cd
照射度	ルクス	lx	lm/m ²	m ² ・m ⁻⁴ ・cd=m ⁻² ・cd
(放射性核種の) 放射能	ベクレル	Bq		s ⁻¹
吸収線量, 質量エネルギー分与, カーマ線量当量, 周辺線量当量, 方向性線量当量, 個人線量当量, 組織線量当量	グレイ	Gy	J/kg	m ² ・s ⁻²
	シーベルト	Sv	J/kg	m ² ・s ⁻²

- (a) ラジアン及びステラジアンの使用は、同じ次元であっても異なった性質をもった量を区別するときの組立単位の表し方として利点がある。組立単位を形作る時のいくつかの用例は表4に示されている。
- (b) 実際には、使用する時には記号rad及びsrが用いられるが、習慣として組立単位としての記号“1”は明示されない。
- (c) 測光学では、ステラジアンの名称と記号srを単位の表し方の中にそのまま維持している。
- (d) この単位は、例としてミリセルシウス度m°CのようにSI接頭語を伴って用いても良い。

表4. 単位の中に固有の名称とその独自の記号を含むSI組立単位の例

組立量	SI 組立単位		
	名称	記号	SI 基本単位による表し方
粘力のモーメント	パスカル秒	Pa・s	m ⁻¹ ・kg ² ・s ⁻¹
表面張力	ニュートンメートル	N・m	m ² ・kg ² ・s ⁻²
角速度	ニュートン毎メートル	N/m	kg ² ・s ⁻²
角加速度	ラジアン毎秒	rad/s	m ² ・m ⁻¹ ・s ⁻¹ =s ⁻¹
熱流密度, 放射照度	ラジアン毎平方メートル	rad/s ²	m ² ・m ⁻¹ ・s ⁻² =s ⁻²
熱容量, エントロピー	ジュール毎平方メートル	W/m ²	kg ² ・s ⁻³
質量熱容量 (比熱容量), 質量エントロピー	ジュール毎キログラム	J/K	m ² ・kg ² ・s ⁻² ・K ⁻¹
質量エネルギー (比エネルギー)	ジュール毎キログラム	J/(kg・K)	m ² ・s ⁻² ・K ⁻¹
熱伝導率	ワット毎メートル毎ケルビン	J/(m・K)	m ² ・s ⁻² ・K ⁻¹
体積エネルギー	ジュール毎立方メートル	W/(m・K)	m ² ・kg ² ・s ⁻³ ・K ⁻¹
電界の強さ	ジュール毎立方メートル	J/m ³	m ⁻¹ ・kg ² ・s ⁻²
体積電荷	ボルト毎メートル	V/m	m ² ・kg ² ・s ⁻³ ・A ⁻¹
電気変位	クーロン毎立方メートル	C/m ³	m ⁻³ ・s・A
誘電率	クーロン毎平方メートル	C/m ²	m ⁻² ・s・A
透磁率	ファラド毎メートル	F/m	m ⁻³ ・kg ⁻¹ ・s ⁴ ・A ²
モルエネルギー	ヘンリー毎メートル	H/m	m ² ・kg ² ・s ⁻² ・A ⁻²
モルエントロピー	ジュール毎モル	J/mol	m ² ・kg ² ・s ⁻² ・mol ⁻¹
モル熱容量	ジュール毎モル毎ケルビン	J/(mol・K)	m ² ・kg ² ・s ⁻² ・K ⁻¹ ・mol ⁻¹
照射線量 (X線及びγ線)	クーロン毎キログラム	C/kg	kg ⁻¹ ・s・A
吸収線量	グレイ毎秒	Gy/s	m ² ・s ⁻³
放射強度	ワット毎ステラジアン	W/sr	m ⁴ ・m ⁻² ・kg ² ・s ⁻³ =m ² ・kg ² ・s ⁻³
放射輝度	ワット毎平方メートル毎ステラジアン	W/(m ² ・sr)	m ² ・m ⁻² ・kg ² ・s ⁻³ =kg ² ・s ⁻³

表6. 国際単位系と併用されるが国際単位系に属さない単位

名称	記号	SI 単位による値
分	min	1 min=60s
時	h	1 h =60 min=3600 s
日	d	1 d=24 h=86400 s
度	°	1°=(π/180) rad
分	′	1′=(1/60)°=(π/10800) rad
秒	″	1″=(1/60)′=(π/648000) rad
リットル	l, L	1 l=1 dm ³ =10 ⁻³ m ³
トン	t	1 t=10 ³ kg
ネーパ	Np	1 Np=1
ベル	B	1 B=(1/2) ln10 (Np)

表7. 国際単位系と併用されこれに属さない単位で SI単位で表される数値が実験的に得られるもの

名称	記号	SI 単位であらわされる数値
電子ボルト	eV	1 eV=1.60217733(49)×10 ⁻¹⁹ J
統一原子質量単位	u	1 u=1.6605402(10)×10 ⁻²⁷ kg
天文単位	ua	1 ua=1.49597870691(30)×10 ¹¹ m

表8. 国際単位系に属さないが国際単位系と併用されるその他の単位

名称	記号	SI 単位であらわされる数値
海里	海里	1 海里=1852m
ノット	ノット	1 ノット = 1 海里毎時=(1852/3600)m/s
アール	a	1 a=1 dam ² =10 ² m ²
ヘクタール	ha	1 ha=1 hm ² =10 ⁴ m ²
バール	bar	1 bar=0.1MPa=100kPa=1000hPa=10 ⁵ Pa
オングストローム	Å	1 Å=0.1nm=10 ⁻¹⁰ m
バール	b	1 b=100fm ² =10 ⁻²⁸ m ²

表9. 固有の名称を含むCGS組立単位

名称	記号	SI 単位であらわされる数値
エルグ	erg	1 erg=10 ⁻⁷ J
ダイン	dyn	1 dyn=10 ⁻⁵ N
ポアズ	P	1 P=1 dyn・s/cm ² =0.1Pa・s
ストークス	St	1 St=1cm ² /s=10 ⁻⁴ m ² /s
ガウス	G	1 G=10 ⁴ T
エルステッド	Oe	1 Oe=(1000/4π)A/m
マクスウェル	Mx	1 Mx=10 ⁻⁸ Wb
スチル	sb	1 sb=1cd/cm ² =10 ⁴ cd/m ²
ホト	ph	1 ph=10 ⁴ lx
ガリ	Gal	1 Gal=1cm/s ² =10 ⁻² m/s ²

表10. 国際単位に属さないその他の単位の例

名称	記号	SI 単位であらわされる数値
キュリー	Ci	1 Ci=3.7×10 ¹⁰ Bq
レントゲン	R	1 R = 2.58×10 ⁻⁴ C/kg
ラド	rad	1 rad=1cGy=10 ⁻² Gy
レム	rem	1 rem=1 cSv=10 ⁻² Sv
X線単位	X unit	1 X unit=1.002×10 ⁻⁴ nm
ガンマ	γ	1 γ=1 nT=10 ⁻⁹ T
ジャンスキー	Jy	1 Jy=10 ⁻²⁶ W・m ⁻² ・Hz ⁻¹
フェルミ	fm	1 fermi=1 fm=10 ⁻¹⁵ m
メートル系カラット	carat	1 metric carat = 200 mg = 2×10 ⁻⁴ kg
トル	Torr	1 Torr = (101 325/760) Pa
標準大気圧	atm	1 atm = 101 325 Pa
カリ	cal	
マイクロ	μ	1 μ =1um=10 ⁻⁶ m

